Title	Preparing Artificial Biocatalysts for Guaiacol Oxidation and Phenylacetylene Polymerization by Placing a Metal Complex within an Engineered Hemoprotein Cavity
Author(s)	福本, 和貴
Citation	大阪大学, 2014, 博士論文
Version Type	VoR
URL	https://doi.org/10.18910/34492
rights	
Note	

Doctoral Dissertation

Preparing Artificial Biocatalysts for Guaiacol Oxidation

and Phenylacetylene Polymerization by Placing a Metal

Complex within an Engineered Hemoprotein Cavity

Kazuki Fukumoto

January 2014

Graduate School of Engineering,

Osaka University

Contents

General Introduction

Metalloenzyme

A metalloenzyme contains a metal ion or metal complex within a naturally-optimized protein matrix, and catalyzes high reactive and selective reactions under mild conditions (in water and at ordinary temperature and pressure). For example, nitrogenase has a FeMo cluster and reduces nitrogen to ammonia (Figure 1a). Cytochrome P450 has an iron porphyrin to insert an oxygen atom into a C–H bond of benzoic or aliphatic compounds (Figure 1b). Methane monooxygenase has a diiron core and catalyzes the hydroxylation of methane (Figure 1c). Although the native metalloenzymes can smoothly catalyze difficult reactions, they can only promote a specific transformation because of enzymatic regulations such as substrate specificity and pH dependence. To broaden the scope of enzymatic transformation, many efforts have been devoted until now.

a)   b)   c)

Nitrogenase   Cytochrome P450   Methane monooxygenase
[Fe][Mo]   [Fe]   [Fe][Fe]

$N_2 \longrightarrow NH_3$ $\longrightarrow$ OH $CH_4 \longrightarrow CH_3OH$
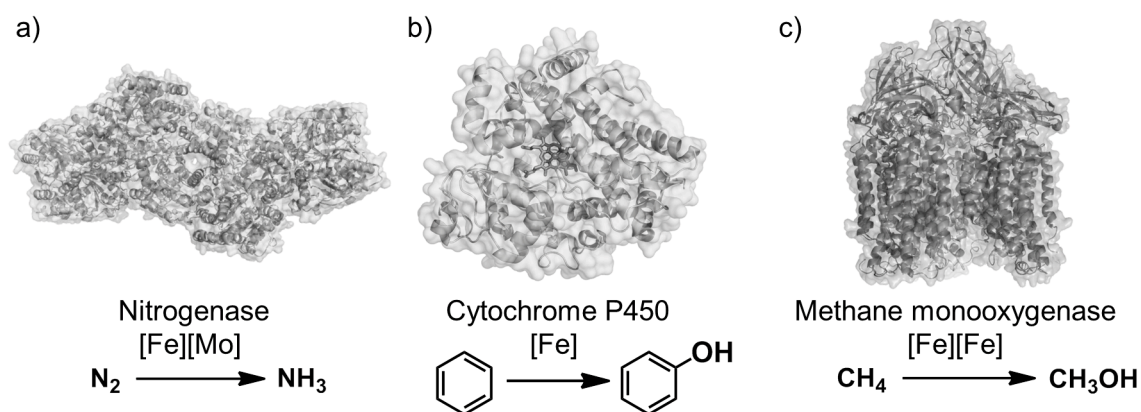
Figure 1. Representative examples of metalloenzymes in nature.

Artificial Biocatalyst

An artificial biocatalyst, which is constructed by the combination of a synthetic metal complex and a protein matrix, is one of the strategies to prepare a metalloenzyme (Figure 2). The synergy between the metal complex as an active center and the protein matrix with a well-defined chemical environment will provide a unique catalysis.

In the 1970s, Whitesides *et al.* opened the door to prepare artificial biocatalysts.[1] They produced the artificial biocatalyst by insertion of a rhodium complex with a biotin moiety into (strept)avidin using supramolecular interaction, giving a hydrogenation product in 41% ee (*S*). In the following decades, no major development was made in the artificial biocatalysts, because determining the structural information of the modified proteins was difficult. However, the recent advance in X-ray crystallographical analysis and computational chemistry has dramatically improved the understanding of the structures and functions of proteins at the molecular level, fueling the research on artificial biocatalysts in the last few years. The next paragraph summarizes the methods for the anchoring to combine a metal complex with a protein cavity, as well as the reactions which were demonstrated by artificial biocatalysts (Table 1, Figure 3).
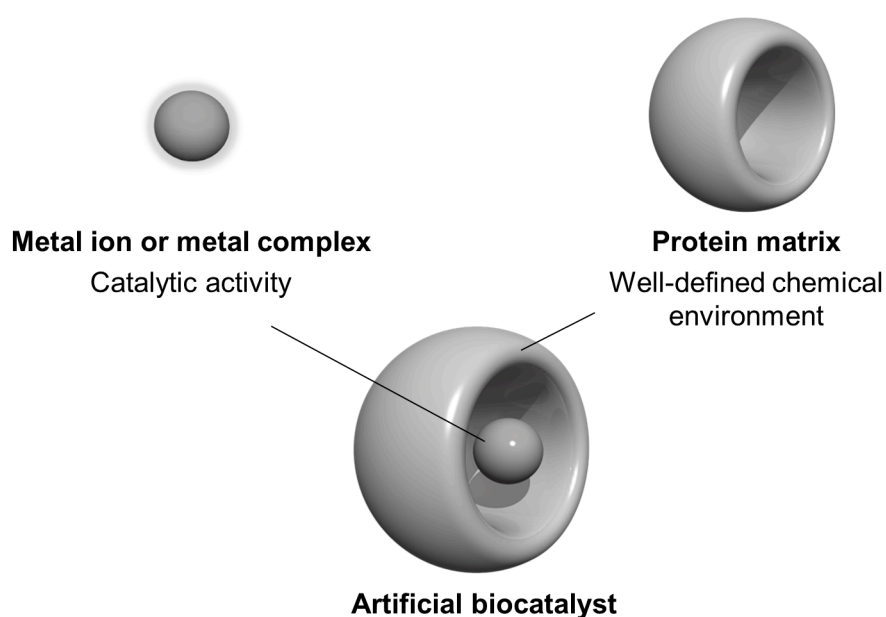

Metal ion or metal complex
Catalytic activity

Protein matrix
Well-defined chemical environment

Artificial biocatalyst

Figure 2. The concept of an artificial biocatalyst.

Table 1. The anchoring methods and recently reported reactions.

Anchoring methods	Reactions	Metal complexes	Protein matrices	Ref.
Supramolecular (biotin-avidin)	H_2 hydrogenation	Rh phosphine complex	(Strept)avidin	[1, 2, 18–20]
	Transfer hydrogenation	M (Rh, Ir and Ru) pianostool complex	(Strept)avidin	[21b, 22]
	Sulfoxidation	Mn salen complex	(Strept)avidin	[3]
	Olefin metathesis	Ru Grubbs complex	(Strept)avidin	[4]
	Benzannulation	Rh Cp* complex	(Strept)avidin	[5]
Supramolecular (heme insertion)	Sulfoxidation	Mn corrole complex	BSA[a]	[28]
		Cr or Mn salen complex	Mb[b]	[27]
	Epoxidation	Mn porphyrin and Mn salen complex	Xylanase	[31]
	Diels-Alder	Cu phthalocyanine complex	BSA	[23]
	Hydroxylation	Mn porphycene complex	Mb	[6]
Dative	Hydrogenation	Rh	CA[c]	[8a]
	Hydroformylation	Rh	CA	[8b, 30]
	Sulfoxidation	VO_4^{3-}	phytase	[26]
	Diels-Alder	Cu	tHisF	[24]
	Epoxidation	Mn	CA	[29]
	Polymerization	Rh	Ferritin	[9]
Covalent	Hydrogenation	Rh bipyridine complex	Papain	[13]
	Epoxidation	Mn salen complex	Papain	[13]
	Sulfoxidation	Mn salen complex	Mb	[14]
	Hydrolysis	Cu phenanthroline complex	LmrR[d]	[15]
	Olefin metathesis	Ru Grubbs complex	Chymotrypsin	[16a]
		Ru Grubbs complex	HSP[e]	[16b]
	ROMP	Ru Grubbs complex	FhuA	[17]
		Cu dipicolylamine complex	SCP-2L[f]	[12a]
	Diels-Alder reaction	Cu phenantroline complex	LmrR	[12b]
		Ru arene complex	Papain	[12c]

[a] BSA (bovine serum albumin). [b] Mb (myoglobin). [c] CA (carbonic anhydrase). [d] LmrR (lactococcal multidrug resistance regulator). [e] HSP (heat shock protein). [f] SCP-2L (sterol carrier protein type 2 like domain).

Anchoring Methods

A metal complex has been introduced into a protein matrix by mainly three anchoring methods (a) supramolecular anchoring, (b) dative anchoring, and (c) covalent anchoring (Figure 3).
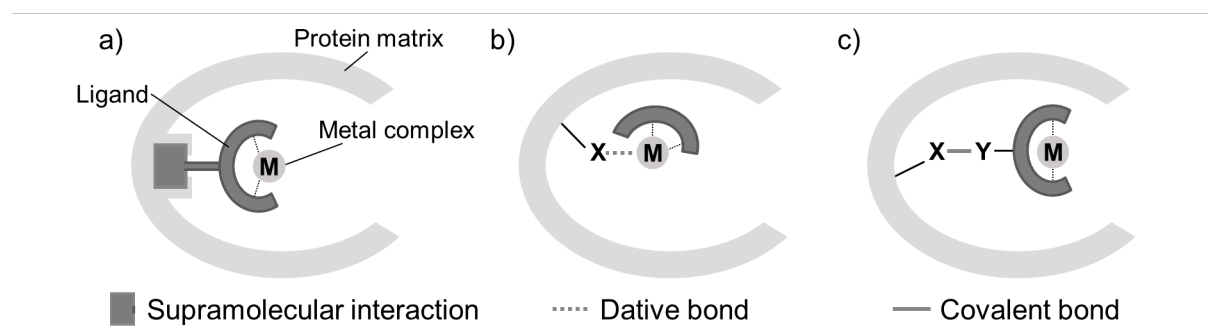

Figure 3. (a) Supramolecular, (b) dative, and (c) covalent anchoring.

(a) The supramolecular anchoring is based on the protein–substrate or protein–cofactor interaction. In 1978, the strong avidin–biotin interaction with very low dissociation constant ($K_d = 10^{-15}$) was used to tightly embed a metal complex within a protein matrix.[1] Using the protein-substrate interaction, Ward *et al*. have reported successful examples of the artificial biocatalysts prepared by the avidin–biotin interaction, which carry out hydrogenation reaction,[2] sulfoxidation,[3] olefin metathesis reaction,[4] and benzannulation reaction.[5] As an alternative approach to prepare an artificial biocatalyst, there is the interaction between a protein cavity and a heme cofactor analogue. A hemoprotein and serum albumin with a hydrophobic cavity usually are capable of binding to introduce the heme cofactor analogues including phthalocyanine, corrole and Schiff base complex in their protein cavity. Recently, Hayashi *et al*. have sophisticatedly exploited the interaction to prepare an artificial metalloenzyme containing a Mn porphycene within myoglobin to carry out a $C(sp^3)$–H bond activation.[6]

(b) The dative anchoring provides the artificial biocatalyst by the direct coordination of N, O, or S atom of amino acid residues to a metal ion. To introduce the metal ion, the native metal binding site in metalloproteins is usually applied. Kaiser *et al*. firstly proposed this approach to prepare artificial biocatalyst by substituting a zinc(II) ion for a copper(II) ion in carboxypeptidase A toward the oxidation of ascorbic acid.[7] In recent report, Kazlauskas *et al*. introduce a rhodium ion into carbonic anhydrase, which naturally contains a zinc(II) ion.[8] Watanabe *et al*. also reported the coordination of rhodium ions on the internal surface of a ferritin cavity.[9]

(c) The covalent anchoring is the conjugation of a functionalized metal complex with an amino acid residue in the protein at the specific position via a covalent linkage in the protein. Kaiser *et al*. firstly reported the covalent conjugation of a bromoacetyl-functionalized flavin with a papain protein.[10] In nearly a decade, artificial biocatalysts by covalent anchoring have been gradually increased. They have demonstrated various reactions such as hydrogenation,[11] Diels-Alder reaction,[12] epoxidation,[13] sulfoxidation,[14] hydrolysis,[15] olefin metathesis,[16] and ring opening metathesis polymerization.[17]

Reactions

Over the last few decades, a variety of reactions have been examined by artificial metalloenzymes. Here, the representative reactions were also summarized (a) hydrogenation, (b) Diels-Alder reaction, (c) peroxidation, (d) polymerization, and (e) the other reactions.

(a) Hydrogenation is the reduction of a double bond such as alkene, ketone and imine by a catalyst in the presence of H_2 gas (H_2 hydrogenation) or the other hydrogen sources such as alcohol and formic acid (transfer hydrogenation). In the H_2 hydrogenation, Whitesides *et al.* firstly reported enantioselective hydrogenation (44 % ee (*S*)) using an artificial biocatalyst, which was combined by a biotinylated rhodium complex and an avidin.[1] After the two decades, Chan *et al.* also reported enantioselective hydrogenation with 48 % ee (*R*) and 15 % ee (*S*) by artificial biocatalysts containing (*S*, *S*) and (*R*, *R*) biotinylated pyrphos rhodium complexes within an avidin protein.[18] To improve the selectivity, there are two strategies. Reetz *et al.* proposed the genetic optimization of the protein matrix in artificial biocatalysts.[19] In this optimization, the appropriate amino acids near the metal complex are combinatorially randomized by saturation mutagenesis. The selectivity in hydrogenation was increased up to 65 % ee (*R*) from 23 % ee (*R*). In the additional strategy, Ward *et al.* demonstrated that the chemogenetic optimization, that is the optimization of both the ligand of metal complex and the protein matrix, provides significant improvement of the enantioselectivity up to 98 % ee (*R*) and (*S*) in hydrogenation.[2, 20] Furthermore, they also demonstrated enantioselective imine[21] and ketone[22] reduction using the same optimization strategy in the transfer hydrogenation. The development of artificial biocatalysts for hydrogenation is approaching the maturity. For the further development, the biocatalysts will be applied to practical fields such as medicinal or industrial applications.

(b) Diels-Alder reaction is a C–C bond formation reaction between a conjugated diene and an alkene. Reetz *et al.* demonstrated the first example of enantioselective Diels-Alder reaction (93 % ee) using the artificial biocatalyst containing a Cu phthalocyanine within BSA via the supramolecular anchoring.[23] In recent researches, enantioselective Diels-Alder reactions were performed by artificial biocatalysts, which introduced a Cu(II) ion into tHisF via dative anchoring[24] and linked a Cu(II) phenanthroline with LmrR via the covalent anchoring.[12b]

(c) Peroxidation is one of representative enzymatic transformations in a native peroxidase such as horseradish peroxidase and chloroperoxidase. Three main substrates, guaiacol (2-methoxyphenol), thioanisole, and styrene derivatives are studied. In the guaiacol oxidation, Hayashi *et al.* dramatically enhanced the catalytic activity of an artificial biocatalyst, which was prepared by the incorporation of a synthetic metal complex into an apomyoglobin mutant, compared with that of native myoglobin.[25] This example gives an important insight into the development of artificial biocatalysts. In other words, the precise design of the metal complex and the protein matrix can enhance not only the selectivity but also the

activity in reactions. In the late 1990s, Sheldon *et al*. reported that enantioselective sulfoxidation of thioanisole derivatives with H_2O_2 was carried out by an artificial biocatalyst datively containing a VO_4^{3-} within a phytase to afford 66% ee (*S*) at 100% conversion.[26] After the pioneering work, Watanabe *et al*. and Lu *et al*. also demonstrated the enantioselective sulfoxidation using a Schiff base complex within an apomyoglobin as an artificial biocatalyst.[14, 27] They provided the lower selectivity (less than 35 % ee) in sulfoxidation. Additionally, one successful example was reported by Gross *et al*.[28] They increased the enantioselectivity of sulfoxidation up to 74 % using a Mn corrole within BSA. Reetz *et al*. firstly reported a Mn Schiff base within a papain for epoxidation of styrene analogues.[13] To provide the enantioselectivity, Kazlauskas *et al*. and Soumillion *et al*. have used a carbonic anhydrase naturally containing a zinc to clearly embed the substituted manganese ion into the protein cavity (67 % ee (*R*) and 40 % ee (*R*), respectively).[29]

(d) There are only three examples including the author's work in the artificial biocatalysts for polymerization, although native enzymes such as DNA polymerases provide polymeric compounds. Watanabe and Ueno *et al*. demonstrated that a rhodium ion was immobilized on the internal surface of a ferritin via the dative anchoring to yield an artificial biocatalyst for phenylacetylene polymerization, and they exploited the ferritin cavity to control the molecular weight distribution of resulting polymers (M_w/M_n = 2.6), compared with that of the rhodium complex without the ferritin (M_w/M_n = 21).[9] Inspired by this work, the author has prepared an artificial biocatalyst for stereoselective phenylacetylene polymerization based on the precise reengineering of an artificial biocatalyst, as described in chapters 2 and 3 of this thesis. In different effort, Okuda and Schwaneberg *et al*. reported ring-opening metathesis polymerization using a Grubbs catalyst covalently linked FhuA, although the stereoselectivity was moderate activity and selectivity (conv. 37 %, *cis*/*trans* = 56/44).[17]

(e) In the other remarkable reactions, hydroformylation (C–C bond formation), olefin metathesis, hydroxylation of ethyl benzene, benzannulation have been reported during past a decade. Marchetti *et al*. reported first example of an rhodium ion datively-loaded HSA for the regioselective hydroformylation of styrene to provide the formyl-branched product (branched : linear = 9 : 1).[30] Kazlauskas *et al*. also demonstrated regioselective hydroformylation to yield the formyl-linear product (branched : linear = 1 : 8.4) using an artificial biocatalyst containing a rhodium ion within a carbonic anhydrase.[8] These two previous works clearly show that the selection of a protein matrix is crucial. Three groups were reported about a Grubbs catalyst-loaded protein for olefin metathesis almost at the same time. Hilvert *et al*. demonstrated olefin metathesis reaction using an artificial biocatalyst, which has a Grubbs catalyst on the surface of a heat shock protein via the cysteine-maleimide coupling.[16b] Matsuo *et al*. prepared an artificial biocatalyst for olefin metathesis using the inhibitor system to covalently anchor a Grubbs catalyst within a chymotrypsin.[16a] Furthermore, Ward *et al*. also reported an artificial biocatalyst containing a biotinylated Grubbs catalyst within an avidin via the supramolecular interaction to carry out olefin

metathesis.[4]   However, these biocatalysts had moderate activities in olefin metathesis.   In the hydroxylation of alkane species, Hayashi *et al*. reported that the insertion of a Mn porphycene into an apomyoglobin provides an artificial biocatalyst for the activation of a $C(sp^3)$-H bond in ethyl benzene.[6] In the other elegant work, Ward *et al*. reported the enantio- and regio- selective benzannulation reaction using Rh(III)Cp* complex-loaded avidin mutants via dual anchoring combining of the supramolecular and dative anchoring.[5]   This reaction was not achieved yet in the organometallic catalyst at the moment.

References

[1]   M. E. Wilson, G. M. Whitesides, *J. Am. Chem. Soc.* **1978**, *100*, 306–307.

[2]   T. R. Ward, *Acc. Chem. Res.* **2011**, *44*, 47–57.

[3]   T. R. Ward, A. Pordea, D. Mathis, *J. Organomet. Chem.* **2009**, *694*, 930–936.

[4]   C. Lo, M. R. Ringenberg, D. Gnandt, Y. Wilson, T. R. Ward, *Chem. Commun.* **2011**, *47*, 12065–12067.

[5]   T. K. Hyster, L. Knörr, T. R. Ward, T. Rovis, *Science* **2012**, *338*, 500–503.

[6]   K. Oohora, Y. Kihira, E. Mizohata, T. Inoue, T. Hayashi, *J. Am. Chem. Soc.* **2013**, *135*, 17282–17285.

[7]   K. Yamamura, E. T. Kaiser, *J. Chem. Soc., Chem. Commun.* **1976**, 830–831.

[8]   a) Q. Jing, K. Okrasa, R. J. Kazlauskas, *Chem. Eur. J.* **2009**, *15*, 1370–1376; b) Q. Jing, R. J. Kazlauskas, *ChemCatChem* **2010**, *2*, 953–957.

[9]   S. Abe, K. Hirata, T. Ueno, K. Morino, N. Shimizu, M. Yamamoto, M. Takata, E. Yashima, Y. Watanabe, *J. Am. Chem. Soc.* **2009**, *131*, 6958–6960.

[10] H. L. Levine, E. T. Kaiser, *J. Am. Chem. Soc.* **1978**, *100*, 7670–7677.

[11] L. Panella, J. Broos, J. Jin, M. W. Fraaije, D. B. Janssen, M. Jeronimus-Stratingh, B. L. Feringa, A. J. Minnaard, J. G. de Vries, *Chem. Commun.* **2005**, *0*, 5656–5658.

[12] a) P. J. Deuss, G. Popa, A. M. Z. Slawin, W. Laan, P. C. J. Kamer, *ChemCatChem* **2013**, *5*, 1184–1191; b) J. Bos, F. Fusetti, A. J. M. Driessen, G. Roelfes, *Angew. Chem. Int. Ed.* **2012**, *51*, 7472–7475; c) B. Talbi, P. Haquette, A. Martel, F. de Montigny, C. Fosse, S. Cordier, T. Roisnel, G. Jaouen, M. Salmain, *Dalton Trans.* **2010**, *39*, 5605–5607.

[13] M. T. Reetz, M. Rentzsch, A. Pletsch, M. Maywald, *Chimia* **2002**, *56*, 721–723.

[14] a) J. R. Carey, S. K. Ma, T. D. Pfister, D. K. Garner, H. K. Kim, J. A. Abramite, Z. Wang, Z. Guo, Y. Lu, *J. Am. Chem. Soc.* **2004**, *126*, 10812–10813; b) J. L. Zhang, D. K. Garner, L. Liang, Q. Chen, Y. Lu, *Chem. Commun.* **2008**, 1665–1667.

[15] J. Bos, A. García-Herraiz, G. Roelfes, *Chem. Sci.* **2013**, *4*, 3578–3582.

[16] a) T. Matsuo, C. Imai, T. Yoshida, T. Saito, T. Hayashi, S. Hirota, *Chem. Commun.* **2012**, *48*,

1662–1664; b) C. Mayer, D. G. Gillingham, T. R. Ward, D. Hilvert, *Chem. Commun.* **2011**, *47*, 12068–12070.

[17] F. Philippart, M. Arlt, S. Gotzen, S.-J. Tenne, M. Bocola, H.-H. Chen, L. Zhu, U. Schwaneberg, J. Okuda, *Chem. Eur. J.* **2013**, 13865–13871.

[18] C. C. Lin, C. W. Lin, A. S. C. Chan, *Tetrahedron: Asymmetry* **1999**, *10*, 1887–1893.

[19] M. T. Reetz, J. J.-P. Peyralans, A. Maichele, Y. Fu, M. Maywald, *Chem. Commun.* **2006**, 4318–4320.

[20] M. Creus, T. R. Ward, *Org. Biomol. Chem.* **2007**, *5*, 1835–1844.

[21] a) F. W. Monnard, E. S. Nogueira, T. Heinisch, T. Schirmer, T. R. Ward, *Chem. Sci.* **2013**, *4*, 3269–3274; b) J. M. Zimbron, T. Heinisch, M. Schmid, D. Hamels, E. S. Nogueira, T. Schirmer, T. R. Ward, *J. Am. Chem. Soc.* **2013**, *135*, 5384–5388.

[22] a) T. R. Ward, C. Letondor, N. Humbert, *Proc. Natl. Acad. Sci. U.S.A.* **2005**, *102*, 4683-4687; b) C. Letondor, A. Pordea, N. Humbert, A. Ivanova, S. Mazurek, M. Novic, T. R. Ward, *J. Am. Chem. Soc.* **2006**, *128*, 8320–8328.

[23] M. T. Reetz, N. Jiao, *Angew. Chem. Int. Ed.* **2006**, *45*, 2416–2419.

[24] J. Podtetenieff, A. Taglieber, E. Bill, E. J. Reijerse, M. T. Reetz, *Angew. Chem. Int. Ed.* **2010**, *49*, 5151–5155.

[25] a) H. Sato, T. Hayashi, T. Ando, Y. Hisaeda, T. Ueno, Y. Watanabe, *J. Am. Chem. Soc.* **2004**, *126*, 436–437; b) T. Matsuo, K. Fukumoto, T. Watanabe, T. Hayashi, *Chem. Asian. J.* **2011**, *6*, 2491–2499.

[26] F. van de Velde, L. Konemann, F. van Rantwijk, R. A. Sheldon, *Chem. Commun.* **1998**, 1891–1892.

[27] a) T. Ueno, T. Koshiyama, S. Abe, N. Yokoi, M. Ohashi, H. Nakajima, Y. Watanabe, *J. Organomet. Chem.* **2007**, *692*, 142–147; b) T. Ueno, T. Koshiyama, M. Ohashi, K. Kondo, M. Kono, A. Suzuki, T. Yamane, Y. Watanabe, *J. Am. Chem. Soc.* **2005**, *127*, 6556–6562.

[28] A. Mahammed, Z. Gross, *J. Am. Chem. Soc.* **2005**, *127*, 2883–2887.

[29] a) K. Okrasa, R. J. Kazlauskas, *Chem. Eur. J.* **2006**, *12*, 1587–1596; b) A. Fernández-Gacio, A. Codina, J. Fastrez, O. Riant, P. Soumillion, *ChemBioChem* **2006**, *7*, 1013–1016.

[30] M. Marchetti, G. Mangano, S. Paganelli, C. Botteghi, *Tetrahedron Lett.* **2000**, *41*, 3717–3720.

[31] M. Allard, C. Dupont, V. M. Robles, N. Doucet, A. Lledos, J. D. Marechal, A. Urvoas, J. P. Mahy, R. Ricoux, *ChemBioChem* **2012**, *13*, 240–251.

[32] Q. Jing, K. Okrasa, R. J. Kazlauskas, *Chem. Eur. J.* **2009**, *15*, 1370–1376.

Outline of This Thesis

The author constructed an artificial biocatalyst with the high catalytic activity beyond the natural metalloenzyme (chapter 1) and the non-natural reactivity and selectivity (chapters 2 and 3).

Chapter 1 (*Precise Design of an Artificial Heme Cofactor to Enhance Peroxidase Activity of an Engineered Myoglobin*)

In this chapter, a H64D myoglobin mutant was reconstituted with two different types of synthetic heme cofactors that have aromatic rings and a carboxylate-based cluster attached to the terminus of one or both of the heme-propionate moieties, thereby forming a "single-winged heme" and "double-winged heme," respectively. The reconstituted mutant myoglobins have smaller K_m values with respect to guaiacol oxidation activity relative to the parent mutant with a native heme. This suggests that the attached moiety functions as a substrate-binding domain. However, the k_{cat} value of the mutant myoglobin with the double-winged heme is much lower than that of the mutant with the native heme. In contrast, the mutant reconstituted with the single-winged heme has a larger k_{cat} value, thereby resulting in overall catalytic activity essentially equivalent to that of the native horseradish peroxidase. Enhanced peroxidase activity was also observed for the mutant myoglobin with the single-winged heme, thus indicating that the introduction of an artificial substrate-binding domain at only one of the heme propionates in the H64D mutant is the optimal engineering strategy for dramatically improving the peroxidase activity of myoglobin.

Chapter 2 (*A Rhodium Complex-linked Nitrobindin as an Artificial Biocatalyst for Phenylacetylene Polymerization*)

In this chapter, the author prepared a rhodium complex with a maleimide moiety at the peripheral position of the Cp (cyclopentadienyl) ligand for an active center in an artificial biocatalyst. The rhodium complex was then inserted into a β-barrel protein scaffold of an aponitrobindin mutant NB(Q96C) via a covalent cysteine-maleimide coupling to yield an artificial biocatalyst. The biocatalyst is found to carry out the phenylacetylene polymerization, and produces 50 % *trans*-selective poly(phenylacetylene) (PPA), although the rhodium complex without the protein scaffold produces *cis* PPA.

Chapter 3

(*Reengineering of a Rhodium Complex-linked Nitrobindin to Increase trans-selectivity for Phenylacetylene Polymerization*)

In this chapter, the appropriate structural optimization of the protein cavity by computationally guided-mutagenesis is found to enhance the stereoselectivity of the polymer with the *trans* content of 82% at 25 °C in pH 8.0. The X-ray crystal structure of one of the reengineered artificial biocatalysts at a resolution of 2.0 Å reveals that the rhodium complex is located in the β-barrel cavity without any perturbation of the whole protein structure. The crystal structure and molecular modeling support the fact that the stereoselectivity is enhanced by effective control of monomer access to the rhodium complex within the limited space of the protein cavity.

Chapter 1

Precise Design of an Artificial Heme Cofactor
to Enhance Peroxidase Activity of an Engineered Myoglobin

1-1. Introduction

To create an artificial enzyme with high catalytic activity, we should consider the elementary processes of enzymatic reactions: substrate-binding and the chemical catalytic process. These processes are apparently qualified by K_m and k_{cat} in Michaelis-Menten kinetics, respectively. Having a solid understanding of the general concepts of supramolecular chemistry is needed to improve a substrate-binding process (decrease in K_m value).[1, 2] Enhancement of catalytic steps (increase in k_{cat} value) is related to regulation of reactive intermediates (their rates of formation, lifetimes and intrinsic reactivities). Controlling both substrate-binding and chemical processes will be required for effective molecular design of an artificial enzyme that exhibits high catalytic activity equivalent or superior to that of naturally occurring enzymes.

Myoglobin (Mb), an oxygen-storage hemoprotein, is an easily obtainable protein which is suitable for use as a scaffold to engineer the native functions by genetic and/or chemical modifications.[3] The native Mb contains native heme at the active site (Figure 1-1). This prosthetic group is responsible for the reversible binding of dioxygen.[4] Although the heme of Mb is the same as that of horseradish peroxidase (HRP), the catalytic oxidation activity of Mb is much lower than that of HRP. This is because Mb lacks a specific binding site for substrates and a general acid-base catalytic system to smoothly generate the oxoferryl species, a key intermediate in the catalytic oxidation cycle. Possible strategies for introducing these factors into Mb are (i) genetic mutations to provide an HRP-like environment at the heme distal site, (ii) attachment of an artificial substrate binding domain at the termini of the heme propionates and (iii) replacement of the native heme with a more reactive heme analog. The first approach is attained by the H64D mutant, where the introduced Asp residue works as a general acid-base unit to activate H_2O_2.[5] In the second strategy, a variety of designed substrate-binding domains have been suggested, including boronic acid,[6] aromatic rings,[7] peptides,[8] and DNA,[9] among others. The third method involves the insertion of an iron complex of porphycene[10] or corrole[11] into the heme pocket of Mb.
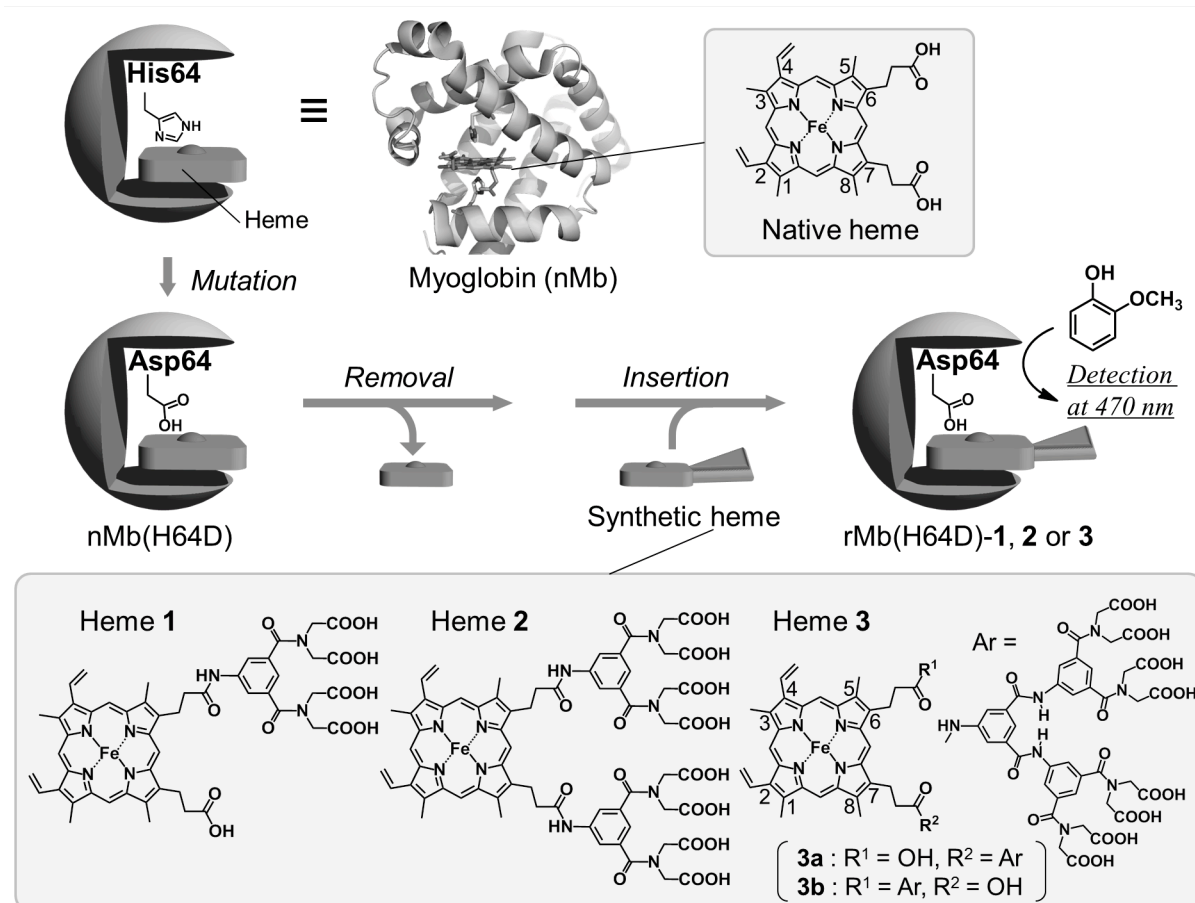
Figure 1-1. Schematic representation.

Parallel to the above-mentioned approaches, the combination of these strategies is also promising to enhance peroxidase activity of Mb. In our previous paper,[12] the author described a reconstituted Mb(H64D) with a "double-winged heme" **2**, rMb(H64D)-**2** (wherein the notation "Mb(H64D)-**X**" indicates Mb(H64D) with heme **X**) (Figure 1-1). This is designated "hybrid Mb". The aromatic moiety introduced at both of the heme propionates was found to function as an effective binding site for hydrophobic substrates such as 2-methoxyphenol (Guaiacol). This leads to a reduction of the K_m value, indicating that binding is more effective. As described above, the introduction of an effective H_2O_2 activation system by genetic mutation and the attachment of a substrate-binding domain by synthetic chemical strategy are indeed useful to the remarkably enhance overall peroxidase activity of the native Mb. It was disclosed, however, that the k_{cat} values unexpectedly decreased by replacement of the native heme with **2** when these values for the two rMb(H64D)s, Mb(H64D)-**1** and Mb(H64D)-**2**, were compared. This finding suggests that modification of the heme propionates often causes negative effects on the chemical processes in the catalytic cycle. Our independent investigations have also indicated that the interactions between the heme propionates and nearby amino acid residues in some hemoproteins are related with the reactivity of the heme iron as well as the thermostability of

11

the proteins.[13]   The next approach to enhance the peroxidase activity of Mb is to improve the overall catalytic activity without negative effects in chemical processes.   In this chapter, the author describes a systematic investigation of the results of heme modification with a "single-winged heme" **3** which was developed for Mb reconstitution in order to obtain key insights with respect to the creation of artificial enzymes optimized for both substrate binding and chemical processes.

1-2. Results and Discussion

Reconstitution of the H64D Myoglobin Mutant with the Single-winged Heme and NMR Study of Heme Orientation

Single-winged heme **3** was prepared by partial condensation of protoporphyrin IX with aniline derivatives, followed by iron insertion and alkaline hydrolysis (See experimental section).   Because the condensation at the propionate side chain occurs non-selectively, the 1:1 mixture of regioisomers **3a** and **3b** was obtained.   It is difficult to separate them (Figure 1-10).   Sperm whale Mb(H64D) expressed by *E. coli* was reconstituted with single-winged heme **3** to obtain Mb(H64D)-**3**, after removal of the native heme. The UV-vis spectrum of Mb(H64D)-**3** shows bands at the same wavelengths as those for nMb(H64D), indicating that heme **3** occupies the same space in the heme pocket as the native heme (Figure 1-7).   This includes coordination of the His93 imidazole to the heme iron.   Although the two regioisomers were inserted into the apoprotein together, the NMR study for the prepared Mbs suggests that each isomer is accommodated so that the unmodified propionate preferentially interacts with Arg45 (*vide infra*).

Mb(H64D)-**3** may theoretically contain four possible configurations, because a mixture of the two regioisomers, **3a** and **3b**, was employed for reconstitution of the H64D mutant and each regioisomer has two possible orientations within the heme pocket (normal and reversed orientations) as a result of a 180° rotation of the heme about the heme α–γ *meso*-axis ("Normal orientation" is a fashion of the major heme orientation, where 6-propionate forms a hydrogen bonding with Arg45, Figure 1-6).   One useful method to elucidate the heme orientations in the heme pocket of Mb is the ^{1}H NMR measurement for cyanomet Mb, because the paramagnetic shift of the methyl protons on the periphery of the heme framework is affected by orientation of proximal His93 and is useful information of the heme orientation in the myoglobin matrix.[14]   This methodology is applicable for mutant Mbs.[14c]

Figure 1-2 shows the ^{1}H NMR spectra of the cyanomet wild-type and Mb(H64D)s obtained in D$_2$O. The assignments of the selected heme methyl peaks were made based on the knowledge obtained in the previous reports.[14]   The numbering of the heme framework is indicated in Figure 1-1.   The assignment indicated in Figure 1-2c was conducted with reference to the previous data obtained in the NMR measurements before the heme orientation reached to equilibrium.[14]   The pattern of the singlet peaks for 5-, 1-, and 8-methyl protons for cyanomet nMb(H64D) in Figure 1-2b is similar to that observed for

wild-type Mb in Figure 1-2a. This suggests that native heme in the protein interior of nMb(H64D) also adopts the normal orientation observed for wild-type Mb.[15] Especially, the chemical shift of 5-methyl proton is affected by the existence of the hydrogen bonding between 6-propionate and Arg45 located in the entrance of the heme pocket: La Mar *et al.* reported that cyanomet Mb reconstituted with 6-methyl-6-despropionate hemin, where a hydrogen bond between 6-propionate and Arg45 is lacking, has a downfield-shifted peak of the 5-methyl protons at 28 ppm.[14, 16] The observation of the 5-methyl proton peak at the same chemical shift (26.8 ppm) supports the fact that the hydrogen bonding between 6-propionate and Arg45 in nMb(H64D) is conserved.
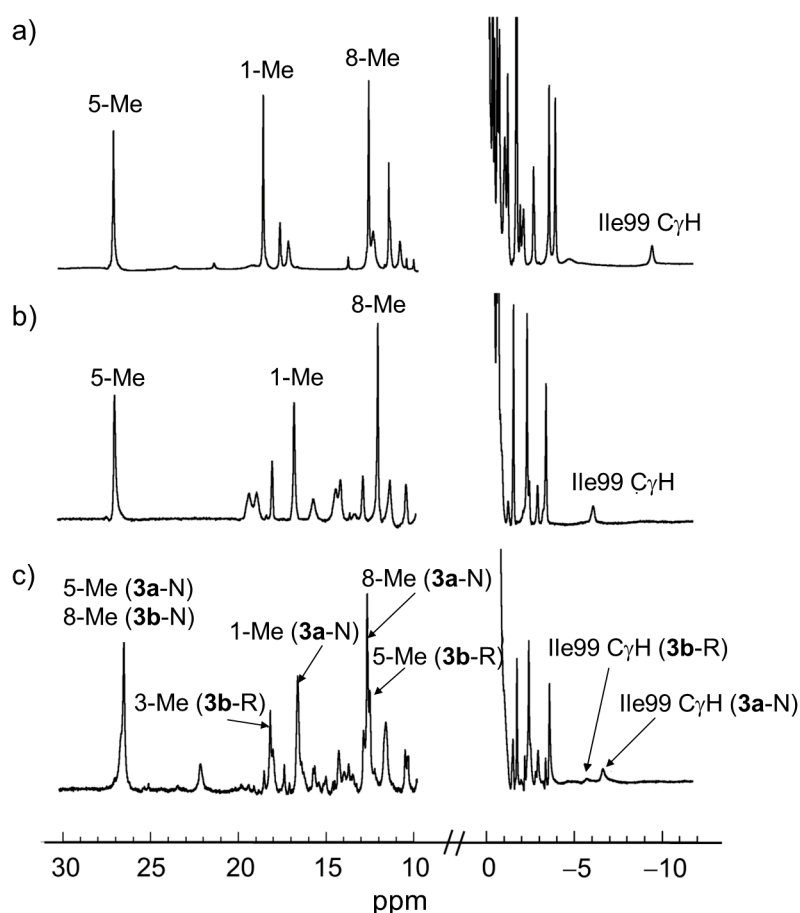
Figure 1-2. ^{1}H NMR spectra of cyanomet Mbs: (a) nMb, (b) nMb(H64D) and (c) rMb(H64D)-**3** in KPi D$_2$O buffer (10 mM, pD = 7.4) at 25 $^\circ$C. The numbering of the heme framework is indicated in Scheme 1. The designations **3a**-N and **3b**-R indicate Mb(H64D) reconstituted with heme **3a** in the normal orientation and **3b** in the reversed orientation, respectively.

In contrast, it is expected that cyanomet rMb(H64D)-**3** shows a complicated peak pattern on the ^{1}H NMR spectrum because of the possibility to take several heme configurations. However, as shown in figure 1-2c, the characteristic heme methyl peaks are relatively simple. In particular, only one signal appeared at 26.5 ppm. The chemical shift is very similar to that observed for nMb(H64D). When the

H64D mutant was reconstituted with 6-methyl-6-despropionate heme, the 5-methyl proton peak appeared at 28 ppm in the same manner as the wild-type Mb reconstituted with this propionate-truncated heme (Figure 1-8), although no peak was observed around 28 ppm in figure 1-2c.   This result indicates that the hydrogen bonding between a propionate side chain and Arg45 is conserved also in rMb(H64D)-**3**. Therefore, the mechanism to account for this spectrum is that heme **3** in the heme pocket should take an orientation allowing interaction between the propionate and Arg45: Isomer **3b** takes the reversed heme orientation to attain the hydrogen bonding with Arg45 (Figure 1-9).[17]   In the reversed orientation, the 8-methyl group should be located in the position where the 5-methyl group in the normal heme orientation occupies, resulting in the similar chemical shift (26.5 ppm for the 5-mehtyl proton in the normal orientation of **3a** and 8-mehtyl proton in the reversed orientation of **3b**) and vice versa.   The rather broad peak at 26.5 ppm also supports the existence of the two conformations.[18]   In contrast, the chemical shifts of the 1-methyl and 3-methyl protons are significantly affected by the accommodated position in the heme pocket, because the positions of these methyl groups are not symmetrical about the heme α–γ *meso*-axis. These findings suggest that the hydrogen bonding at Arg45 is essential for the stability of a reconstituted Mb with the propionate-modified heme[19] and that the hydrogen bonding a between a heme propionate and Arg45 might indeed contribute to the regulation of the heme iron reactivity (*vide infra*).

Steady-state Kinetics for 2-Methoxyphenol Oxidation

For evaluation of the peroxidase activities of Mb(H64D)s, the oxidation of 2-methoxyphenol (also known as guaiacol) was investigated (Scheme 1-1).[20]

Figure 1-3 shows the time-courses of the absorbance changes at 470 nm during 2-methoxyphenol oxidation catalyzed by the rMb(H64D)s in the presence of excess H_2O_2.   The protein showing the most effective catalytic activity is rMb(H64D)-**3**.   Table 1-1 lists the Michaelis-Menten parameters of 2-methoxyphenol oxidation.[21]   In order to compare the effects of heme structures on the catalytic activity, the previously reported kinetic parameters for apo Mb(H64D) with native heme and with double-winged heme **2** are also described.[12]   For the purpose of discussing the effect of the propionate modification on the catalytic activities (*vide infra*), the kinetic parameters for Mb(H64D)-**1**, in which the four-carboxylate moiety is attached at one heme-propionate (Figure 1-1), are also included.
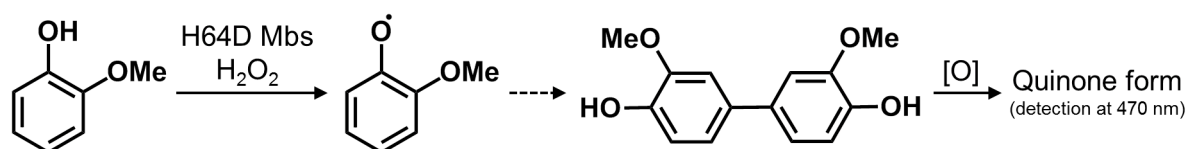
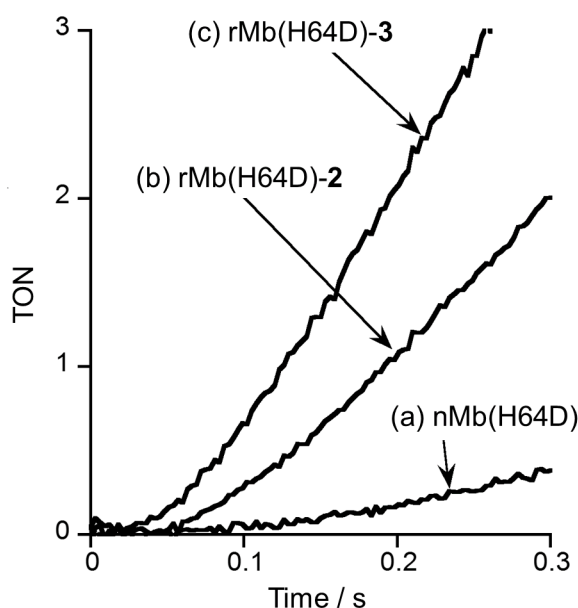**Scheme 1-1.** 2-Methoxyphenol oxidation mediated by rMb(H64D)s.

14

Figure 1-3. Time-courses of 2-methoxyphenol oxidations catalyzed by (a) nMb(H64D), (b) rMb(H64D)-**2** and (c) rMb(H64D)-**3** in sodium malonate buffer (20 mM, pH 6.0) at 25 °C; [Mb(H64D)] = 2.0 μM, [2-methoxyphenol]$_0$ = 0.5 mM, [H$_2$O$_2$]$_0$ = 15 mM.   TON = turnover number.

Table 1-1. Kinetic parameters for 2-methoxyphenol oxidations catalyzed by Mb(H64D) mutants.[a]

Artificial biocatalyst	k_{cat} (s^{-1})	K_m (mM)	k_{cat}/K_m (M^{-1}s^{-1})
nMb(H64D)	9.0 ± 1.2[b]	1.8 ± 0.4[b]	5,100[b]
rMb(H64D)-**1**	13 ± 1	0.63 ± 0.08	21,000
rMb(H64D)-**2**	1.2 ± 0.1[b]	0.052 ± 0.016[b]	23,000[b]
rMb(H64D)-**3**	24 ± 2	0.29 ± 0.06	85,000

[a] Sodium malonate buffer (20 mM, pH 6.0) at 25 °C, [Mb] = 4.0 μM, [H$_2$O$_2$]$_0$ = 100 mM.   [b] Ref. [12].

According to the previous report,[12] the kinetic parameter for the wild-type Mb was found to be k_{cat}/K_m = 52 M^{-1}s^{-1}.   When His64 in the wild-type protein was converted into Asp, the obtained nMb(H64D) showed the *ca*. 100-fold catalytic activity (k_{cat}/K_m = 5100 M^{-1}s^{-1}) as also reported in Watanabe and co-workers.[5]   When the further engineering of H64D mutant was conducted by the replacement of the native heme heme with a synthetic heme **2** or **3**, the overall catalytic activities of the hybrid proteins, rMb(H64D)-**2** and rMb(H64D)-**3**, were remarkably enhanced.   The main factor of the enhancement in the catalytic activity is the decrease in K_m values.   This is because the introduced aromatic moieties at the termini of the propionate side chains function to facilitate the access of the hydrophobic substrate to the vicinity of the reaction site.

On the other hand, the k_{cat} value for rMb(H64D)-**2** significantly decreased from nMb(H64D), which is a negative effect from the aspects of the enhancement of the peroxidase activity in Mb.   The

15

decrease in k_{cat} observed for rMb(H64D)-**2** implies that the modification of *both* propionates causes a decrease in the reactivities of the oxoferryl species, a reactive intermediate responsible for a substrate oxidation (See below for the investigation of the reaction intermediates).   In contrast, the k_{cat} value of rMb(H64D)-**3** is rather improved from nMb(H64D).   This tendency is also observed in rMb(H64D)-**1**, in which one heme propionate is unmodified as in **3** (Table 1-1).   The result provides useful insights into the design of an ideal synthetic heme: *retaining one unmodified propionate is essential to prevent the k_{cat} value from decreasing along with enhancement of the substrate binding process.* Consequently, rMb(H64D)-**3** has an extraordinary enhancement of the overall catalytic activity (k_{cat}/K_m = 85,000 $M^{-1}s^{-1}$).   The catalytic activity of this engineered Mb is, interestingly, almost equivalent to that of a naturally occurring peroxidase under the same reaction conditions (For HRP, k_{cat}/K_m = 72,000 $M^{-1}s^{-1}$ at pH = 6.0, 25 °C, [H_2O_2] = 1.0 mM).[21, 22]   This result indicates that the combination of a point mutation and precise design of an appropriate chemically-modified heme have enabled us to construct an "ultra-native" biocatalyst.

2-Methoxyphenol Binding

In order to directly evaluate the effects of the attached moiety on the substrate affinity, the binding of 2-methoxyphenol to the engineered Mb(H64D)s was observed by a UV-vis spectral titration in the absence of H_2O_2.   The calculated dissociation constants (K_{d1} and K_{d2}) are summarized in Table 1-2.   The spectral changes for the Mb(H64D)s are shown in Figures 1-4.

   For nMb(H64D), the absorbance of the Soret band slightly increases upon addition of 2-methoxyphenol, which could be caused by small conformational changes in the protein due to the access of the substrate to the vicinity of the heme-propionates.   In contrast, Mb(H64D)s reconstituted with the synthetic hemes **2** or **3** exhibit quite different spectral changes (Figure 1-4).   The variances of those changes are much larger in the latter two Mb(H64D)s, indicating that significant perturbations of the π-conjugation system of hemes **2** and **3** are induced during the access of the organic substrate to the heme pocket of these proteins.[23]   Moreover, for nMb(H64D), the absorbance changes can be analyzed as a single substrate-binding model, whereas the decay of the Soret band for Mb(H64D)-**2** or Mb(H64D)-**3** observed during the titrimetric measurements requires two-phase analysis.   With respect to the two dissociation constants obtained for 2-methoxyphenol (K_{d1} and K_{d2}), the lower K_{d1} values for the Mb(H64D)s with modified heme **2** or **3** are attributed to the attached hydrophobic aromatic moieties.   These lower K_{d1} values are in agreement with the low K_m values (Table 1-2).
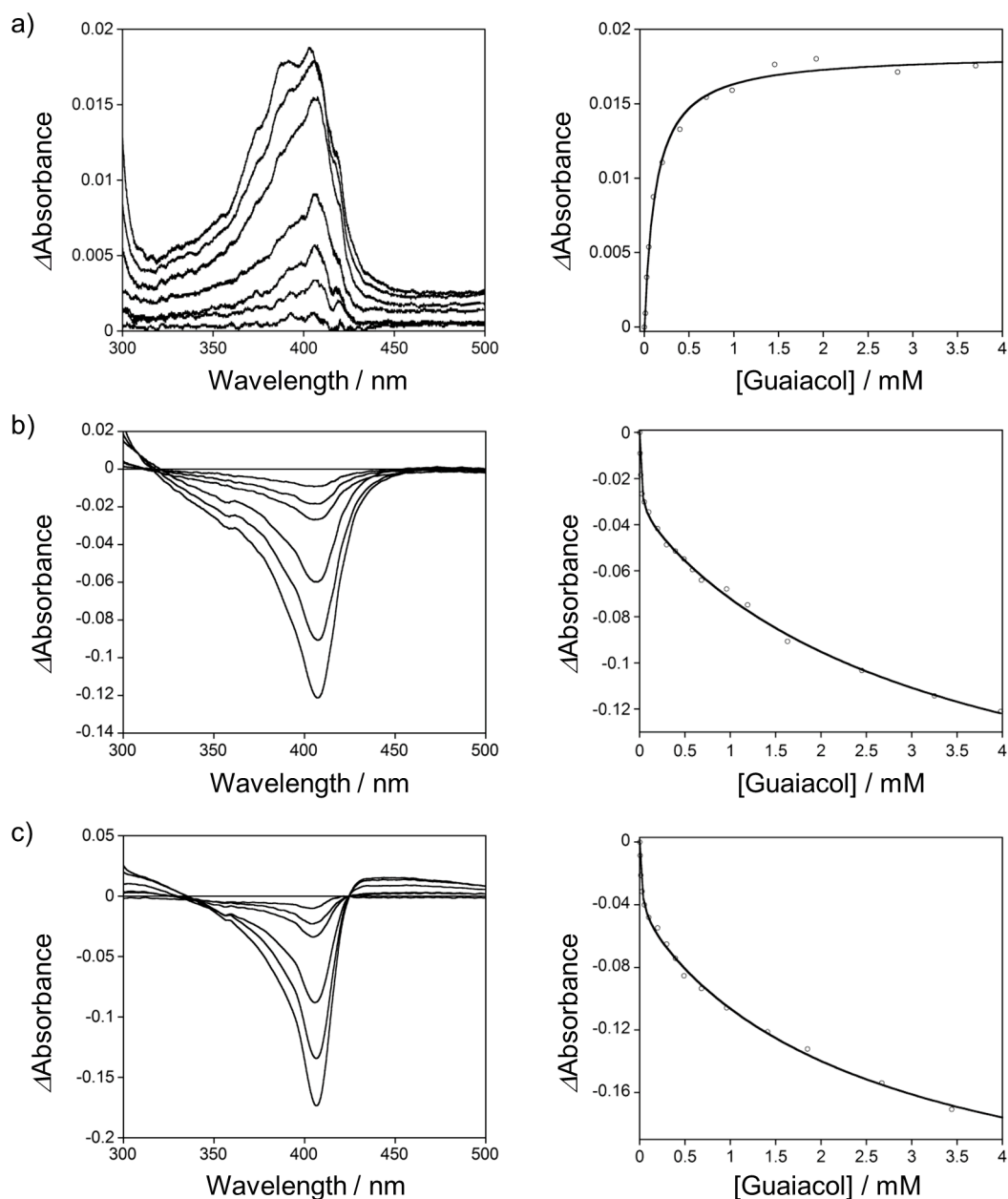
Figure 1-4. UV/Vis spectral changes (left) and dependency of the absorbance at 408 nm (right) in the binding of 2-methoxyphenol to (a) nMb(H64D), (b) rMb(H64D)-**2** and (c) rMb(H64D)-**3** in sodium malonate buffer (20 mM, pH 6.0) at 25 °C.　　Error bars are drawn based on an estimation of 10% error.

**Table 1-2.** Dissociation constants for 2-methoxyphenol binding to Mb(H64D) mutants.[a]

Artificial biocatalyst	K_{d1} (mM)	K_{d2} (mM)
nMb(H64D)	0.13 ± 0.01	N.D.[b]
rMb(H64D)-**2**	0.019 ± 0.002	2.6 ± 0.3
rMb(H64D)-**3**	0.014 ± 0.002	3.3 ± 0.3

[a] 20 mM sodium malonate buffer (pH 6.0) at 25 °C, [Mb] = 8.0 μM, [2-methoxyphenol] = 0–4 mM.　　[b] Not determined due to single-phase dependency.

17

Kinetic Analysis for Catalytic Cycle

Next, to evaluate the reactivities of the oxoferryl intermediates, (Compounds I and II), the author determined the two rate constants, k_1 and k_2 (defined in Scheme 1-2). The generation of Compound I (oxoferryl species with a porphyrin π-cation radical) was attained by the reaction of the reconstituted ferric Mb(H64D)s with a slight excess of *m*-chloroperbenzoic acid (*m*CPBA). The rate constants determined in the kinetic study are summarized in Table 1-3, and the representative kinetic trace is shown in Figure 1-5.

The Mb(H64D) with the double-winged heme, Mb(H64D)-**2**, has the smallest k_1 value, indicating that the modification of both heme-propionates lowers the reactivity of the Compound I intermediate. This finding may partially account for the drop in the k_{cat} value for the reaction catalyzed by this protein. However, the k_2 value, which indicates the reactivity of Compound II, is approximately 3-fold greater than that of the other two proteins. Therefore, it is difficult to simply rationalize the catalytic activities of Mb(H64D)-**2** on the basis of the magnitudes of the k_1 and k_2 values. Another possible factor affecting the catalytic activities of the Mb(H64D)s will be discussed in the next section.
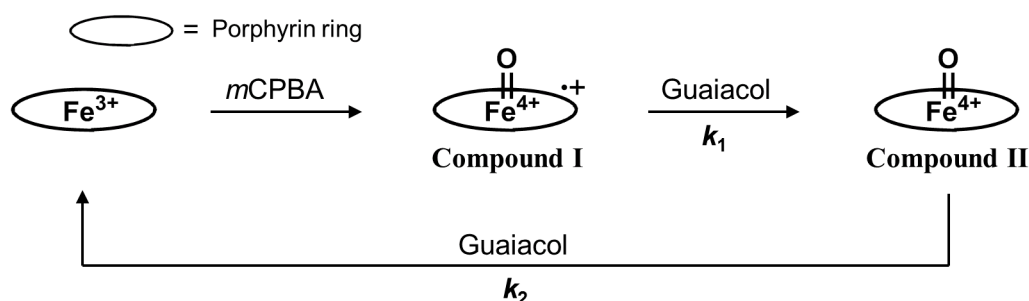
Scheme 1-2. Reaction scheme for the kinetic analysis of the catalytic cycle of the 2-methoxyphenol oxidation mediated by Mb(H64D) mutants.

Table 1-3. Rate constants for elemental processes in 2-methoxyphenol oxidation catalyzed by Mb(H64D) mutants.[a, b]

Artificial biocatalyst	k_1 (M^{-1}s^{-1})[c]	k_2 (M^{-1}s^{-1})[d]
nMb(H64D)	1.1×10^6	1.3×10^4
rMb(H64D)-**2**	0.32×10^6	3.5×10^4
rMb(H64D)-**3**	3.6×10^6	1.2×10^4

[a] Sodium malonate buffer (20 mM, pH 6.0) at 15 $^{\circ}$C, [Mb] = 2.0 μM, [2-methoxyphenol]$_0$ = 10–100 mM. [b] Experimental errors are within 10%. [c] Reduction rate of Compound I. [d] Reduction rate of Compound II.
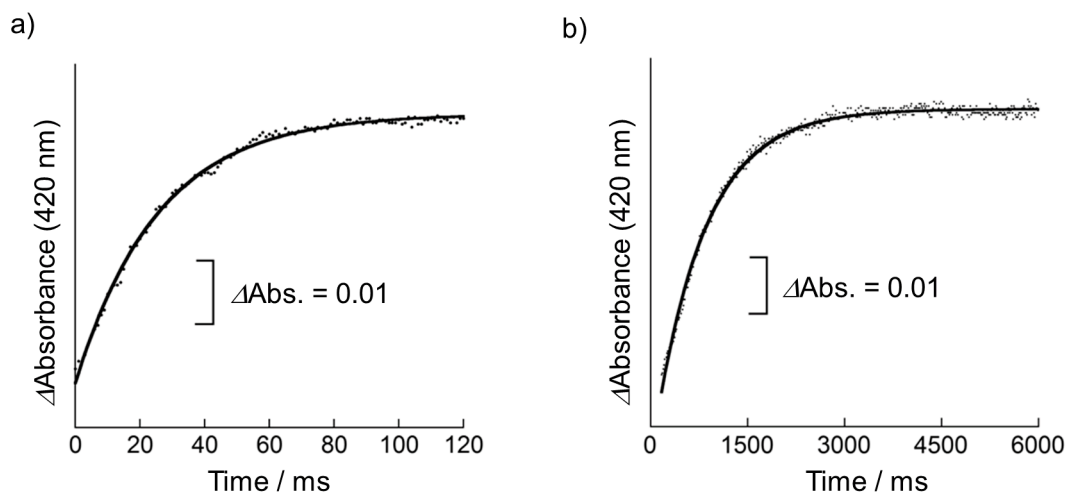
Figure 1-5. Representative absorbance changes for determination of the rate constants k_1 and k_2 for Mb(H64D)-**3**; [Mb]$_0$ = 2 μM, [2-methoxyphenol]$_0$ = 10 mM, [mCPBA] = 1.3 equiv in sodium malonate buffer (20 mM, pH 6.0) at 15 °C.   (a) Initial stage within 120 ms for k_1-step.   (b) Later stage in 6 s for k_2-step.   The fitting assuming a single-phase kinetics is indicated by solid lines.

In the determination of the rate constants k_1 and k_2 for Mb(H64D)-**3**, the absorbance changes were clearly observed to follow single-phase kinetics.   There is a negligible difference in the reactivities of Compounds I and II between the proteins with the normal and reversed heme-orientations.   As indicated by the largest k_1 value in Mb(H64D)-**3**, the reactivity of Compound I is improved with respect to the other two proteins, which is coincide with the fact that this protein has the highest k_{cat} value among the Mbs investigated.   This suggests that there is a relationship between the heme propionate(s)-protein interactions and the reactivity of Compound I.   As indicated in the ^{1}H NMR study (*vide supra*), heme **3** is oriented in the heme pocket of Mb so that the hydrogen bonding interaction between the heme-propionate and Arg45 is retained at the distal site.   These findings suggest that the reactivity of Compound I can be enhanced by two factors: (i) the conservation of the 6-propionate–Arg45 interaction, and (ii) the removal of the interaction between the 7-propionate and the amino acid residues at the proximal site.[24]   The first factor contributes to the maintenance of the distal site structure and the second factor regulates the characteristics of coordination of His93 to the heme iron.   According to the resonance Raman measurements of ferric Mb reconstituted with 7-methyl-7-despropionate heme, where the hydrogen bonding interaction between the 7-propionate and Ser92 is disrupted, the Fe–His93 stretching mode is slightly stronger because there is no regulation of proximal ligand coordination by the hydrogen bonding network at the proximal site.[13a] The author expects that a similar mechanism is operating with respect to Mb(H64D)-**3**).[25]

Efficiency of Generation of the Compound I Intermediate

The catalytic activity of Mbs may also be controlled by the process of O–O bond cleavage after the formation of the hydroperoxo species (Fe(III)–OOH), because the Compound I intermediate, the highly reactive oxidizing species, is only produced by heterolytic cleavage of the O–O bond. In order to evaluate the efficiency of Compound I generation, an analysis of the reaction between ferric Mb and cumene hydroperoxide (CHPO) was examined.[5a] Table 1-4 summarizes the ratio of O–O bond heterolysis and homolysis, based on the product yields of cumyl alcohol and acetophenone, respectively (Scheme 1-3).

The total amounts of organic products obtained by rMb(H64D)-**2** and rMb(H64D)-**3** were increased, relative to the amounts of products obtained by nMb(H64D). This is because CHPO can easily bind to the artificial binding domain. However, the ratio in rMb(H64D)-**2** is relatively small, indicating that the efficiency of Compound I generation is lower than that of the other engineered proteins. Based on the data described in Tables 1-3 and 1-4, the modification of *both* propionates gives rise to negative effects with respect to generation of Compound I.
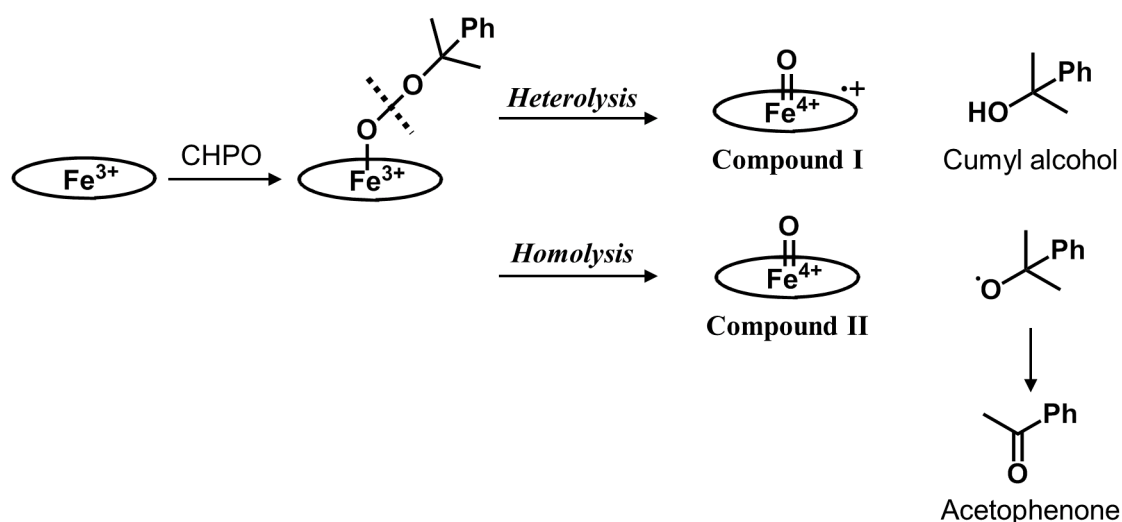
Scheme 1-3. Reaction of ferric Mb with cumene hydroperoxide (CHPO).

**Table 1-4.** Reaction of cumene hydroperoxide (CHPO) with the ferric Mb(H64D) mutants.[a]

Artificial biocatalyst	Total amounts of products (μM)[b]	Heterolysis/Homolysis[c]
nMb(H64D)	25	15
rMb(H64D)-**2**	146	7
rMb(H64D)-**3**	100	13

[a] Sodium malonate buffer (20 mM, pH 6.0), 15 $^{\circ}$C, [Mb] = 20 μM, [CHPO] = 200 μM. [b] Total amounts of acetophenone and cumyl alcohol as a product produced over 5 min. [c] Calculated from [cumyl alcohol]/[acetophenone].

20

Two-electron Oxidations Catalyzed by Mb(H64D) Reconstituted with Single-winged Heme 3

Next, the author observed the H_2O_2-dependent oxidation of thioanisole (oxygen-atom transfer) and ethylbenzene (hydroxylation) catalyzed by Mbs (Scheme 1-4).

As expected, rMb(H64D)-**3** also exhibits the highest catalytic activity toward the two-electron oxidations among the engineered Mbs (Table 1-5). In the case of oxygen transfer to thioanisole, a four-electron oxidation product, sulfone, was also observed for all of the reconstituted Mbs proteins examined. The protein with the highest peroxygenase activity yielding both sulfoxide and sulfone is rMb(H64D)-**3**. Interestingly, catalytic hydroxylation is also observed in rMb(H64D)-**3**, although such activity is very rare for most Mb mutants.[26] Catalysis of hydroxylation of a C–H bond by heme enzymes in nature has only been observed for *S*-coordinated hemoproteins such as cytochrome P450s and chloroperoxidase. Therefore, it is a remarkable finding that rMb(H64D)-**3**, whose heme iron is coordinated by a neutral imidazole, demonstrates hydroxylation activity. These results reflect the synergetic effects derived from the enhanced reactivity of Compound I (increased k_1) and efficient substrate-binding (decreased K_m).[25, 26, 27]
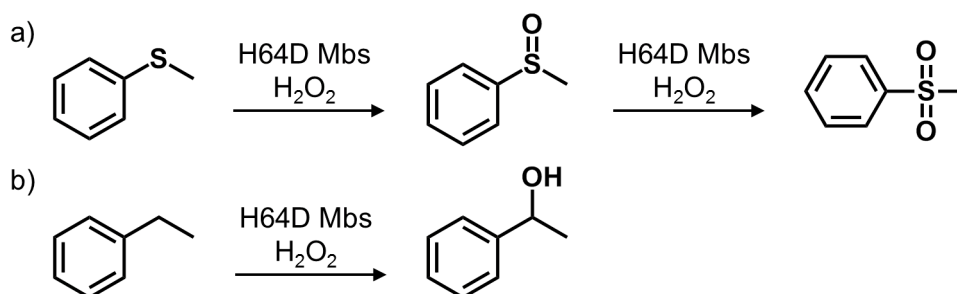
Scheme 1-4. (a) Thioanisole and (b) ethylbenzene oxidation catalyzed by Mb(H64D) mutants.

Table 1-5. Turnover numbers for thioanisole and ethylbenzene oxidation catalyzed by Mb(H64D) mutants.[a]

Artificial biocatalyst	Thioanisole oxidation[b]		Ethylbenzene oxidation[c]
	Sulfoxide (min^{-1})[d]	Sulfone (min^{-1})[e]	2-Phenylethanol (min^{-1})[f]
nMb(H64D)	25[g]	2.6[h]	N.D.[i]
rMb(H64D)-**2**	33[g]	2.0[h]	N.D.[i]
rMb(H64D)-**3**	49[g]	3.8[h]	0.3[j]

[a] KPi buffer (100 mM, pH 7.0) at 25 °C. [b] [Mb] = 2.0 μM, $[H_2O_2]_0$ = 1.0 mM, $[thioanisole]_0$ = 0.5 mM. [c] [Mb] = 20 μM, $[H_2O_2]_0$ = 1.0 mM, $[ethylbenzene]_0$ = 0.5 mM. [d] Product of oxygen transfer to thioanisole. [e] Product of oxygen transfer to methylphenyl sulfoxide. [f] Product of hydroxylation at the benzyl position (as racemic forms). [g] Calculated from the amount of the sulfoxide divided by [Mb]. The ratio of *R* and *S* isomers was not determined.[27] [h] Calculated from the amount of the sulfone divided by [Mb]. [i] Not determined because there was no observation. [j] Calculated from the amount of 2-phenylethanol produced divided by [Mb].

1-3. Summary

In this research, it was demonstrated that the incorporation of a single-winged heme into apoH64D Mb enhances the reactivities of the oxidizing intermediates as well as facilitating the binding of substrates. The replacement of His64 with Asp by genetic mutation contributes to the smooth H_2O_2 activation mediated by a general acid-base catalysis of the Asp residue (improvement of chemical processes). The introduction of the aromatic moiety at the termini of the heme propionate side chains is useful to create a substrate-binding domain (improvement of substrate-binding process). The kinetic analysis for each step of the catalytic cycle, however, suggests that retaining one unmodified propionate is important to control the reactivity of the Compounds I and II, leading to more effective improvement of the peroxidase activity in Mb. The significance of one unmodified propionate is the formation of hydrogen bonding between the heme propionate and Arg45 and the stabilization of the heme orientation in the heme pocket of Mb. Furthermore, precise design of a synthetic heme enables us to endow an appropriate myoglobin mutant with enhanced catalytic activity toward two-electron oxidation through oxo-transfer and C–H bond activation. The findings demonstrated in this paper will provide important insights into the methodologies required for engineering of chemically- and biologically-attractive biocatalysts.

1-4. Experimental Section

Instruments

^{1}H NMR spectra were measured using a Bruker DPX 400 spectrometer. The measurements of UV-vis spectra and the titrations of 2-methoxyphenol to monitor the binding of substrate to protein were carried out using a Shimadzu UV-3210 double beam spectrophotometer. Kinetic measurements were conducted using an RSP-1000 stopped-flow system constructed by Unisoku, Co., Ltd. (Osaka, Japan). The HPLC analyses were conducted using a Shimadzu HPLC LC-VP system. The GC/FID measurements were made using a Shimadzu GC-2014 gas chromatography system. The mass analyses (FAB-MS and ESI-MS) were conducted using a JEOL JMS-700 mass spectrometer.

Materials

All reagents and chemicals were obtained from commercial sources and were used as received unless otherwise noted. The H64D myoglobin mutant was expressed from *E. coli.* and purified by column chromatography through CM-52 (Whatman) and Sephadex G-25 (GE healthcare) columns.[5a] The preparation of compound **5**, compound **6** and heme **2** was described in the previous report.[7] Hemes **1** and **3** were synthesized as described in the Supporting Information. The reconstituted Mb(H64D)s were prepared as described in the previous report,[12] after the removal of the native heme by Teale's 2-butanone method.[28] The reconstituted Mbs were purified with a Sephadex G-25 column (2 × 50 cm, 100 mM KPi, pH 7.0, 4 ℃) and were found to be stable at −80 ℃ for at least one month as a frozen solution (*ca*. 1 mM).

Preparation of Artificial Heme 3
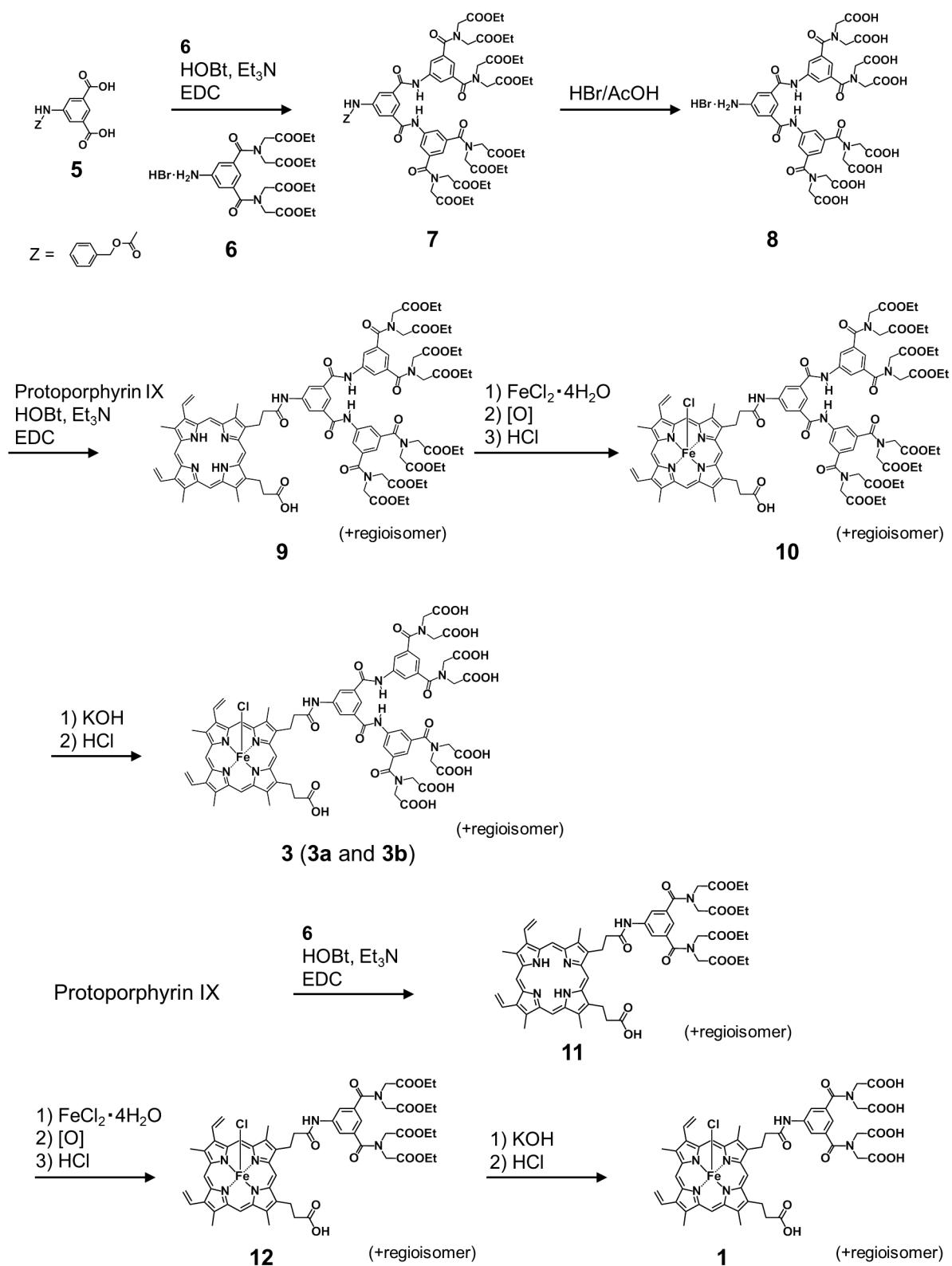
Scheme 1-5. Synthetic scheme of hemes **1** and **3**.

Compound 7. Compound **5** (350 mg, 1.1 mmol) was treated with SOCl$_2$ (10 mL) in the presence of aliquot DMF at 90 $^\circ$C for 3 h.   After cooling, the solution was concentrated under reduced pressure. The obtained residue was dissolved in dry CH$_2$Cl$_2$ (10 mL) under a N$_2$ atmosphere, and compound **6** (2.1 g, 3.4 mmol) and dry Et$_3$N (6 mL) were added.   The reaction mixture was stirred at room temperature for 24 h.   The solution was subsequently washed with 0.1 M HCl*aq.*, water and brine, and then the solvent was evaporated.   The residue was subjected to silica gel column chromatography (hexane/AcOEt = 1/9) to obtain yellowish solid **7** (1.0 g, 68% yield). ^{1}H NMR (400 MHz; CDCl$_3$, residual proton of the solvent) δ = 9.33 (2H, s), 8.30 (1H, s), 8.05 (2H, s), 7.94 (1H, s), 7.87 (4H, s), 7.36 (5H, m), 7.11 (2H, s), 5.21 (2H, s), 4.24–4.18 (32H, m), 1.25 (24H, m).

Compound 8. Compound **7** (1.03 g, 0.75 mmol) was dissolved in 25% HBr-acetic acid solution under a N$_2$ atmosphere and stirred at room temperature for 4 h.   The addition of ether gave white solids, which was collected by filtration.   The solid was dried *in vacuo* and found to be **8** by ^{1}H NMR measurement (0.82 g, 85% yield). ^{1}H NMR (400 MHz; DMSO-d_6, residual proton of the solvent) δ = 10.68 (2H, s), 8.01 (1H, s), 7.93 (4H, s), 7.56 (2H, s), 6.92 (2H, s), 4.10 (32H, m), 1.22 (12H, t, J = 7.2 Hz), 1.14 (12H, t, J = 7.2 Hz).

Compound 9. Protoporphyrin IX (160 mg, 0.13 mmol), compound **8** (88.2 mg, 0.16 mmol), 1-hydroxybenzotriazol monohydrate (HOBt·H$_2$O, 110 mg, 0.82 mmol) and dry triethylamine (290 mg, 2.88 mmol) were dissolved in dry DMF (5 mL) and cooled with an ice bath.   After 1-Ethyl-3-(3'-dimethylaminopropyl)carbodiimide hydrochloride (EDC·HCl, 110 mg, 0.57 mmol) was added to the solution, the reaction mixture was stirred at 0 $^\circ$C for 1 h.   After further the addition of EDC·HCl (100 mg, 0.52 mmol), the reaction mixture was then stirred at room temperature for 24 h. The solvent was evaporated, and the residue was dissolved in CH$_2$Cl$_2$.   The solution was subsequently washed with 0.1 M HCl*aq.*, saturated NaHCO$_3$ and brine.   The organic phase was dried over Na$_2$SO$_4$ before the solvent was removed under reduced pressure.   The residue was subjected to silica gel column chromatography (CHCl$_3$/MeOH = 50/1) and the brown band was collected.   The collected materials were purified by GPC, and compound **9** was obtained as oily brown product (36 mg, yield 16%). ^{1}H NMR (DMSO-d_6, residual proton of the solvent) δ = 10.70 (s, 2H), 10.40 (s, 1H), 10.05–9.75 (m, 4H), 8.30 (m, 2H), 7.90 (s, 4H), 6.95 (s, 2H), 6.36 (m, 2H) 6.15 (m, 2H), 4.42 (m, 4H), 4.15–3.91 (m, 32H), 3.70–3.55 (m,12H), 1.21 (t, J = 6.8 Hz, 12H), 1.09 (t, J = 6.8 Hz, 12H).

Compound 10. Compound **9** (33.5 mg, 0.019 mmol), FeCl$_2$·4H$_2$O (57.0 mg, 0.29 mmol) and NaHCO$_3$ (10.4 mg, 0.12 mmol) were dissolved in N$_2$-purged CHCl$_3$/CH$_3$CN (3/7, 10 mL) under a N$_2$ atmosphere, and the mixture was stirred at 55 $^\circ$C for 2 h.   After cooling, the reaction solution was

diluted with CHCl$_3$ and washed with 0.1 M HClaq., brine and water.   The organic phase was dried over Na$_2$SO$_4$, and the solvent was evaporated.   The obtained residue was purified by silica gel column chromatography (CHCl$_3$/MeOH = 50/1), and the brown band was collected.   The evaporation of the solvent gave brown solid **10** (15.1 mg, yield 44% as chloride coordinated form).

Compound 11. Protoporphyrin IX (70.2 mg, 0.13 mmol), compound **6** (120 mg, 0.20 mmol) and HOBt·H$_2$O (68.5 mg, 0.51 mmol) were dissolved in dry DMF (4 mL), and dry triethylamine (36.0 mg, 0.358 mmol) was added.   The solution was stirred at 0 $^\circ$C for 15 min before the addition of EDC·HCl (36.0 mg, 0.188 mmol).   The reaction mixture was stirred at 0 $^\circ$C for 1 h and allowed to warm up to room temperature.   The solution was further stirred at room temperature for 25 h.   The solution was diluted with CHCl$_3$ (50 mL) and subsequently washed with water, 0.1 M HClaq., sat. NaHCO$_3$ and brine.   The organic phase was dried over Na$_2$SO$_4$, and the solvent was evaporated.   The obtained residue was subjected to silica gel column chromatography (CHCl$_3$/MeOH = 50/1) for eluting the compound in which both propionates reacted, followed by eluting compound **11** with CHCl$_3$/MeOH = 30/1.   The solvent was evaporated to isolate compound **11** as wine-red solid (18.6 mg, yield 14 %). ^{1}H NMR (DMSO-d_6, residual proton of the solvent) δ = 12.30 (s, 1H), 10.35 (s, 1H), 10.07 (s, 1H), 9.97 (s, 1H), 9,.92 (s, 2H), 8.32 (s, 2H), 7.73 (s, 2H), 6.83 (s, 1H), 6.34 (d, J = 11 Hz, 2H), 6.16 (d, J = 11 Hz, 2H), 4.35 (m, 4H), 4.21 (s, 4H), 4.11 (q, J = 7.0 Hz, 4H), 4.07 (s, 4H), 4.02 (q, J = 7.0 Hz, 4H), 3.56 (s, 12H), 3.31 (m, 4H), 1.17 (t, J = 7.0 Hz, 6H), 1.02 (t, J = 7.0 Hz, 6H), −3.90 (br, 2H).

Heme 1. The synthesis of heme **1** was conducted as described in the preparation of heme **3** from compound **11** *via* compound **12**.   UV-vis (λ_{max} (nm) in water): 400, 498, 622; FAB-HRMS (positive mode): calcd for C$_{50}$H$_{47}$O$_{13}$N$_7$Fe: 1009.2581; [M]$^+$ found: 1009.2600.

Heme 3. Compound **10** (10.1 mg, 5.5 μmol) was dissolved in a mixed solvent of THF (9 mL) and MeOH (9 mL).   After the addition of 0.2 M KOHaq. (9 mL), the reaction mixture was stirred at room temperature for 12 h.   The complete of the reaction was confirmed by TLC, and 0.1 M HClaq. was slowly added till the pH of the solution became around 6.   The solution was then concentrated under reduced pressure, and the residue was subjected to size exclusion gel column chromatography (LH-20, GE healthcare) with the elution of water.   The brown band was collected, and brown solid **3** was obtained as a mixture of the regioisomers, **3a** and **3b**, after lyophilization (quant).   The purity was confirmed by the observation of a single peak in the HPLC analysis (Figure 1-10).   UV-vis (λ_{max} (nm) in water): 400, 498, 622; ESI-MS (positive mode): calcd for C$_{74}$H$_{67}$FeN$_{11}$O$_{25}$: 1565.36 [M]$^+$; found: 1565.32.

Determination of Dissociation Constants (K_{d1} and K_{d2})

Mb(H64D) (8 μM) was dissolved in 20 mM KPi (pH = 6.0) and titrated with 2-methoxyphenol. The UV-vis spectra were measured in the range 350 nm to 450 nm with dropwise additions of 2-methoxyphenol. The dependency of the absorbance change at 408 nm (Δabs_{408}) on concentrations of 2-methoxyphenol was analyzed by the following equation:

$$\Delta abs_{408} = (A \cdot K_{d2} \cdot [S] + B \cdot [S]^2) / (K_{d1} \cdot K_{d2} + K_{d2} \cdot [S] + [S]^2)$$

where [S] is the concentration of 2-methoxyphenol, A and B are constants and K_{d1} and K_{d2} are the first and second dissociation constants of 2-methoxyphenol, respectively.

Steady-state Kinetics for 2-Methoxyphenol Oxidation

Steady-state kinetic measurements for 2-methoxyphenol oxidation catalyzed by Mb(H64D) mutants were carried out using the stopped-flow method at 25 ℃. A mixture of Mb and various concentrations of 2-methoxyphenol in 20 mM sodium malonate buffer (pH = 6.0) was rapidly mixed with H_2O_2 in the same buffer after incubation at 25 ℃ in the sample reservoirs. The final concentrations are as follows: [Mb] = 4 μM, [2-methoxyphenol] = 0.025–3 mM and [H_2O_2] = 100 mM. The oxidation reactions were monitored by observing the increase in absorbance at 470 nm. The initial rates were calculated using the molar absorption coefficient of the oxidation product; $\varepsilon = 26,600$ $M^{-1}cm^{-1}$.[29]

Determination of the Rate Constants for the Elemental Processes in 2-Methoxyphenol Oxidations

The reactions were carried out in 20 mM sodium malonate buffer (pH = 6.0) at 15 ℃ using a double-mixing stopped-flow apparatus equipped with a PDA detector. A Mb solution (8.0 μM) was mixed with 10.4 μM *m*CPBA in a first mixing shot to generate the Compound I species. After an aging period of 700–1200 ms, the generated intermediate was mixed with 2-methoxyphenol (20–200 μM) in a second mixing shot. The spectral changes after the second mixing shot were monitored by collecting the transient spectra every 10–100 ms. The absorbance changes at 408 nm were analyzed according to pseudo-first-order kinetics.

Catalytic Activities toward Thioanisole and Ethylbenzene Oxidations

The reactions were carried out in 100 mM KPi buffer (pH = 7.0) at 25 ℃. A buffer solution of Mb, thioanisole and benzyl alcohol (internal standard) was incubated prior to addition of H_2O_2 to start the reaction. The final concentrations were: [Mb] = 2.0 μM, [thioanisole] = 0.5 mM, [benzyl alcohol] = 5.0 μM and [H_2O_2] = 1.0 mM. After a reaction period of 5 min, ether was added and the reaction mixture was vigorously shaken using a vortex mixer to extract the organic materials. The separated organic phase was concentrated by evaporation with streaming N_2 gas, and the residues were analyzed using a GC/FID

system equipped with a DB-1 column.   The oxidation of ethylbenzene was carried out according to the same procedure.

Reaction of Myoglobins with Cumene Hydroperoxide (CHPO)

A Mb solution was reacted with cumene hydroperoxide ([Mb] = 20 μM, [CHPO] = 200 μM) in 1 mL of 20 mM sodium malonate buffer (pH = 6.0) at 25 °C for 5 min.   After the addition of benzyl alcohol (10 μM), the reaction mixture was filtered using a Centricon concentrator, and the filtrate was analyzed by an HPLC system equipped with a YMC Pro-C18 column, 150 × 4.6 mm at a flow rate of 0.8 mL/min with elution by addition of a 1:1 mixture of H₂O/MeOH to determine the amounts of acetophenone and cumyl alcohol formed by cleavage of CHPO based on the intensity ratios of these materials against that of a benzyl alcohol standard.
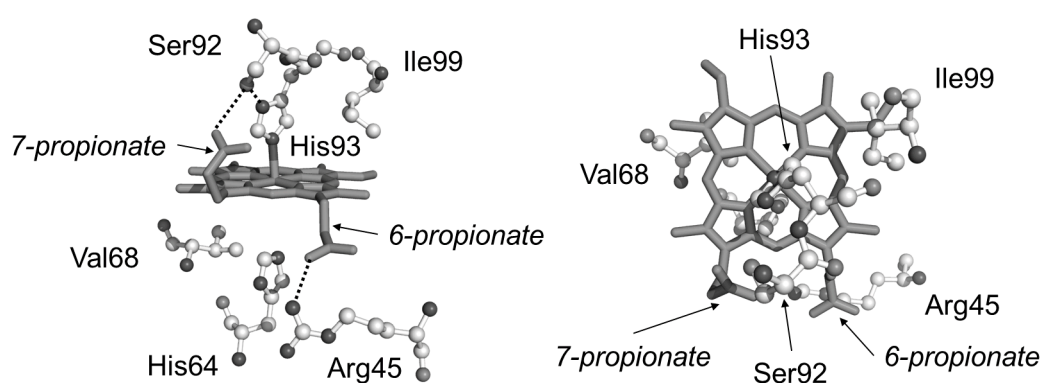
Figure 1-6. Structure of the heme pocket in aquomet wild-type Mb (extracted from PDB: 1JP8); (a) side view; (b) view from the proximal site (His 93 side).   The heme is indicated by a purple wireframe.   The dotted lines indicate hydrogen bonds.
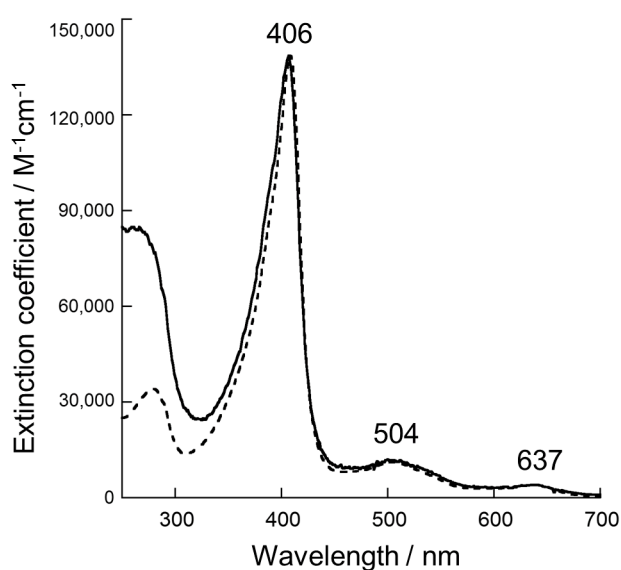
Figure 1-7. UV-vis spectra of nMb(H64D) and Mb(H64D)-**3** in 100 mM KPi (pH = 7.0).   The dotted line for nMb(H64D) and the solid line for Mb(H64D)-**3**.
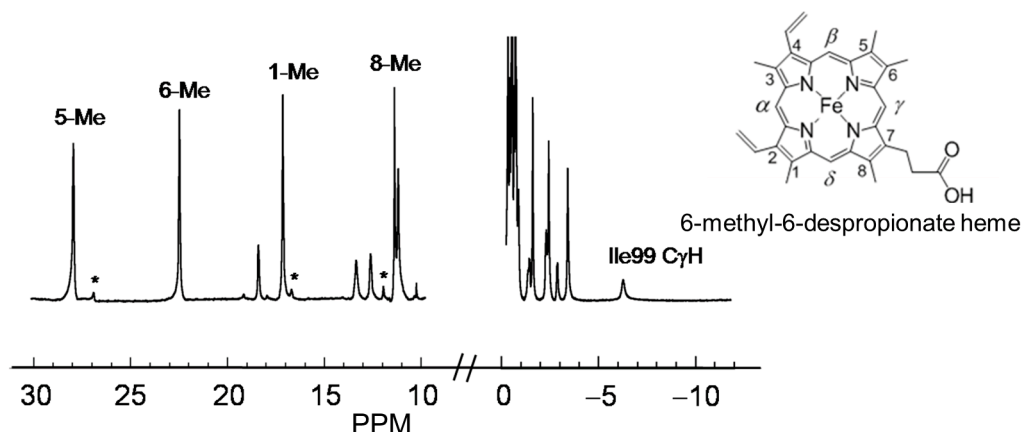
28

Figure 1-8. ^{1}H NMR spectrum of cyanomet Mb(H64D) mutant reconstituted with 6-methyl-6-despropionate heme in 10 mM KPi D$_2$O buffer (pD = 7.4) at 25 °C. The peaks with an asterisk are assignable to the heme methyl protons accommodated in the reversed orientation.
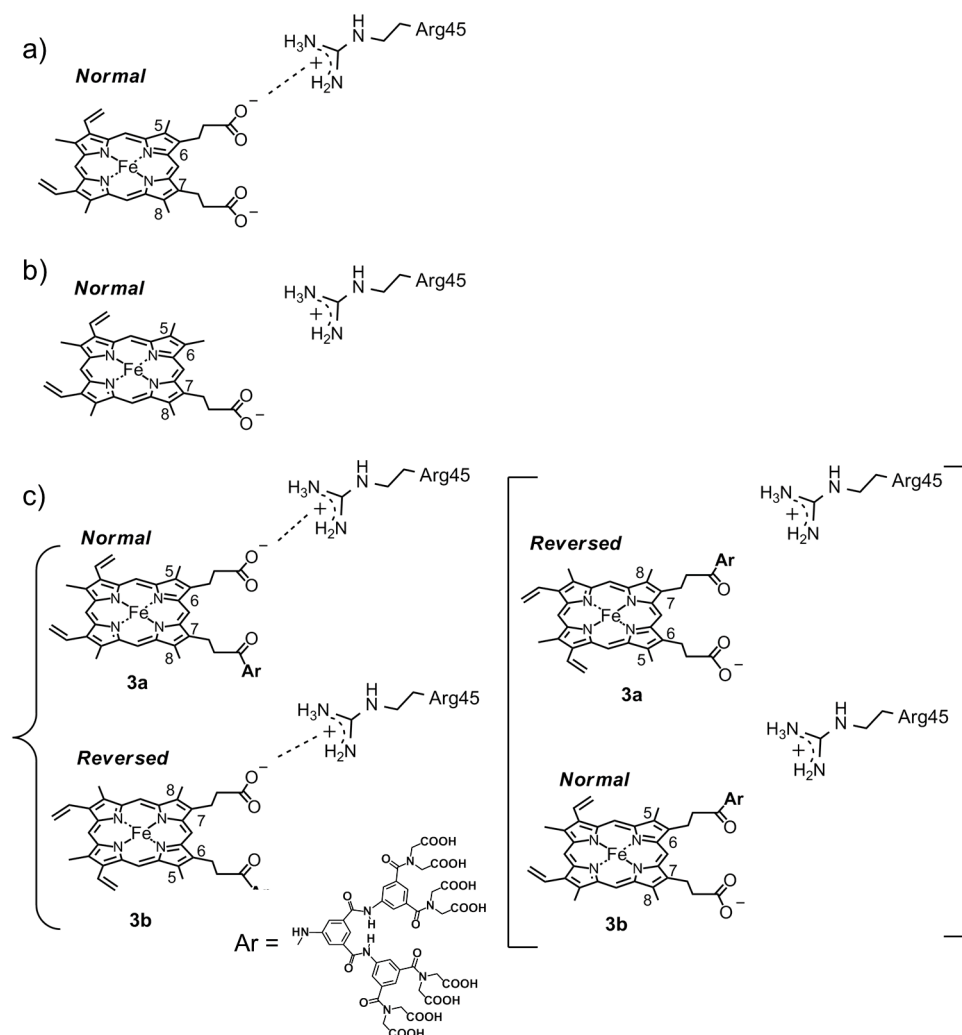

Figure 1-9. Plausible orientations of heme hemes in Mbs suggested by the result of ^{1}H NMR measurement for cyanomet form of (a) wild-type Mb or nMb(H64D), (b) Mb(H64D) reconstituted 6-methyl-6-despropionate heme and (c) Mb(H64D)-**3**. ^{1}H NMR study suggests that the reversed orientation for **3a** and the normal orientation for **3b** (shown in the brackets) can be ruled out.
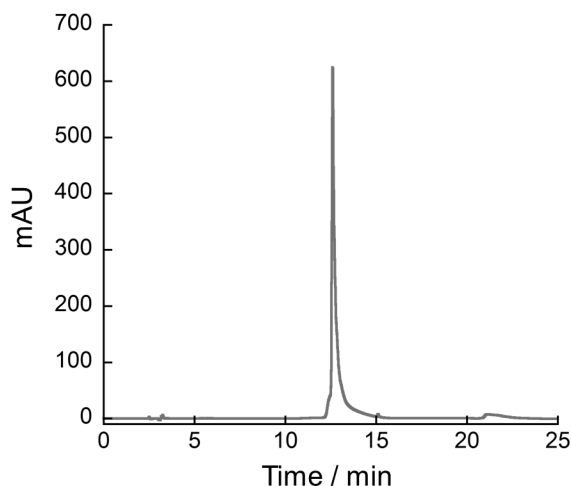
29

Figure 1-10. Reversible HPLC chromatogram for compound **3** (mixture of regioisomers **3a** and **3b**). (YMC-Pro C-18 column (150 x 4.6 mm) eluted with a mixed solvent of water and MeCN; MeCN concentration 20% (0–5 min), followed by linear gradient to 100% over 5 min and finally eluted with MeCN for 15 min; detection at 400 nm). The single peak in spite of the mixture suggests the impossibility of the separation.

References and Notes

[1]   P. D. Beer, P. A. Gale, D. K. Smith, in *Supramolecular Chemistry*; Oxford University Press Inc, New York, **2003** and reference therein.

[2]   J.-M. Lehn, in *Supramolecular Chemistry*, Wiley-VCH, Weinheim, **1995** and reference therein.

[3]   a) E. L. Raven, A. G. Mauk, in *Advances in Inorganic Chemistry* Vol. 51, Academic Press, San Diego, **2000**, pp. 1–49; b) T. Hayashi, Y. Hisaeda, *Acc. Chem. Res.* **2002**, *35*, 35–43; c) T. Ueno, S. Abe, N. Yokoi, Y. Watanabe, *Coord. Chem. Rev.* **2007**, *251*, 2717–2731; d) M. D. Toscano, K. J. Woycechowsky, D. Hilvert, *Angew. Chem. Int. Ed.* **2007**, *46*, 3212–3236; e) L. Fruk, J. Müller, G. Weber, A. Narváez, E. Domínguez, C. M. Niemeyer, *Chem. Eur. J.* **2007**, *13*, 5223–523; f) Y. Lu, D. K. Garner, J.-L. Zhang, in *Wiley Encyclopedia of Chemical Biology*, Vol.1 (Eds: T. P. Begley), John Wiley & Sons, Inc., Hoboken, N. J., **2008**, pp. 124–133; g) L. Fruk, C.-H. Kuo, E. Torres, C. M. Niemeyer, *Angew. Chem. Int. Ed.* **2009**, *48*, 1550–1574; h) J. Steinreiber, T. R. Ward, *Coord. Chem. Rev.* **2008**, *252*, 751–756; i) T. Matsuo, T. Hayashi, *J. Porphyrins Phthalocyanines.* **2009**, *13*, 1082–1089.

[4]   E. Antonini, M. Brunori, in *Hemoglobin and Myoglobin in Their Reaction with Ligands*, North-Holland, Amsterdam, **1971**.

[5]   a) T. Matsui, S. Ozaki, Y. Watanabe, *J. Am. Chem. Soc.* **1999**, *121*, 9952–9957; b) T. D. Pfister, T. Ohki, T. Ueno, I. Hara, S. Adachi, Y. Makino, N. Ueyama, Y. Lu, Y. Watanabe, *J. Biol. Chem.* **2005**, *280*, 12858–12866 and references therein.

[6]   I. Hamachi, T. Nagase, Y. Tajiri, S. Shinkai, *Chem. Commun.* **1996**, 2205–2206.

[7]   a) T. Hayashi, Y. Hitomi, T. Ando, T. Mizutani, Y. Hisaeda, S. Kitagawa, H. Ogoshi, *J. Am. Chem. Soc.* **1999**, *121*, 7747–7750; b) T. Hayashi, T. Matsuda, Y. Hisaeda, *Chem. Lett.* **2003**, *32*, 496–497.

[8]   E. Monzani, G. Alzuet, L. Casella, C. Redaelli, C. Bassani, A. M. Sanangelantoni, M. Gullotti, L. D. Gioia, L. Santagostini, F. Chillemi, *Biochemistry*, **2000**, *39*, 9571–9582.

[9]   S. Sakamoto, K. Kudo, *Bull. Chem. Soc. Jpn*. **2005**, *78*, 1749–1756.

[10] a) T. Hayashi, D. Murata, M. Makino, H. Sugimoto, T. Matsuo, H. Sato, Y. Shiro, Y. Hisaeda, *Inorg. Chem.* **2006**, *45*, 10530–10536; b) T. Matsuo, D. Murata, H. Hori, Y. Hisaeda, T. Hayashi, *J. Am. Chem. Soc.* **2007**, *129*, 12906–12907.

[11] T. Matsuo, A. Hayashi, M. Abe, T. Matsuda, Y. Hisaeda, T. Hayashi, *J. Am. Chem. Soc.* **2009**, *131*, 15124–15125

[12] H. Sato, T. Hayashi, T. Ando, Y. Hisaeda, T. Ueno, Y. Watanabe, *J. Am. Chem. Soc.* **2004**, *126*, 436–437.

[13] a) K. Harada, M. Makino, H. Sugimoto, S. Hirota, T. Matsuo, Y. Shiro, Y. Hisaeda, T. Hayashi, T. *Biochemistry*, **2007**, *46*, 9406–9416 and references therein; b) T. Hayashi, K. Harada, K. Sakurai, H. Shimada, S. Hirota, *J. Am. Chem. Soc.* **2009**, *131*, 1398–1400 and reference therein.

[14] a) G. N. La Mar, U. Pande, J. B. Hauksson, R. K. Pandey, K. M. Smith, *J. Am Chem. Soc.* **1989**, *111*, 485–491; b) G. N. La Mar, H. Toi, R. Krishnamoorthi, *J. Am. Chem. Soc.* **1984**, *106*, 6395–6401; c) Y. Wu, E. Y. T. Chien, S. G. Sligar, G. N. La Mar, *Biochemistry*, **1998**, *37*, 6979–6990 and reference therein.

[15] The X-ray structures of similar mutants, H64D/V68A and H64D/V68S Mbs, show the normal heme orientation in the heme pocket.   H.-J. Yang, T. Matsui, S. Ozaki, S. Kato, T. Ueno, G. N. Phillips, Jr., S. Fukuzumi, Y. Watanabe, *Biochemistry*, **2003**, *42*, 10174–10181.

[16] The propionate-truncated heme is also accommodated in the normal orientation when equilibrium is attained.   The crystal structure of the Mb reconstituted with 6-methyl-6-despropionate heme reveals the normal orientation of the heme.   See refs. 13a and 14.

[17] La Mar and coworkers reported that the interaction of Arg45–6-propionate is stronger than that of Ser92–7-propionate in sperm whale myoglobin.   Our observation that the non-substituted propionate in **3** prefers the interaction with Arg45 will be consistent with that observed by La Mar's group.   See refs. 13a and 14.

[18] The two sets of distinct peaks with the intensity ratio of 1:1 were observed immediately after the incorporation of the hemin into the apoprotein.   See ref. 13b.

[19] Similar behavior was observed in Mb with a flavin-pendant hemin, where the flavin moiety was linked to one of the two propionates.   T. Matsuo, T. Hayashi, Y. Hisaeda, *J. Am. Chem. Soc.* **2002**, *124*, 11234–11235.

[20] The latest report regarding product analysis of 2-methoxyphenol oxidation mediated by peroxidases proposed that 3,3′-dimethoxy-4,4′-biphenylquinone is formed as the main product.   D. R. Doerge, R. L. Divi, M. I. Churchwell, *Anal. Biochem.* **1997**, *250*, 10–17.

[21] It was confirmed that the kinetic parameters were independent of the concentrations of H_2O_2 under the conditions employed.   Therefore, the k_{cat} values shown in Table 1 directly reflect the process of oxidation of 2-methoxyphenol.

[22] M. I. Savenkova, J. M. Kuo, P. R. Ortiz de Montellano, *Biochemistry*, **1998**, *37*, 10828–10836.

[23] The spectral changes would be caused by the change in the polarity at the distal site.

[24] There are interactions of the heme-propionate with amino acid residues at the distal and the proximal sites in Mb(H64D)-**1**, whereas these interactions do not exist for Mb(H64D)-**2**.

[25] The strong coordination of the proximal ligand to the heme iron is recognized as a "push-effect" which controls the reactivities of the high-valent species in native heme-containing oxidases.   See ref. 3d.

[26] The intramolecular hydroxylation of the amino acid residue at the distal site has been reported for the F43W/H64D/V68I myoglobin mutant.   T. D. Pfister, T. Ohki, T. Ueno, I. Hara, S. Adachi, Y. Makino, N. Ueyama, Y. Lu, Y. Watanabe, *J. Biol. Chem.* **2005**, *280*, 12858–12866.

[27] For thioanisole oxidation using $H_2{}^{18}O_2$, the complete incorporation of ^{18}O into the products was confirmed by GC-MS.   The enantiometric excess value (*ee*) for methyl phenyl sulfoxide was not determined in this research, because the value would be time-dependent: Both stereoisomers of the sulfoxide product can be converted into the sulfone through the second oxygen transfer.   The sequential oxidation will bring about the change in the ratio of the stereoisomers in the transiently formed sulfoxide product unless the second oxidation becomes quite negligible.   The previous paper reported the slightly preferential production of (*S*)-isomer (6% *ee*) in the oxidation of thioanisole mediated by Mb(H64D)-**1** (reference 5a and correction: *Biochemistry*, **2008**, *47*, 2700).

[28] F. W. Teale, *Biochim. Biophys. Acta*, **1959**, *35*, 543.

[29] a) G. D. DePillis, B. P. Sishta, A. G. Mauk, P. R. Ortiz de Montellano, P. R. *J. Biol. Chem.* **1991**, *266*, 19334–19341; b) B. Chance, A. C. Maehly, *Methods Enzymol.* **1955**, *2*, 764–775.

Chapter 2

A Rhodium Complex-linked Nitrobindin as an Artificial Biocatalyst
for Phenylacetylene Polymerization

2-1. Introduction

Efforts to develop biocatalysts with new chemical reactivity and selectivity different from that found in Nature indicate that promising strategies involve construction of artificial metalloenzymes generated by incorporation of a metal containing moiety into protein scaffolds.[1] For example, sophisticated anchoring systems for attachment of an artificial metal heme into a desired specific site within a protein matrix using covalent,[2] dative,[3] or supramolecular approaches[4] have been developed over the last decade. Although many of the previous challenges have achieved a variety of intriguing reactions, such as enantioselective hydrogenation and asymmetric alkylation,[4c, d] artificial metalloenzymes catalyzing polymerization reaction with C–C bond formation have been quite limited.[3h] In contrast, a variety of transition metal catalysts that produce chemoselective and stereoselective polymers have been extensively studied, and several synthetic polymers have been used to produce useful materials. For example, transition metal complexes have been found to catalyze polymerization of phenylacetylene.[5] This compound produces some of the most intriguing synthetic polymers due to its remarkable electrical conductivity, paramagnetism, and photoconductivity.[6] In particular, a rhodium (Rh)-based complex has been considered as an attractive target for development of a polymerization catalyst because Rh complexes are capable of catalyzing stereoselective living polymerization to yield poly(phenylacetylene) (PPA) with high cis stereoregularity even in water.[7] Such a polymerization with C–C bond formation has not been observed in Nature. Inspired by this knowledge, the author envisioned that a ''hybrid catalyst'' with a synthetic metal catalyst engineered into the protein scaffold could achieve heretofore unexploited and well-controlled polymerization within a chiral protein environment. A Rh complex immobilized within the discrete space of a spherical ferritin cage with a diameter of roughly 8 nm was recently reported to catalyze polymerization of phenylacetylene with restricted molecular weight. The stereostructure of this complex was not discussed.[3h] In this chapter, the author demonstrates that our hybrid catalyst containing a Rh active site in the β-barrel concave structure of nitrobindin (Figure 2-1), which inherently transports an NO molecule in *Arabidopsis thaliana*, produces the trans conformer of PPA. This proves that the protein environment adjacent to an artificial metal heme has an important effect on tailored polymerization.
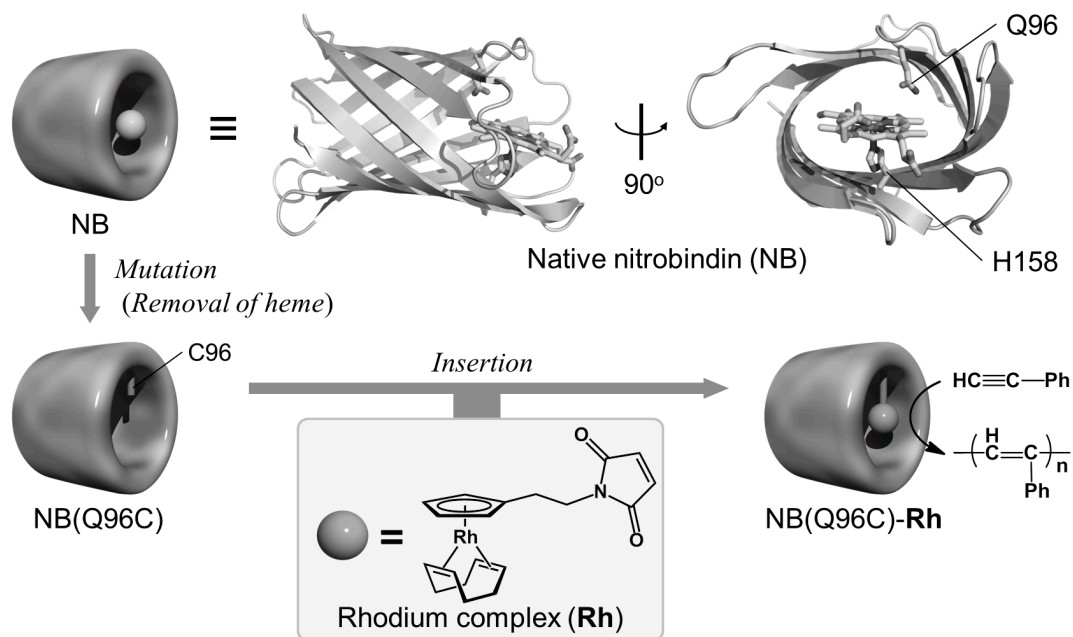
Figure 2-1. Schematic representation.

2-3. Results and Discussion

Preparation of Rhodium Complex (Rh)

The author designed a Rh complex with cyclopentadiene (Cp) and cyclooctadiene (COD) ligands as an artificial active site of a Rh–nitrobindin hybrid catalyst with the objective of catalyzing polymerization of phenylacetylene (Figure 2-4a).   To anchor the Rh complex onto the specific site of the protein, the author used the Cp ligand, which binds tightly to the metal.   This ligand also possesses a maleimide group which forms a covalent linkage with a Cys residue.   The Rh(I) catalyst (**Rh**) with the maleimide group was synthesized via two steps from Cp and characterized by ESI-TOF MS and ^{1}H NMR spectroscopy.   The crystal structure analysis indicated that the Cp and cod ligands bind to the Rh ion with η^5 and η^2 coordination modes, respectively (Figure 2-4b).   These modes are commonly found in the analogous Rh complexes.   To ensure that a Cys residue selectively reacts with the maleimide group in **Rh**, the author investigated a simple model reaction with cysteine in a THF–H_2O co-solvent.   The desired reaction was easily monitored by the ^{1}H NMR signals and the concomitant increase in the exact mass assignable to the coupling product (calcd for $C_{22}H_{29}N_2O_8Rh_1S_1$ 521.108, found 521.098).   This indicates that the maleimide group of **Rh** reacts selectively with the cysteine thiol to form a covalent linkage.

Preparation of Nitrobindin Mutant NB(Q96C)

Next, to incorporate the Rh complex, a rigid protein scaffold containing a suitable-sized cavity is required as a host. Here, a β-barrel structure is expected to provide an appropriate structural motif in various protein scaffolds. The author thus selected nitrobindin (NB), which contains a heme molecule within the cavity surrounded by eight β-strands. Such a β-barrel structure provides a remarkably rigid platform to construct an artificial active site, because proteins of the NB family retain their inherent barrel folding even in an apo-form obtained by removal of the heme heme.[9] In addition, a relatively hydrophobic environment without cysteine residues in NB is expected to be useful in further shaping the active site. As our first trial, Gln96 was identified as a possible single anchoring site. This residue, which is located in the entrance of the cavity in NB, was mutated to a Cys residue to covalently bind the Rh complex **Rh** through the maleimide moiety. According to the X-ray crystal structure of **Rh** (Figure 2-4b), the molecular size of **Rh** would be expected to be suitable for anchoring within the cavity. The NB(Q96C) protein expressed in *E. coli* was obtained as the apo-form and purified by an anion exchange column (Figure 2-2).
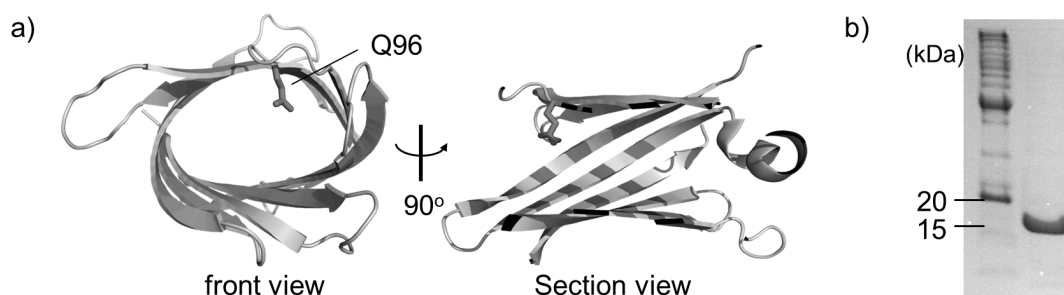

Figure 2-2. (a) The mutation position (Q96) of NB and (b) SDS-PAGE of NB(Q96C).

Preparation of NB(Q96C)-Rh

The NB mutant (10 μM) in 5 mL of a 10 mM Tris-HCl buffer (pH 8.0) was supplemented with DTT to reduce a thiol group of the NB protein. The reduced NB protein was concentrated and purified using a HiTrap™ desalting column equilibrated with 10 mM Tris-HCl (pH 8.0). The collected NB protein solution was slowly supplemented with **Rh** in DMSO and the mixed solution was incubated at room temperature for 30 min. The partially precipitated Rh complex was removed by filtration with a membrane filter (0.44 μm) and the filtrate was again concentrated, followed by purification to yield the **Rh**–NB-hybrid catalyst (NB(Q96C)-**Rh**). The MALDI-TOF MS spectrum of NB(Q96C)-**Rh** indicated the desired molecular weight of the corresponding protein with the covalently linked Rh moiety (calcd 18424.94, found 18425.83) (Figure 2-3a). The successful conjugation was also confirmed by the content of the Rh ion (0.94 eq.) derived from an ICP experiment. Protein folding of the hybrid catalyst was analyzed by CD spectroscopy (Figure 2-3b). The CD spectrum of NB(Q96C)-**Rh** is consistent with that

observed for apo-NB with a characteristic negative band at 220 nm due to the rigid β-barrel structure. This indicates that the introduction of **Rh** into the entrance of the cavity has no serious influence on the β-barrel structure. To visualize the orientation of the Rh active site within the cavity, the structure of the hybrid catalyst covalently bound to NB was calculated (Figure 2-5). Two favorable binding modes were determined, suggesting that the Rh active site fits well within the NB cavity.
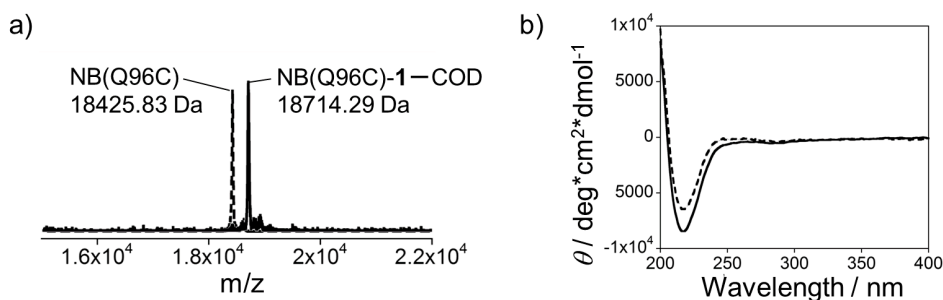

Figure 2-3. (a) MALDI-TOF MS and (b) CD spectra of NB(Q96C) in dashed line and NB(Q96C)-**Rh** in solid line.

Polymerization of Phenylacetylene

Phenylacetylene polymerization catalyzed by the hybrid protein was monitored by color changes of the reaction mixture from colorless to pale yellow. A gel permeation chromatography (GPC) analysis was also performed. The trans/cis ratio of the product was determined according to a previously reported method using ^{1}H NMR spectroscopy (Table 2-1).[10] The polymerization of phenylacetylene proceeded smoothly in a Tris-HCl buffer (pH 8), giving the polymer with an Mn value of 42,600 at 25 °C. Interestingly, the trans content of PPA is found to be 53% (Table 2-1, entry 1), as supported by a characteristic broad ^{1}H NMR signal at about 7 ppm which is assigned as the trans isomer. On the other hand, the **Rh** without the protein scaffold predominantly provided PPA with a *cis* content of greater than 93% (Table 2-1, entry 2).

A sharp signal of the vinyl proton in the cis isomer was clearly observed at 5.40 ppm. In addition, a Mb(A125C)-**Rh** as a reference hybrid catalyst, where **Rh** was conjugated to the surface of A125C mutant myoglobin, is also found to give *cis* PPA (Table 2-1, entry 3). These findings support our proposal that the otherwise favorable production of the *cis* conformer of PPA is restrained by the concave shape of the Rh active site with its surrounding amino acid residues. This leads to the generation of trans PPA.[11] Surprisingly, in the polymerization catalyzed by NB(Q96C)-**Rh** at lower temperature (Table 2-1, entries 4 and 5), the trans content of PPA decreases to 30%, while **Rh** on the surface in Mb(A125C)-**Rh** mainly produces *cis* PPA. Therefore, it is expected that the neighboring protein environment of the Rh complex in NB(Q96C)-**Rh** kinetically perturbs the approach of the monomer to the growing polymer chain to yield *cis* PPA. As a result, *trans*-rich PPA is available within the protein matrix, although *cis* PPA is thermodynamically more favorable. Finally, the polymerization catalyzed by the hybrid is found to

proceed under basic conditions (pH > 8; Table 2-1, entry 6). This suggests that the base would be required to abstract the acidic hydrogen of the phenyl acetylene to form an alkynyl–Rh(I) species in the initiation step.

Table 2-1. Polymerization of phenylacetylene catalyzed by artificial biocatalyst.[a]
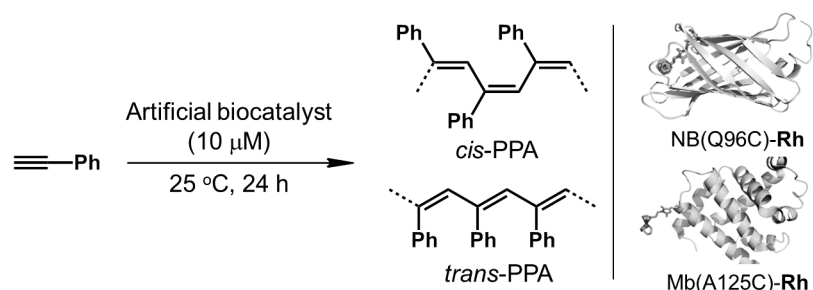
Entry	Artificial biocatalyst	Buffer (pH)	M_n[b]	M_n / M_w[b]	trans / cis[c]
1	NB(Q96C)-**Rh**	Tris-HCl (pH 8)	42,600	2.1	53 : 47
2	Rhodium complex (**Rh**)	THF	22,900	2.6	7 : 93
3	Mb(A125C)-**Rh**	Tris-HCl (pH 8)	55,700	2.2	7 : 93
4[d]	NB(Q96C)-**Rh**	Tris-HCl (pH 8)	80,000	1.8	30 : 70
5[d]	Mb(A125C)-**Rh**	Tris-HCl (pH 8)	64,800	1.9	5 : 95
6	NB(Q96C)-**Rh**	Tris-HCl (pH 7)	No reaction		

[a] All emulsion polymerizations were carried out by using the hybrid catalyst (10 μM) and phenylacetylene (1 M) in a buffer solution at 25 ^{o}C for 24 h. After the reaction, the polymer in the organic phase was lyophilized, extracted with CH_2Cl_2 and purified. [b] Determined by GPC in CH_2Cl_2. [c] Determined by ^{1}H NMR (Figure 2-6). The deviation is less than 3%. [d] The reaction was performed at 2 ^{o}C for 24 h.

1-3. Summary

In conclusion, the author has developed an artificial biocatalyst for polymerization of phenylacetylene by conjugating a Rh complex to a β-barrel NB protein. To the best of our knowledge, the present work provides the unique example of C–C bond formation and subsequent polymerization, which is not seen in Nature. While the content of *trans* PPA is remarkably increased by the hybrid catalyst, the *trans* conformer content is not completely predominant, because two plausible conformations appear to exist in the Rh-complex in the protein matrix (Figure 2-5). Therefore, the author expects that the *trans* conformer content could be increased by optimizing the attachment site of the Rh complex in the protein. Finally, the present results indicate that a rigid and chiral protein scaffold can function as a powerful platform for regulation of recognition of a monomer during a propagation reaction. Enhancement of the *trans* conformer content is currently in progress and several hybrid biocatalysts are being developed with different sites in the NB protein substituted with cysteine to produce various Rh-complex linkage sites.

2-4. Experimental Section

Instruments

^{1}H NMR spectra were recorded on a Bruker DPX400 NMR spectrometer. Highresolution magic angle spinning (HR-MAS) experiments were performed on a Varian Unity Inova 600 MHz NMR spectrometer equipped with a 4 mm gHX Nanoprobe. Chemical shifts were reported in ppm relative to the residual solvent resonances. ESI-TOF MS analyses were performed on an Applied Biosystems Mariner API-TOF Workstation or a Bruker micrOTOF focus III mass spectrometer and MALDI-TOF MS analyses were performed on a Bruker autoflex III mass spectrometer. UV-vis experiments were conducted using a Shimadzu UV-3150 double-beam spectrophotometer equipped with a thermostated cell holder with a 0.1 °C deviation. Purification of the proteins was performed using a GE healthcare ÄKTA Purifier system at 4 °C. Circular dichroism (CD) spectra were recorded by JASCO J720S spectrometer. ICP-OES was performed on a Shimadzu ICPS-8100 emission spectrometer. The pH values were monitored with a Horiba F-52 pH meter. Air-sensitive manipulations were performed in an MBraun glovebox. Gel permeation chromatography was performed on a TOSOH SC8020 apparatus with a refractive index detector with the TOSOH TSKgel G4000HHR column.

Materials

The pUC57 plasmid containing optimized nitrobindin (NB) (M75L, M148L) gene was purchased from GeneScript. Oligonucleotides were obtained from Invitrogen, Inc. (Japan). Restriction enzymes were obtained from Takara Bio Inc. (Japan). Nucleotide sequences were determined by Fasmac (Japan). All reagents of the highest guaranteed grade were purchased and used as received unless otherwise noted. A standard rhodium solution for inductively coupled plasma optical emission spectroscopy (ICP-OES) was purchased from Wako (Japan). Distilled water was demineralized by a Barnstead NANOpure DIamond^{TM} apparatus. [Rh(COD)Cl]$_2$ was synthesized according to the previous report.

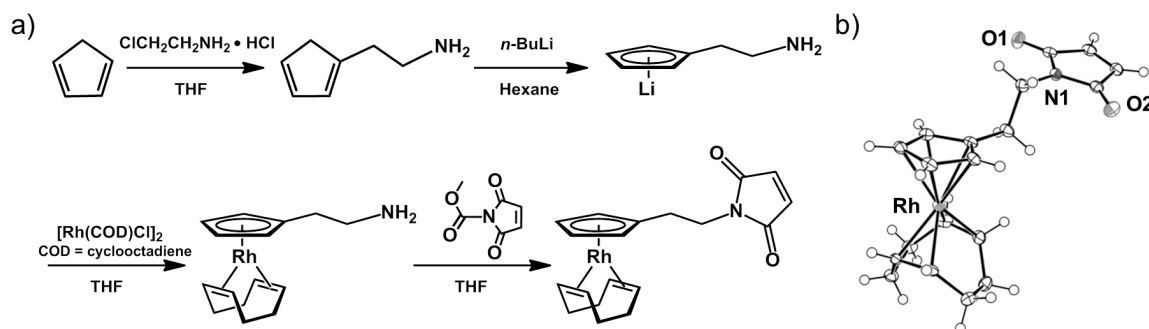**Preparation of the Rhodium Complex (Rh)**

Figure 2-4. (a) Synthetic route and (b) crystal structure of **Rh**.

Synthesis of LiC₅H₄CH₂CH₂NH₂ To a solution of freshly prepared cyclopentadiene (20 mL, 240 mmol) in THF (300 mL) was added NaH (12.0 g, 290 mmol) at 0 °C, and the mixture was stirred at 0 °C for 30 min and at room temperature for additional 30 min. To the solution was added ClCH₂CH₂NH₂·HCl (13.5 g, 120 mmol) and the mixture was stirred at room temperature for 10 h. The reaction was quenched by the addition of H₂O and the product was extracted with pentane. The organic phase was concentrated and mixed with 2 M HCl*aq.* until the aqueous phase was adjusted to pH 1. The product was further extracted with an acidic solution and additional portion of 0.1 M HCl*aq.*, and the combined aqueous solution was then adjusted to pH 14 with 4 M NaOH*aq.* The product was again extracted with pentane and the organic phase was dried over Na₂SO₄. The product in pentane solution was concentrated to ca. 10 mL and the solution was mixed with excess amount of *n*-BuLi (1.6 M in hexane, 15 mL). The product precipitated was collected by filtration and dried in vacuo to give air- and moisture-sensitive white powder (660 mg, 4.8%): ¹H NMR (400 MHz, THF-*d₈*): δ 5.61 (t, 2H, *J* = 2.4 Hz), 5.45 (t, 2H, *J* = 2.4 Hz), 2.69 (tt, 2H, *J* = 6.0 Hz, 6.0 Hz), 2.54 (t, 2H, *J* = 6.0 Hz), 1.08 (t, 2H, *J* = 6.0 Hz).

Synthesis of Rhodium Complex (Rh) [Rh(COD)Cl]₂ (79 mg, 0.16 mmol) and LiC₅H₄CH₂CH₂NH₂ (40 mg, 0.37 mmol) were dissolved in 5 mL of THF and the solution was stirred at room temperature for 30 min. To the solution was added *N*-methoxycarbonylmaleimide (55 mg, 0.37 mmol) in 10 mL of THF and the mixed solution was stirred at room temperature for 24 h. The product was purified by column chromatography (Al₂O₃, THF) under N₂ and dried in vacuo. The residue was recrystallized from hexane to give air-stable yellow crystal **Rh** (22 mg 14.9 %): ¹H NMR (400 MHz, C₆D₆): δ 5.71 (s, 2H), 4.85 (m, 2H), 4.80 (m, 2H), 3.83 (m, 4H), 3.57 (m, 2H), 2.28 (m, 6H), 1.96 (m, 4H); ¹³C NMR (100 MHz, C₆D₆): δ 169.9, 133.1, 102.0, 86.8, 85.8, 63.9, 38.7, 32.7, 26.7; ESI-TOF MS (positive mode) *m/z* calcd for C₁₉H₂₂NO₂Rh [M + H]⁺ 400.078, Found 400.090.

Crystal Structure Determination

The crystal of **Rh** was mounted on a glass fiber, and the X-ray data was collected at 108 K on a Rigaku VariMax RAPID imaging plate area detector with graphite monochromated Mo-Kα radiation (0.71075 Å). The basic crystallographic parameters for **Rh** are listed in Table S1.   The structure was solved by the direct method and expanded using SIR92.   Nonhydrogen atoms were refined anisotropically and all H atoms were located at the calculated positions.   All structures in the final stages of refinement showed no movement in the atom positions.   The calculations were performed using Single-Crystal Structure Analysis Software, CrystalStructure (version 3.8.2) and SHELXL-97.

Table 2-1. Crystallographic data for **Rh**.

Parameters	Rhodium complex
Empirical formula	$C_{19}H_{22}NO_2Rh_1$
Formula weight	399.29
Crystal system	Monoclinic
a, Å	6.3936(2)
b, Å	11.9067(4)
c, Å	21.0945(6)
α, deg	90.00
β, deg	91.9750(10)
γ, deg	90.00
V, Å^3	90.00
β, deg	91.9750(10)
γ, deg	90.00
V, Å^3	1604.90(9)
Space group	$P2_1/n$
Z	4
ρ_{calc}, g cm^{-1}	0.064 (0.300)
μ (MoKα), cm^{-1}	96.5 (89.7)
Temp	108
Data	15370
Unique data	3679
R_1	2.96
wR_2	5.80
GOF	1.054

[a] $R_1 = \Sigma(|F_o| - |F_c|)/ \Sigma |F_o|$.   [b] $wR_2 = \{\Sigma(w(F_o^2 - F_c^2)^2)/\Sigma w(F_o^2)^2\}^{1/2}$.

Expression and Purification of the Nitrobindin Proteins

The pUC57 plasmid containing optimized NB (M75L, M148L) gene was used as a template for PCR with oligonucleotide primers (i)5′-GGGGACAAGTTTGTACAAAAAAGCAGGCTTCGAAGGAGATAGAA CCATGAATCAACTGCAACAACTGC-3′ and (ii) 5′-GGGGACCACTTTGTACAAGAAAGCTGGGTC CTATTACAGTTTGTCCAGGATGGC-3′. The PCR product was inserted into pDONR vector and then pDEST14 expression vector by the standard protocols for Gateway technology (Invitrogen). Successful mutagenesis, Q96C, was achieved with the QuickChange Mutagenesis kit (StrataGene). DNA sequencing was performed to verify the correct insertion of the gene sequence into the expression vector. The resulting expression plasmid, NB, was transformed into *E. coli* BL21(DE3). Each 1 L of a TB medium containing ampicillin (50 mg) and 1% (v/v) glucose was inoculated with 10 mL of the culture (OD$_{600}$ = 0.5) of the relevant transformed cells. After the cells were grown aerobically with vigorous shaking at 37 ℃ until the OD$_{600}$ reached ~0.5, isopropyl-β-D-1-thiogalactopyranoside (IPTG) was added to a final concentration of 0.5 mM to induce the protein expression. The incubation was continued at 37 ℃ for approximately 6 h. The cells were harvested by centrifugation at 4000 ×g for 10 min. Tricine SDS-PAGE analysis showed that both the supernatant and pellet from the lysed cells contained an overexpressed protein (~18k Da). The harvested cells from 4 L of culture were re-suspended in ca. 100 mL of a 20 mM Tris-HCl buffer (pH 8.0) containing 15 mM PMSF, 1mM EDTA, and 10 mM DTT and cell lysed by freeze–thaw cycles, followed by a reaction with 10 μL of benzonase® nuclease (Novagen) for 30 min at 4 ℃. The lysate was then centrifuged and the collected supernatant was dialyzed three times against 1 L of a 20 mM Tris-HCl buffer (pH 8.0). The dialyzed solution was loaded onto an anion-exchange column with HiTrap DEAE Fast Flow (GE healthcare) which was pre-equilibrated in a 5 mM Tris-HCl buffer (pH 9.0). The fraction of the target protein was collected by a 5 mM Tris-HCl buffer (pH 9.0) and 0.5 M NaCl, and concentrated using an Amicon stirred ultrafiltration cell with a 10 kDa molecular weight cut-off membrane (Millipore). The purified fractions were characterized by SDS-PAGE and MALDI-TOF MS. MALDI-TOF MS (positive mode) NB(Q96C): *m/z* calcd for C$_{830}$H$_{1304}$N$_{222}$O$_{248}$S$_2$ [M + H]$^+$18424.94, found 18425.83.

・Optimized codon sequence of NB (M75L, M148L):

AATCAACTGCAACAACTGCAAAATCCGGGC**G**AGAGTCCGCCGGTTCATCCGTTCGTGGCACC
GCTGTCCTATCTGCTGGGTACCTGGCGCGGCCAGGGTGAAGGCGAGTATCCGACCATTCCGA
GCTTTCGCTATGGCGAAGAGATCCGTTTCAGCCATTCGGGTAAACCGGTGATTGCCTATACCC
AAAAAACGTGGAAACTGGAATCGGGTGCACCGCTGCACGCAGAGAGTGGTTATTTTCGCCCG
CGTCCGGATGGTTCTATTGAAGTGGTTATCGCACAGTCGACCGGTCTGGTGGAAGTTCAAAAA
GGCACGTATAATGTGGATGAGCAGAGTATTAAACTGAAATCTGACCTGGTGGGCAACGCGTC
CAAAGTTAAAGAAATCAGCCGCGAATTCGAGCTGGTTGACGGTAAACTGAGTTATGTGGTTC
GTCTGAGCACGACCACGAATCCGCTGCAACCGCACCTGAAAGCCATCCTGGACAAACTGTAA

・Amino acid sequence of NB (M75L, M148L):

MNQLQQLQNPGESPPVHPFVAPLSYLLGTWRGQGEGEYPTIPSFRYGEEIRFSHSGKPVIAYTQ
KTWKLESGAPLHAESGYFRPRPDGSIEVVIAQSTGLVEVQKGTYNVDEQSIKLKSDLVGNASK
VKEISREFELVDGKLSYVVRLSTTTNPLQPHLKAILDKL

・Forward primer for Gateway cloning:

5′-GGGGACAAGTTTGTACAAAAAAGCAGGCTTCGAAGGAGATAGAACCATGAATCAACTGCA
ACAACTGC-3′.

・Reverse primer for Gateway cloning:

5′-GGGGACCACTTTGTACAAGAAAGCTGGGTCCTATTACAGTTTGTCCAGGAT-GGC-3′.

・Forward primers for NB(Q96C):

5′-GTTCTATTGAAGTGGTTATCGCATGCTCGACCGGTCTGGTGGAAG-3′.

・Reverse primers for NB(Q96C):

5′-CTTCCACCAGACCGGTCGAGCATGCGATAACCACTTCAATAGAAC-3′

Conjugation of Rhodium Complex (Rh) with NB Mutant

The NB mutant (10 μM) in 5 mL of a 10 mM Tris-HCl buffer (pH 8.0) was added DTT (2 mg/mL) to reduce a thiol group of the protein.   The mixed solution was incubated at 4 ºC for 30 min and concentrated to 0.5 mL using an Amicon stirred ultrafiltration cell with a 10kDa molecular weight cut-off membrane (Millipore).   The reduced protein was purified using a HiTrap desalting column (GE healthcare) equilibrated with a 10 mM Tris-HCl buffer (pH 8.0).   The collected protein solution (1.5 mL) was slowly added to **Rh** in DMSO (0.1 mg/20 μL) and the mixed solution was incubated at room temperature for 30 min.   The precipitate of the rhodium complex was removed by filtration with membrane filters (0.44 μm) and the solution was again concentrated to 0.5 mL.   The NB(Q96C)-**Rh** was purified by the HiTrap desalting column eluting with a 10 mM Tris-HCl buffer (pH 8.0).   The purified fractions were characterized by MALDITOF MS.   MALDI-TOF MS (positive mode) NB(Q96C)-**Rh**: m/z calcd for $C_{830}H_{1304}N_{222}O_{248}S_2$ $[M - COD]^+$ 18424.94, found 18425.83.

Conjugation of Rhodium Complex with Mb(A125C)

The conjugation of **Rh** with Mb(A125C) mutant was performed by the method similar to NB(Q96C)-**Rh**. The purified fractions were characterized by MALDI-TOF MS.   MALDI-TOF MS (positive mode) Mb(A125C)-**Rh**: m/z calcd for $C_{830}H_{1304}N_{222}O_{248}S_2$ $[M - COD]^+$ 17653.10, found 17653.81.

Polymerization of Phenylacetylene

All emulsion polymerizations were carried out by the hybrid catalyst (10 μM) and phenylacetylene (1 M) in 1.5 mL of a buffer at 25 ºC for 24 h.   After polymerization, the organic phase was separated by microsyringe and evaporated to dryness.   The residue was washed with hexane and methanol to remove the unreacted monomer and dried in vacuo to give a poly(phenylacetylene) (PPA) product.

Gel Permeation Chromatography (GPC)

Chloroform was used as an eluent at a flow rate of 1.0 mL/min.   The molecular weight calibration curve was obtained with standard polystyrenes.

Determination of Stereostructure of PPAs

The PPA product dissolved in $CDCl_3$ was transferred to a 4 mm magic angle spinning (MAS) rotor and the NMR spectrum was recorded by high-resolution magic angle spinning (HR-MAS) method.   The ratio of *cis* and *trans* PPAs was determined based on the peak intensities of each signal.

Molecular Modeling of Hybrid Catalyst

Modeling of the hybrid catalyst was performed using YASARA Structure Vers. 11.6.16 employing force field AMBER03 for protein residues and GAFF using AM1/BCC partial charges for the catalyst covalently bound to Cys96.   The X-ray structure of **Rh** was used as the starting structure.   The metal was replaced by cobalt, since no parameters are available for rhodium.   To maintain the correct coordination geometry, the distances from the metal to all five carbon atoms of the Cp ligand were constrained to 2.2 Å and the η^5 coordination is represented by five force field arrows.   To maintain η^2 coordination of the cod ligand, four force field arrows were defined and the distances were constrained to 2.0 Å, according to the X-ray structure of **Rh**.   The total charge of **Rh** was set to zero and the charge of the metal was set to +1 for Rh^+. The bond orders for the Cp ligand were defined as 1.67 Å to maintain an aromatic system.   As basis for the hybrid catalyst, the X-ray structure of NB with bound heme ligand (PDB: 3EMM) was used.   The author removed the heme ligand and water molecules and mutated Gln96 to cysteine.   The catalyst was placed manually in the cavity with its maleimide moiety adjacent to Cys96 and defined a bond from Cys Cγ atom to the C1 or C2 atom of the maleimide group.   The constructed hybrid catalyst was solvated in a box of TIP3P water molecules using periodic boundaries at pH 7 and a density of 0.997 g/mL.   Several starting structures were analyzed and two favorable orientations were identified for covalent attachment to the reactive maleimide atoms by steepest descent minimization and simulated annealing.   The minimized structures were relaxed using molecular dynamics calculations at 298 K for 500 ps and snapshots were

taken every 25 ps to analyze the binding modes. In the case of the hybrid catalyst linked via C1 of maleimide, the binding mode was not stable after 500 ps and an additional 2000 ps of MD-simulation was performed. The most favorable two binding modes are shown in Figure 2-5.
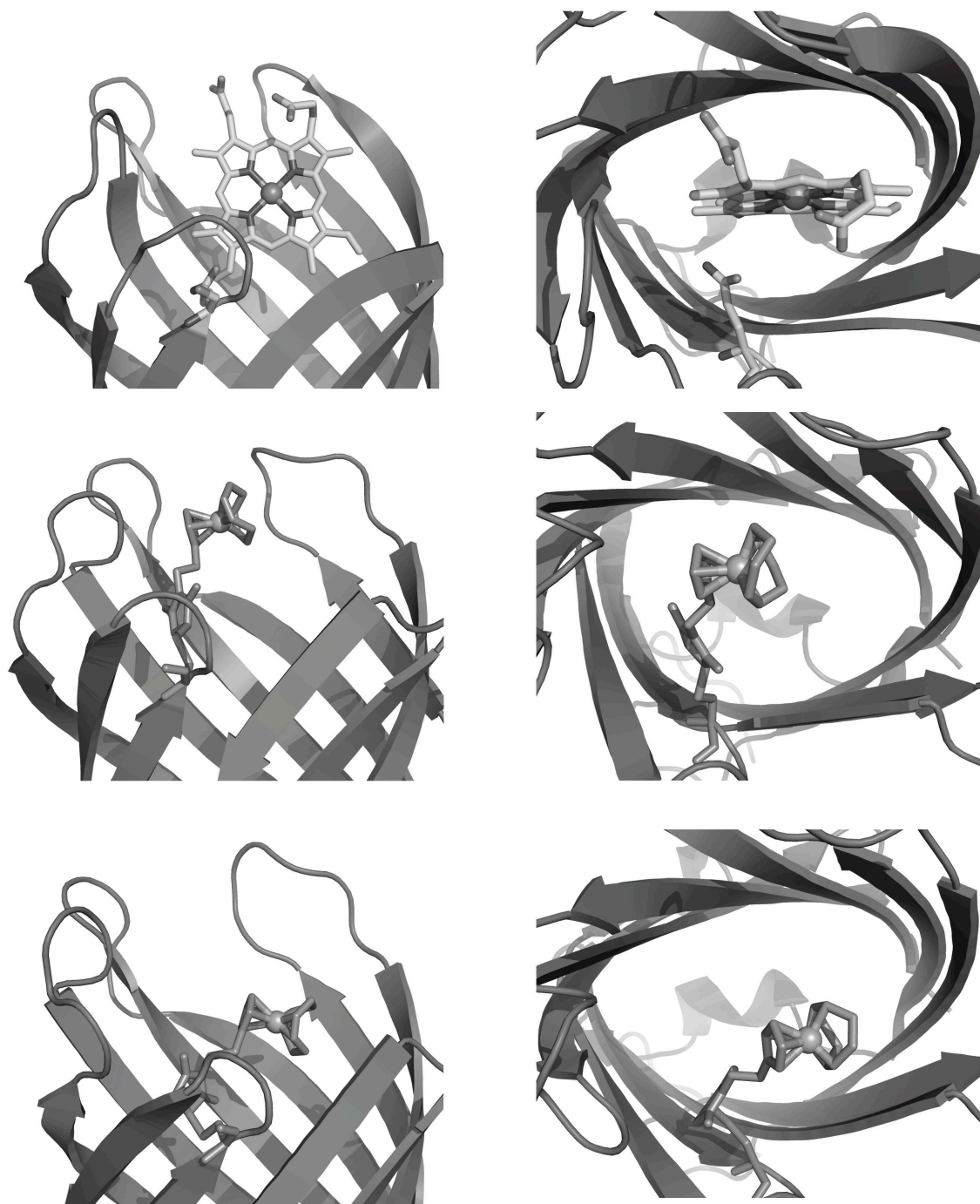

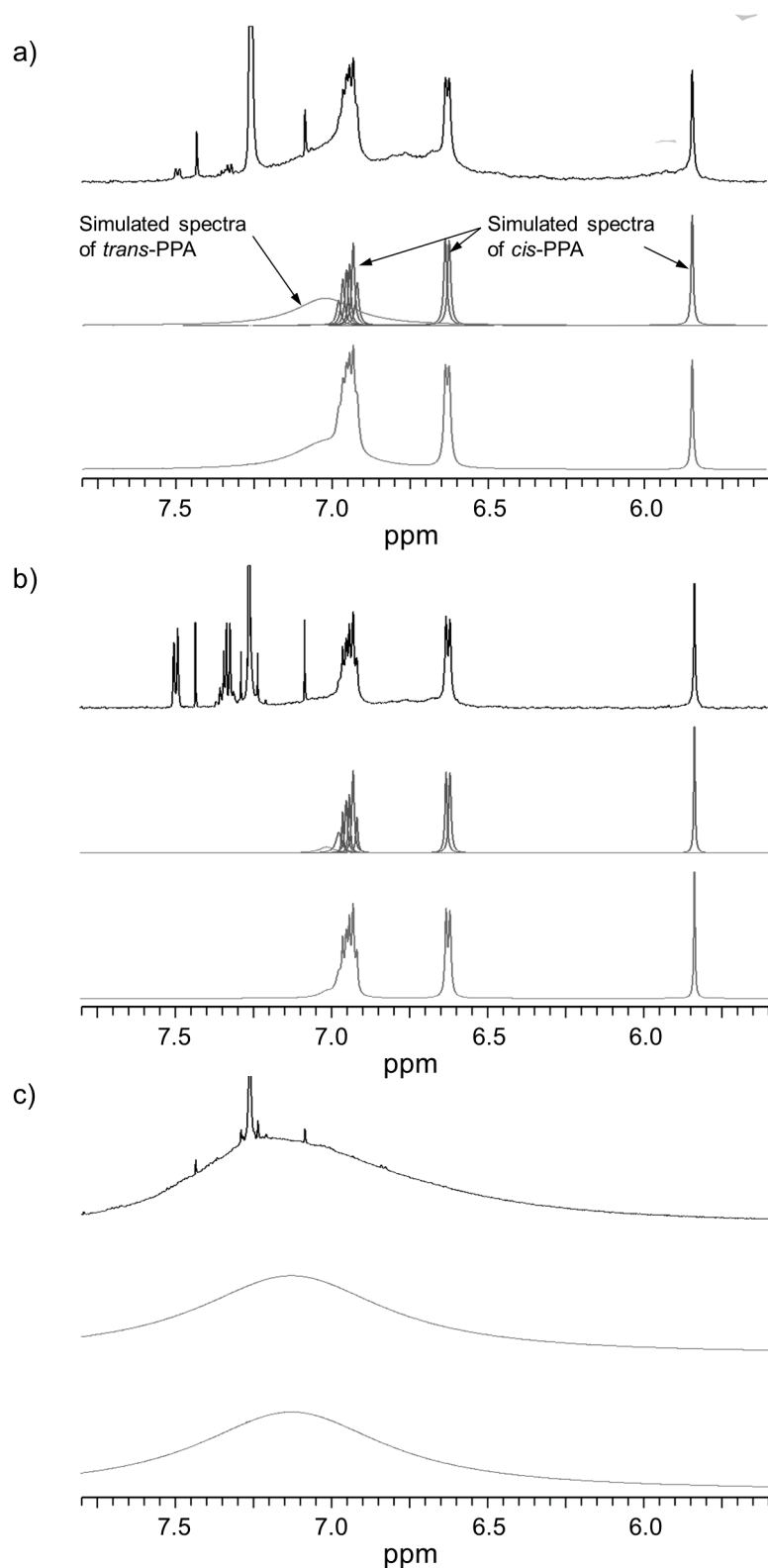**Figure 2-5.** The most favorable structures of NB(Q96C)-**Rh**.

Figure 2-6. Determination of stereostructure of PPAs by ^{1}H NMR (600 MHz). The spectra were recorded by the high-resolution magic angle spinning (HR-MAS) method. (a) PPA prepared by NB(Q96C)-**Rh**. (b) PPA prepared by **Rh**, and (c) reference sample for *trans*-PPA prepared by WCl$_6$ catalyst. In each spectrum, the observed spectra (black and top), simulated spectra of *cis* (blue and middle) and *trans* (red and middle), and the sum of the simulated spectra (purple and bottom).

References and Notes

[1] (a) Y. Lu, N. Yeung, N. Sieracki, N. M. Marshall, *Nature*, **2009**, *460*, 855–862; b) M. T. Reetz, M. Rentzsch, A. Pletsch, M. Maywald, P. Maiwald, J. J. P. Peyralans, A. Maichele, Y. Fu, N. Jiao, F. Hollmann, R. Mondiere, A. Taglieber, *Tetrahedron*, **2007**, *63*, 6404–6414; c) T. Heinisch and T. R. Ward, *Curr. Opin. Chem. Biol.* **2010**, *14*, 184–199; d) T. R. Ward, *Acc. Chem. Res.* **2011**, *44*, 47–57; e) T. Hayashi and Y. Hisaeda, *Acc. Chem. Res.* **2002**, *35*, 35–43; f) P. J. Deuss, R. den Heeten, W. Laan and P. C. J. Kamer, *Chem.–Eur. J.* **2011**, *17*, 4680–4698.

[2] (a) Z. P. Wu and D. Hilvert, *J. Am. Chem. Soc.* **1989**, *111*, 4513–4514; b) D. Qi, C. M. Tann, D. Haring and M. D. Distefano, *Chem. Rev.* **2001**, *101*, 3081–3111; c) J. R. Carey, S. K. Ma, T. D. Pfister, D. K. Garner, H. K. Kim, J. A. Abramite, Z. Wang, Z. Guo, Y. Lu, *J. Am. Chem. Soc*. **2004**, *126*, 10812–10813; d) C. Mayer, D. G. Gillingham, T. R. Ward and D. Hilvert, *Chem. Commun.* **2011**, 47, 12068–12070; e) T. Matsuo, C. Imai, T. Yoshida, T. Saito, T. Hayashi and S. Hirota, *Chem. Commun.* **2012**, *48*, 1662–1664; f) P. Haquette, B. Talbi, L. Barilleau, N. Madern, C. Fosse and M. Salmain, *Org. Biomol. Chem.* **2011**, *9*, 5720–5727.

[3] (a) M. Ohashi, T. Koshiyama, T. Ueno, M. Yanase, H. Fujii and Y. Watanabe, *Angew. Chem., Int. Ed.* **2003**, *42*, 1005–1008; b) Q. Jing, K. Okrasa and R. J. Kazlauskas, *Chem.–Eur. J.* **2009**, *15*, 1370–1376; c) J. Podtetenieff, A. Taglieber, E. Bill, E. J. Reijerse and M. T. Reetz, *Angew. Chem., Int. Ed.* **2010**, *49*, 5151–5155; d) Y. Sano, A. Onoda and T. Hayashi, *Chem. Commun.* **2011**, *47*, 8229–8231; e) T. Matsuo, A. Hayashi, M. Abe, T. Matsuda, Y. Hisaeda and T. Hayashi, *J. Am. Chem. Soc.* **2009**, *131*, 15124–15125; f) B. V. Popp and Z. T. Ball, *J. Am. Chem. Soc.* **2010**, *132*, 6660–6662; g) R. Sambasivan and Z. T. Ball, *J. Am. Chem. Soc.* **2010**, *132*, 9289–9291; h) S. Abe, K. Hirata, T. Ueno, K. Morino, N. Shimizu, M. Yamamoto, M. Takata, E. Yashima and Y. Watanabe, *J. Am. Chem. Soc.* **2009**, *131*, 6958–6960.

[4] (a) M. E.Wilson and G. M.Whitesides, *J. Am. Chem. Soc.* **1978**, *100*, 306–307; b) T. R. Ward, J. Collot, J. Gradinaru, N. Humbert, M. Skander and A. Zocchi, *J. Am. Chem. Soc.* **2003**, *125*, 9030–9031; c) J. Collot, J. Gradinaru, N. Humbert, M. Skander, A. Zocchi and T. R. Ward, *J. Am. Chem. Soc.* **2003**, *125*, 9030–9031; d) J. Pierron, C. Malan, M. Creus, J. Gradinaru, I. Hafner, A. Ivanova, A. Sardo and T. R. Ward, *Angew. Chem., Int. Ed.* **2008**, *47*, 701–705; e) H. Yamaguchi, T. Hirano, H. Kiminami, D. Taura and A. Harada, *Org. Biomol. Chem.* **2006**, *4*, 3571–3573.

[5] (a) T. Masuda, N. Sasaki and T. Higashimura, *Macromolecules*, **1975**, *8*, 717–721; b) B. Z. Tang, K. T. Xu, H. Peng, J. W. Y. Lam, T. W. H. Poon, Y. P. Dong, H. Y. Xu, Q. H. Sun, K. K. L. Cheuk, F. Salhi and P. P. S. Lee, *Macromolecules,* **2000**, *33*, 6918–6924.

[6] (a) A. G. MacDiarmid, *Angew. Chem., Int. Ed.* **2001**, *40*, 2581–2590; b) H. Shirakawa, A*ngew. Chem., Int. Ed.* **2001**, *40*, 2575–2580; c) A. J. Heeger, *Angew. Chem., Int. Ed.* **2001**, *40*, 2591–2611.

[7] (a) T. Ikariya, Y. Kishimoto, P. Eckerle, T. Miyatake, M. Kainosho, A. Ono and R. Noyori, *J. Am. Chem. Soc.* **1999**, *121*, 12035–12044; b) B. Z. Tang, J. Z. Liu and J. W. Y. Lam, *Chem. Rev.* **2009**, *109*, 5799–5867; c) E. Yashima, K. Maeda, H. Iida, Y. Furusho and K. Nagai, *Chem. Rev.* **2009**, *109*, 6102–6211; d) Z. F. Ke, S. Abe, T. Ueno and K. Morokuma, *J. Am. Chem. Soc.* **2011**, 133, 7926–7941.

[8] E. Krieger, T. Darden, S. Nabuurs, A. Finkelstein and G. Vriend, *Proteins: Struct. Funct. Bioinf.* **2004**, *57*, 678–683.

[9] (a) A. M. Amoia and W. R. Montfort, *Protein Sci.* **2007**, *16*, 2076–2081; b) G. N. Phillips, C. M. Bianchetti, G. C. Blouin, E. Bitto and J. S. Olson, *Proteins: Struct. Funct. Bioinf.* **2010**, *78*, 917–931.

[10] C. I. Simionescu and V. Percec, *J. Polym. Sci., Part A: Polym. Chem.* **1980**, *18*, 147–155.

[11] It is known that PPA with high trans content is only isolable by using a metal-carbene catalyst with early transition metals, such as Mo and W, via a metathesis mechanism.[12]

[12] Y. Fujita, Y. Misumi, M. Tabata and T. Masuda, *J. Polym. Sci., Part A: Polym. Chem.* **1998**, *36*, 3157–3163.

Chapter 3

Reengineering of a Rhodium Complex-linked Nitrobindin
to Increase *trans*-selectivity for Phenylacetylene Polymerization

3-1. Introduction

A hybrid biocatalyst comprising a synthetic transition metal complex and a well-defined protein scaffold holds promise for development of homogenous catalysts with new chemical reactivity and selectivity.[1] Hybrid biocatalysts have been constructed via dative,[2] supramolecular,[3] or covalent[4] anchoring approaches to catalyze stereoselective reactions such as hydrogenation,[5] Diels-Alder reaction,[6] sulfoxidation,[2b, 7] and benzannulation reaction.[8]   Optimization of employed protein scaffold by amino acid substitutions has been often found to be a powerful strategy for increasing reactivity and enantioselectivity of hydrogenation.[1d, 3d, 9]   One synthetically attractive target will be a new class of hybrid biocatalysts for stereo-controlled C–C bond formation.

   This inspired us to prepare a new hybrid biocatalyst which promotes stereo-controlled polymerization within a precisely designed protein cavity.   The author uses acetylene as a monomer, because polyacetylene derivatives consisting of valuable π-conjugated polyenes provide useful properties such as electrical conductivity, light emission, and liquid crystallinity.[10]   A variety of rhodium complexes have been studied as catalysts for *cis*-selective phenylacetylene polymerization.[11]   One example of catalytic phenylacetylene polymerizations has been demonstrated within an internal surface of a spherical ferritin cage in which the multiple rhodium complexes are immobilized.[12]   In a separate effort, the author recently developed a hybrid biocatalyst containing a mononuclear rhodium active site embedded within a robust 10-stranded β-barrel of a heme-free nitrobindin[13] variant for phenylacetylene polymerization (Figure 3-1).[14]   Interestingly, it was found that incorporation of the rhodium complex into an aponitrobindin variant, NB(Q96C),[15] via a maleimide–thiolate linkage produces an attractive catalyst, NB(Q96C)-**Rh**, which promotes the polymerization of phenylacetylene with approximately 50% *trans* content in polyphenylacetylene (PPA) (Figure 3-1).   The rhodium catalyst without a protein matrix yields *cis*-PPA almost exclusively.   To further enhance the *trans*-stereoselectivity of NB(Q96C)-**Rh** in PPA synthesis, the cavity around the rhodium active site has recently been engineered by site-directed mutagenesis.   The rigid β-barrel structure of aponitrobindin is capable of computationally guided design of the cavity.   In this report, the author describes the crystal structure and catalysis of the optimized rhodium complex-linked hybrid biocatalyst, which preferentially generates *trans*-PPA.
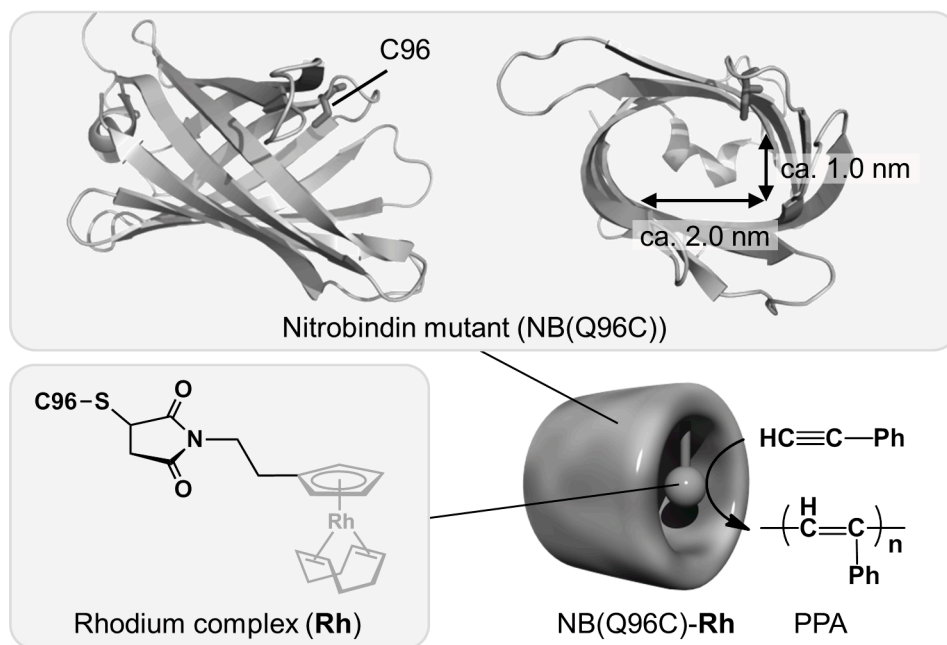
Figure 3-1. Artificial biocatalyst NB(Q96C)-**Rh** with a covalently anchored rhodium complex (**Rh**) within the nitrobindin variant (NB(Q96C) which promotes *trans*-PPA synthesis).

3-2. Results and Discussion

Preparation of Hybrid Catalysts with a Redesigned Cavity

To redesign size and shape of the cavity, the author focused on amino acid residues within a distance of 6 Å from the rhodium center using a calculated structure of the prototype hybrid biocatalyst NB(Q96C)-**Rh** (Figure 3-2a). First, the native His76 and His158 residues, which are closest to the rhodium moiety, were replaced with Ala and/or Leu to enlarge the cavity. In addition, one of the following six residues, Phe44, Leu75, His76, Lys127, Val128 or Leu148, were individually replaced with a Trp residue to increase the tightness of the cavity. Then, a total of ten NB variants that differed in size and shape of the cavity were designed, produced in *E. coli*, purified, and used as a hybrid protein scaffold (Figure 3-2b).

Five of the heme-free variants (Figure 3-2b: NB4, NB5, NB6, NB9 and NB10) were successfully crystallized and the 3D structures were determined by X-ray crystallography at a resolution of 1.10 Å–2.20 Å (Figure 3-7). The reengineered cavities of the other variants (Figure 3-2b: NB1, NB2, NB3, NB7 and NB8) in the apo-form were evaluated by molecular modeling using FoldX plug-in for the YASARA software[16] (Figure 3-8), and the cavity volume of each variant was calculated and summarized in Table 3-5.[17] Notably the structures of the cavities formed by NB's robust β-barrel scaffold in all variants are similar with that of the wild type.

NB1-**Rh**–NB10-**Rh** hybrid biocatalysts were prepared by conjugating the rhodium complex (**Rh**) containing Cp and COD ligands to each of the freshly reduced variant apoproteins via maleimide coupling

to the Cys96 residue.   The NB variant (1 mM, 200 μL) was mixed with DTT (2 mg/mL), and the solution was incubated at 4 ºC for 1 h.   The reduced protein was purified using a HiTrap desalting column, which was equilibrated with 10 mM Tris-HCl (pH 7.3).   The collected protein solution was diluted to 10 μM with 10 mM Tris-HCl (pH 7.3), and the rhodium complex (**Rh**) in DMSO (1 mg/100 μL) was slowly added to the diluted protein solution.   The mixed solution was incubated at room temperature for 30 min. The precipitate of the rhodium complex was removed by filtration and the solution was again concentrated to 200 μL.   The NB variant linked with the rhodium complex was purified using a HiTrap desalting column eluting with a 10 mM Tris-HCl buffer (pH 8.0) to remove the unbound rhodium complex.   All of the conjugates were confirmed by MALDI-TOF MS analyses (Table 3-4).[18]   The amount of attached rhodium ion in NB variants was also determined by ICP-OES and the Bradford assay (Table 3-4).

a)

b)

	Mutation positions	Cavity volume [Å³]
NB1	H76**A**/Q96C/H158**A**	1161
NB2	H76**A**/Q96C/H158**L**	1006
NB3	H76**L**/Q96C/H158**A**	1145
NB4	H76**L**/Q96C/H158**L**	855
NB5	F44**W**/H76**L**/Q96C/H158**L**	850
NB6	L75**W**/H76**L**/Q96C/H158**L**	891
NB7	H76**W**/Q96C/H158**L**	827
NB8	H76**L**/Q96C/K127**W**/H158**L**	889
NB9	H76**L**/Q96C/V128**W**/H158**L**	651
NB10	H76**L**/Q96C/L148**W**/H158**L**	665
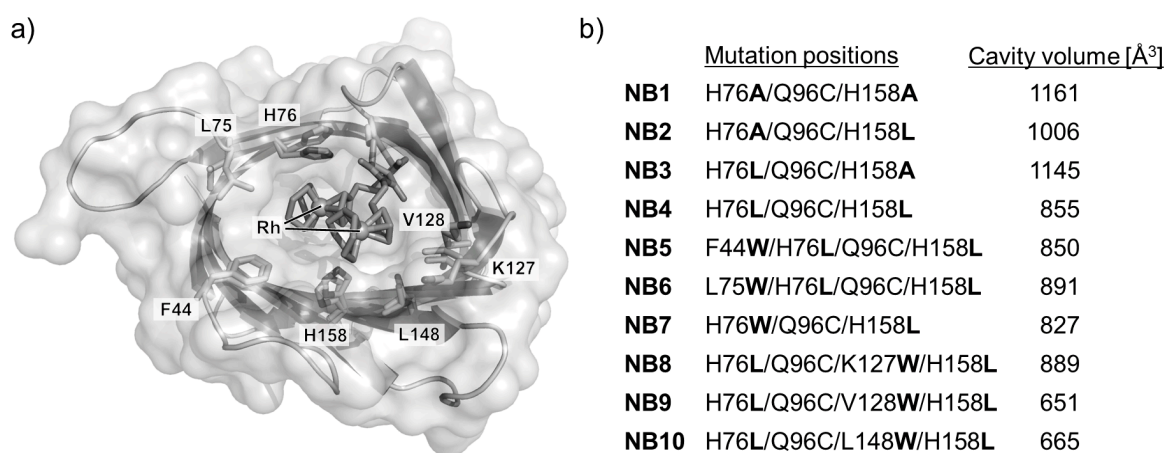
Figure 3-2. Overview on the ten generated NB variants.   (a) The amino acid residues in the vicinity of the rhodium complex within NB(Q96C)-**Rh**.   Two calculated stable conformations of the rhodium complex are shown (the rhodium atom and its ligand are represented by pink and purple sticks, respectively).   Met75 and Met148 were replaced by Leu in all variants.   (b) List of reengineered NB variants for stereoselective PPA synthesis.

Crystal Structure of the Hybrid Catalyst

NB4-**Rh** for the X-ray crystal structure analysis was purified as follows: NB4-**Rh** was loaded onto a HiPrep[TM] 26/60 Sephacryl[TM] S-200 High resolution column equilibrated with 5 mM MES-HCl buffer (pH 6.0) containing NaCl (200 mM).   The fraction of the protein was concentrated to 1 mM.   NB4-**Rh** was then crystallized using the hanging-drop vapor diffusion method at 293 K.

The molecular structure of the hybrid biocatalyst NB4-**Rh**, which represents a **Rh**-linked nitrobindin mutant, NB(H76L/Q96C/H158L), was determined by X-ray crystallography at a resolution of 2.0 Å (Figure 3-3 and Figure 3-9).   The electron density of the rhodium complex anchored to the Cys96 residue via the maleimide linker is clearly observed in the $2F_o - F_c$ map, whereas polyethylene glycol (which is used as a precipitant) is found in the cavity of the crystal structure of apo-NB4 without **Rh** under the same

crystallization conditions (Figure 3-4).[19]   According to the crystal structure, the Cp ligand is located in the hydrophobic surface consisting of L100, V128, I131, L148, L158 and L159 residues.   The catalytically active rhodium center is thus oriented to favor access of the monomer.   It is further noted that the crystal structure correlated well with the structure obtained by the MD simulation data in terms of the position and orientation of the rhodium moiety.   The RMSD for the Cα atoms between NB4-Rh and the apo-NB4 is 0.27 Å.   This indicates that the rigid β-barrel scaffold is retained in the presence of the anchored rhodium complex.   In fact, there is additional support for consistency in the secondary structure of NB4-Rh in the results of CD measurements.   All of the NB hybrids have CD spectra similar to the CD spectra of the rhodium complex-free proteins (Figure 3-10 and 3-11).
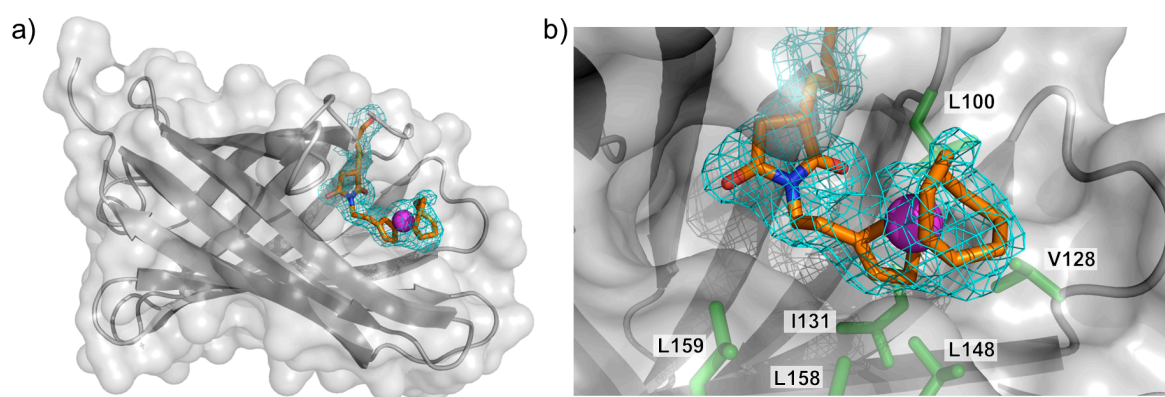
Figure 3-3. Crystal structure of NB4-**Rh** at a 2.0 Å resolution.   **(a)** Whole hybrid catalyst structure and (b) close-up views of the covalently linked rhodium complex.   The $2F_o - F_c$ electron density (1.0 σ) and residues in close proximity are also shown.
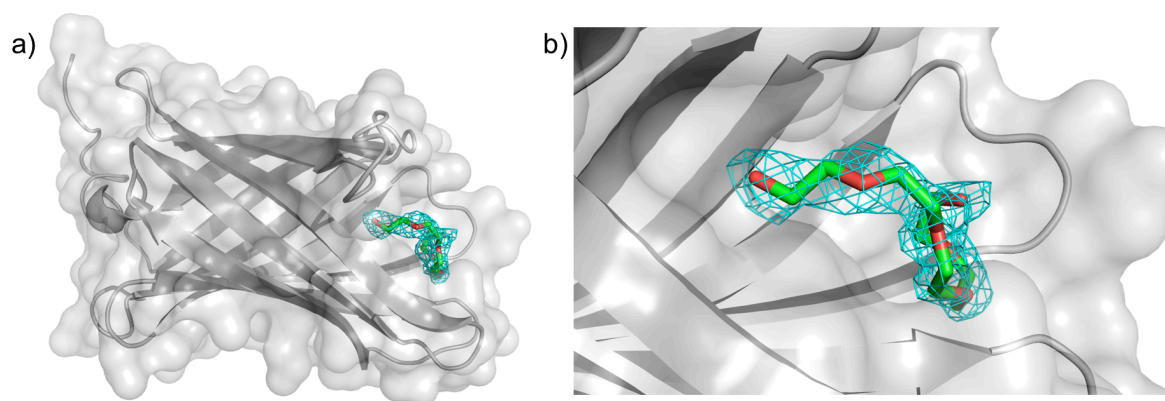
Figure 3-4. Crystal structure of NB4 at a 2.2 Å resolution.   **(a)** Whole structure and (b) close-up views of the polyethylene glycol molecule within the cavity.   The $2F_o - F_c$ electron density (1.0 σ) are shown.

Polymerization of Phenylacetylene

Table 3-1. Polymerization of phenylacetylene at 25 $^{\circ}$C with determined *trans*/*cis* ratios and molecular weight distributions.[a]
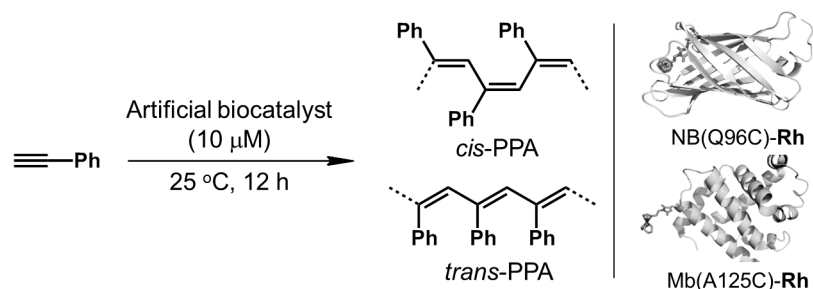
Entry	Artificial biocatalyst	*trans* : *cis*[b]	M_n[c]	M_w/M_n[c]
1	Mb(A125C)-**Rh**	9 : 91	46,500	2.3
2	NB(Q96C)-**Rh**	54 : 46	42,800	2.1
3	NB1-**Rh**	44 : 56	36,500	2.6
4	NB2-**Rh**	45 : 55	38,300	2.2
5	NB3-**Rh**	55 : 45	36,800	2.2
6	NB4-**Rh**	82 : 18	38,900	2.4
7	NB5-**Rh**	77 : 23	38,300	2.3
8	NB6-**Rh**	39 : 61	38,300	2.4
9	NB7-**Rh**	34 : 66	31,100	2.5
10	NB8-**Rh**	28 : 78	31,500	2.4
11	NB9-**Rh**	40 : 60	34,600	2.1
12	NB10-**Rh**	22 : 78	38,600	2.7

[a] The polymerization of phenylacetylene was performed in the presence of the hybrid biocatalyst (10 μM) in a buffer (10 mM Tris-HCl, pH 8.0) under emulsion conditions for 12 h at 25 $^{\circ}$C.   The *trans*/*cis* ratio for 12 h was shown, because the *trans*-selectivity was decreased at 24 h probably due to gradual unfolding of the protein during the polymerization.   [b] Determined by ^{1}H NMR.   [c] Determined by GPC in CHCl$_3$.

All emulsion polymerizations were carried out with an identical hybrid catalyst (10 μM) and phenylacetylene (1 M) in Tris-HCl buffer solution (0.5 mL) at pH 8.0 and room temperature (25 $^{\circ}$C) for 12 h (Table 3-1).   After the polymerization, the reaction mixture was freeze-dried.   The residue was washed with hexane and dried under vacuum to give PPA.   The molecular weights (M_n) and the distribution (M_n/M_w) of PPA were determined by GPC analysis.   Chloroform was used as an eluent at a flow rate of 1.0 mL/min at 40 $^{\circ}$C.   The *trans*/*cis* ratio of PPA was determined by ^{1}H NMR spectroscopy (Figure 3-12). A hybrid biocatalyst, Mb(A125C)-**Rh**, was used as a reference.   This protein has the covalently-linked rhodium complex on the surface of myoglobin and produces PPA with a high *cis* content (>91%) (Table 3-1, entry 1).   In contrast, NB(Q96C)-**Rh** harbors the rhodium complex within the cavity of the

NB(Q96C) and yields PPA with a 54 % *trans* content (Table 3-1, entry2). The reengineered hybrid biocatalysts (NB1-**Rh**, NB2-**Rh**, and NB3-**Rh**), each of which have an enlarged cavity as a result of an Ala replacement, were found to produce PPA with moderate *trans* content of 44%, 45%, and 55%, respectively (see Table 3-1, entries 3–5), which is similar to that of NB(Q96C)-**Rh**. (Table 3-1, entry 2). These results indicate that the larger cavity does not enhance the *trans*-selectivity in PPA production. It is quite interesting that NB4-**Rh** (two His residues are replaced with Leu residues) produces PPA with 82% *trans* content, the highest among all generated hybrid catalysts (Table 3-1, entry 6). The polymer produced by NB5-**Rh,** which has a cavity similar in size and shape to the cavity to NB4-**Rh** (Figure 3-7), produces PPA with a high *trans* content of 77% (Table 3-1, entry 7).

Selective PPA polymerization promoted by the hybrid biocatalysts with small cavities was also evaluated. The hybrids, NB6-**Rh**, NB7-**Rh**, and NB8-**Rh,** have a partially crowded cavity and produce PPAs with lower *trans* content (39, 34 and 28%, see Table 3-1, entries 8–10). The Trp residue comes into contact with the rhodium moiety in NB6–NB8-**Rh** and could interface with the monomer access to the catalytic center (Figure 3-13), resulting in reduction of the *trans* content. NB9-**Rh** and NB10-**Rh** also have a crowded cavity. These variants also produce PPA with lower *trans* content (40 and 22%, see Table 3-1, entries 11 and 12). Consequently, NB5-**Rh** as well as NB4-**Rh** produced PPA with high *trans* content because a large cavity enables a precise positioning of the **Rh** which is a prerequisite to increase the *trans* content in PPA synthesis.

Molecular Dynamic Simulation

As the structural basis for the modeling of the hybrid biocatalysts, the X-ray structure of native nitrobindin (PDB: 2A13) and the NB variants (NB4, 5, 6, 9 and 10), the calculated structures of the NB variants (NB1, 2, 3, 7 and 8) and the high resolution X-ray structure of the rhodium complex (**Rh**) were used. According to the previously published procedure,[14] the modeling was carried out using YASARA[20] Structure Vers. 13.6.16. Superimposed structures of NB1-**Rh**, NB4-**Rh**, and NB6-**Rh** are shown in Figure 3-5. The total energy of the rhodium complex and the surrounding fourteen amino acid residues are plotted against the distance between the rhodium ion and Cα of Leu75, showing the conformational distribution of the rhodium moiety within the cavity. The result of NB1-**Rh** clearly indicates the existence of two major conformations, suggesting the substantial flexibility of the rhodium active site (Figure 3-5a). The NB1-**Rh** biocatalyst produces PPAs with lower *trans* content. The decrease of *trans* selectivity could be thus explained by uncontrolled access of the monomer owing to the flexibility of the rhodium active site. The MD calculation also suggests that the rhodium moiety possesses a defined orientation within the NB4 cavity (Figure 3-5b), thereby providing a confined environment for the stereoselective polymerization of *trans*-PPA. Although the rhodium moiety in NB6 having Trp residue exhibits a narrowly-distributed

conformation, the NB6-**Rh** produces PPA with lower *trans* content.   The bulky Trp residue nearby within the cavity might influence the access of the monomer to the rhodium center (Figure 3-5c).
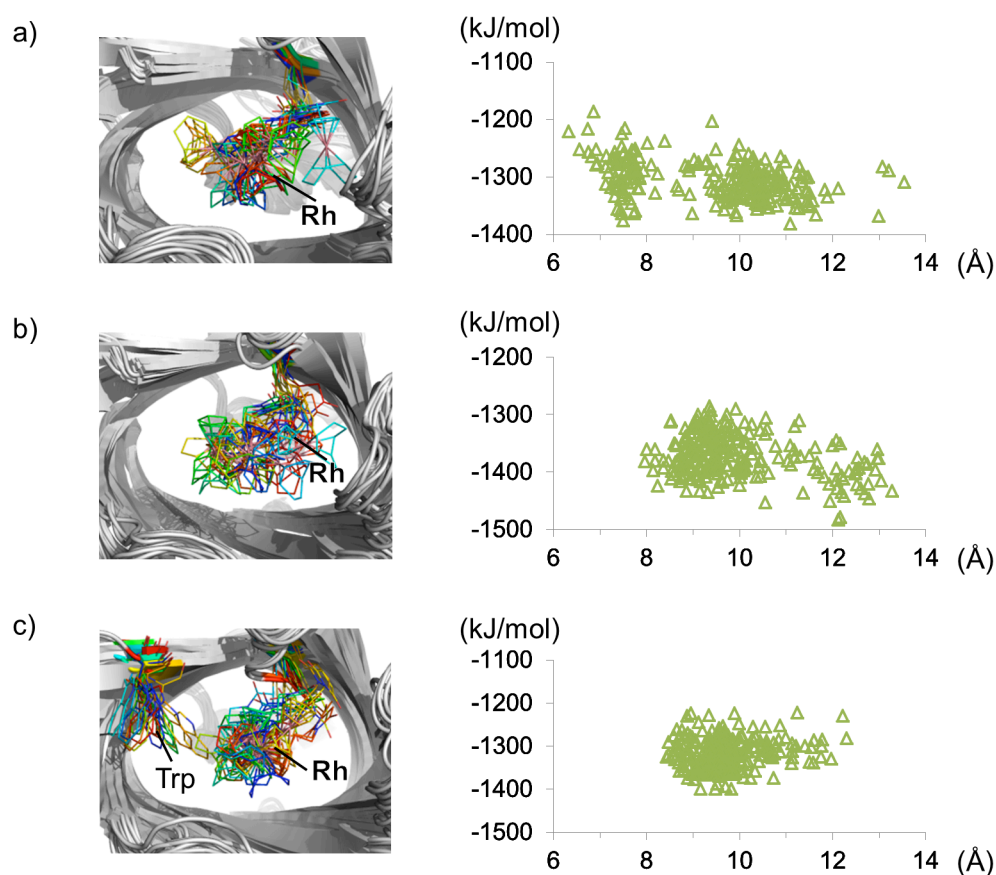

Figure 3-5. The distribution of the rhodium complex within the cavity of (a) NB1-**Rh**, (b) NB4-**Rh**, and (c) NB6-**Rh** during MD calculation at 298K for 1500 ps.   Selected sixteen snapshot structures are shown in rainbow colors (left), and the total energy of the rhodium complex and the surrounding fourteen amino acid residues (position 41, 44, 46, 75, 76, 96, 98, 100, 127, 128, 148, 150, 158, and 159) are plotted against the distance between the rhodium ion and Cα of Leu75 (right).   Total 240 minimized structures are plotted as green triangles.

3-3. Summary

In conclusion, the author reengineered the cavity of rhodium complex-linked nitrobindin by computationally-guided site-directed mutagenesis, resulting in identification of key residues which modulate and significantly improve the trans/cis-stereoselectivity in phenylacetylene polymerization. Particularly, the hybrid biocatalysts, NB4-**Rh** (NB(H76L/Q96C/H158L)-**Rh**) and NB5-**Rh** (NB(F44W/H76L/Q96C/H158L)-**Rh**), yielded an inverted stereopreference trans-PPA synthesis (up to 82% *trans*).   X-ray crystal structure and MD simulation results yielded molecular insights on how stereopreference is guided within NB-**Rh** hybrid catalysts and how monomer access to the rhodium center is controlled.

3-4. Experimental Section

Instruments

^{1}H NMR spectra were recorded on a Bruker DPX400 NMR spectrometer. High-resolution magic angle spinning (HR-MAS) experiments were performed on a Varian Unity Inova 600 MHz NMR spectrometer equipped with a 4 mm gHX Nanoprobe. ESI-TOF MS analyses were performed on an Applied Biosystems Mariner API-TOF Workstation or a Bruker micrOTOF focus III mass spectrometer and MALDI-TOF MS analyses were performed on a Bruker autoflex III mass spectrometer. UV-vis experiments were conducted using a Shimadzu UV-3150 double-beam spectrophotometer and BioSpec-nano. Mutagenesis and Amplification were performed using a Bio-Rad PCR T100[TM] thermal cycler. Purification of the proteins was performed using a GE healthcare ÄKTA Purifier system at 4 ºC. Circular dichroism (CD) spectra were recorded with a JASCO J720S spectrometer. ICP-OES was performed on a Shimadzu ICPS-8100 emission spectrometer. The pH values were monitored with a Horiba F-52 pH meter. Air-sensitive procedures were performed in an MBraun glovebox. Gel permeation chromatography was performed on a TOSOH SC8020 apparatus with a refractive index detector using a TOSOH TSKgel G4000HHR column.

Materials

The oligonucleotides were obtained from Invitrogen, Inc. (Japan). Restriction enzymes were obtained from Takara Bio Inc. (Japan) and New England BioLabs Inc. (Japan). Nucleotide sequences were determined by Fasmac (Japan). The rhodium complex was synthesized as described in the previous report.[14] All reagents of the highest guaranteed grade were purchased and used as received unless otherwise noted. A standard rhodium solution for inductively coupled plasma optical emission spectroscopy (ICP-OES) was purchased from Wako (Japan). Distilled water was demineralized by a Barnstead NANOpure DIamond[TM] apparatus.

Subcloning of Expression Plasmids for NB Variants

The NB(M75L/Q96C/M148L) gene with *Strep*-tag II was amplified as the pDEST14 plasmid encoding the NB(M75L/Q96C/M148L) gene as a template. The forward primer coding the *NdeI* restriction site and *Strep*-tag II gene (i) 5'-ATCTTACATATGTGG-AGCCACCCGCAGTTCGAAAAAAATCAACTGCA ACAACTGCAAAATCCGGGC-3′ and the reverse primer encoding *XhoI* site (ii) 5'-TGGTGCTCGAGCTATTACAGTTT GTCCAGGATGGCTTTCAGGTGC-3′ were used. The PCR product was digested with *NdeI* and *XhoI*, and subcloned into the pET42b(+) vector. The other

expression plasmids for the NB variant were constructed according to the standard protocol of the QuickChangeII site-direct mutagenesis kit (Stratagene) using the expression plasmids for NB(M75L/Q96C/M148L) as a template. The plasmids amplified by PCR using *PfuUltra*^{TM} High-Fidelity DNA Polymerase (Agilent Technologies), and the amplified plasmids were treated with DpnI restriction enzymes (Stratagene). The plasmids for the variant were transformed into DH5α competent cells. The forward and reverse primers used in this study are listed in Scheme 3-1.

Expression and Purification of NB Variants

The resulting expression plasmids encoding the NB variant gene with *Strep*-tag II were transformed into *E. coli* BL21 Star™ (DE3). Each 1.5 L of a LB medium containing kanamycin (50 μg/mL) was inoculated with a 10 mL culture (OD_{600} = 0.5 ~ 0.7) of the transformed cells. The cells were shaken at 37 ºC and 180 rpm until the OD_{600} of the culture reached at approximately 0.5. Isopropyl-β-D-1-thiogalactopyranoside (IPTG) was added to a final concentration of 0.5 mM to induce the expression. The incubation was continued at 30 ºC and 160 rpm for approximately 24 h. The cells were harvested by centrifugation at 12000g for 9 min.

The harvested cells were resuspended in ca. 100 mL of 100 mM Tris-HCl buffer (pH 8.0) containing 1 mM EDTA, 150 mM NaCl, and 10 mM DTT. The cells were lysed by sonication (Branson Sonifier 250, 70% duty cycle, output = 6 cycle for 30 sec). After centrifugation at 12000g for 9 min, benzonase nuclease was added to the collected supernatant. The supernatant was loaded on a Strep-Tactin column (IBA, Germany), which was equilibrated in 100 mM Tris-HCl buffer (pH 8.0) containing 1 mM EDTA and 150 mM NaCl. The target protein was collected in 100 mM Tris-HCl buffer (pH 8.0) containing 1 mM EDTA, 150 mM NaCl, and 2.5 mM desthiobiotin. Furthermore, the protein was purified using a HiTrap DEAE and benzamidine column (GE Healthcare) in 100 mM Tris-HCl buffer (pH 8.0) containing 1mM EDTA and 150 mM NaCl. The target protein was concentrated to approximately 1.0 mM using an Amicon-stirred ultrafiltration cell with a 10-kDa molecular weight cutoff membrane (Millipore). The purified NB mutants were characterized by SDS-PAGE (Figure 3-6) and MALDI-TOF MS (Table 3-2).

Crystallization and Structure Analysis

The NB variants (NB5, NB6, NB9, and NB10) for the X-ray crystal structure analysis were crystallized by a hanging-drop vapor diffusion method at 293 K. The crystals were grown on siliconized coverslips by equilibrating a mixture containing 1.0 μL of the protein solution (1.0 mM protein in 5 mM MES buffer, pH 6.0, 200 mM NaCl, 1 mM dithioerythritol) and 1.0 μL of the reservoir solution (100 mM Tris-HCl buffer, pH 8.0, polyethylene glycol 2000 (18 ~ 20%)) with 100 μL of the reservoir solution (condition 1). The needle-shaped crystals of NB4-**Rh** and NB4 as a reference were obtained by equilibrating a mixture

containing 2.0 μL of the protein solution (1.0 mM protein in 5 mM MES buffer, pH 6.0, 200 mM NaCl) and 2.0 μL of the reservoir solution (100 mM MES buffer, pH 6.5, polyethylene glycol 400 (26%)) with 100 μL of the reservoir solution at 293K using the hanging-drop vapor diffusion method (condition 2).

The crystals of NB5, NB6, NB9, and NB10 grown under the condition 1 were fished with standard nylon loop, soaked in cryoprotectant solution (67%(v/v) Paraton-N, 28%(v/v) paraffin oil, 5%(v/v) glycerol), and flash-cooled in an N_2 gas stream at 100 K. The crystals of NB4-**Rh** and NB4 grown under the condition 2 were fished and directly flash-cooled in the N_2 gas stream. The X-ray diffraction data were collected at SPring-8 BL44XU or using in-house system.

The data were integrated and scaled using the program *HKL2000*,[21] and further processed using the *CCP4* software package.[22] The initial phases were obtained by the molecular replacement method using the program *PHASER*.[23] The reported structure of nitrobindin (PDB code 2A13) was used as a search model. The model was refined with multiple rounds of manual rebuilding using *COOT*,[24] and crystallographic refinement by *REFMAC5*.[25] The data collection and refinement statistics are summarized in Table 3-3. Figures depicting the structure were prepared with *PYMOL* (http://www.pymol.org). The atomic coordinates and structure factors were deposited into the Protein Data Bank, (http://www.rcsb.org/ PDB codes: 3WJB for NB4, 3WJC for NB4-**Rh**, 3WJD for NB5, 3WJE for NB6, 3WJF for NB9, 3WJG for NB10).

Molecular Dynamic Simulation

The modeling was carried out using YASARA[20] Structure Vers. 13.6.16 employing force field AMBER03[26] for protein residues and GAFF[27] using AM1/BCC[28] partial charges for the catalyst covalently bound to Cys96. The metal was replaced by cobalt, since no parameters are available for rhodium. To maintain the correct coordination geometry, the distances from the metal to all five carbon atoms of the Cp ligand were constrained to 2.2 Å and the η^5 coordination is represented by five force field arrows. To maintain η^2 coordination of the COD ligand, four force field arrows were defined and the distances were constrained to 2.0 Å, according to the X-ray structure of **Rh**. The partial charge of the metal was set to +1 and the total charge of **Rh** was set to zero. The bond orders for the Cp ligand were defined as 1.67 Å to maintain an aromatic system. **Rh** was placed manually in the cavity adjacent to Cys96 and a bond was defined from the Cys sulfur atom to the C1 or C2 atom of the maleimide group. The constructed hybrid catalysts were solvated in a box of TIP3P water molecules using periodic boundaries at pH 7 and a density of 0.997 g/mL. Four starting structures representing the cysteine-maleimide linker isomers were analyzed and favorable models were identified for covalent attachment to the reactive maleimide atoms C1 and C2 by simulated annealing and steepest descent minimization. The pre-minimized structures were relaxed using molecular dynamics calculations at 298 K for 1500 ps and snapshots were taken at 25 ps intervals to analyze the binding modes. Each snapshot

was minimized to 0 K by simulated annealing and steepest descent minimization, and then the total energy (kJ/mol) of the 14 specific amino acids (position 41, 44, 46, 75, 76, 96, 98, 100, 127, 128, 148, 150, 158 and 159) and **Rh** in the each minimized structures were analyzed (Figure 3-13–3-16).

Scheme 3-1. The forward and reverse primers for subcloning of expression plasmids.

H76A, forward primer
5'-CTGGAATCGGGTGCACCGGCACTGGCAGAGAGTGGTTATTTTCG-3'

H76A, reverse primer
5'-CGAAAATAACCACTCTCTGCCAGTGCCGGTGCACCCGATTCCAG-3'

H158A, forward primer
5'-CGACCACGAATCCGCTGCAACCGGCACTGAAAGCCATCCTGGAC-3'

H158A, reverse primer
5'-GTCCAGGATGGCTTTCAGTGCCGGTTGCAGCGGATTCGTGGTCG-3'

H76L, forward primer
5'-GTGCACCGCTGCTGGCAGAGAGTGGTTATTTTC-3'

H76L, reverse primer
5'-GAAAATAACCACTCTCTGCCAGCAGCGGTGCAC-3'

H158L, forward primer
5'-GAATCCGCTGCAACCGCTGCTGAAAGCCATCCTG-3'

H158L, reverse primer
5'-CAGGATGGCTTTCAGCAGCGGTTGCAGCGGATTC-3'

F44W, forward primer
5'-CCGACCATTCCGAGCTGGCGCTATGGCGAAGAG-3'

F44W, reverse primer
5'-CTCTTCGCCATAGCGCCAGCTCGGAATGGTCGG-3'

L75W, forward primer
5'-GAATCGGGTGCACCGTGGCTGGCAGAGAGTGG-3'

L75W, reverse primer
5'-CCACTCTCTGCCAGCCACGGTGCACCCGATTC-3'

H76W, forward primer
5'-GTGCACCGCTGTGGGCAGAGAGTGGTTATTTTC-3'

H76W, reverse primer
5'-GAAAATAACCACTCTCTGCCCACAGCGGTGCAC-3'

K127W, forward primer
5'-GTGGGCAACGCGTCCTGGGTTAAAGAAATCAGC-3'

K127W, reverse primer
5'-GCTGATTTCTTTAACCCAGGACGCGTTGCCCAC-3'

V128W, forward primer
5'-GGCAACGCGTCCAAATGGAAAGAAATCAGCCGC-3'

V128W, reverse primer
5'-GCGGCTGATTTCTTTCCATTTGGACGCGTTGCC-3'

L148W, forward primer
5'-GAGTTATGTGGTTCGTTGGAGCACGACCACGAATC-3'

L148W, reverse primer
5'-GATTCGTGGTCGTGCTCCAACGAACCACATAACTC-3'

Table 3-2. MALDI-TOF MS results of nitrobindin variants.

Nitrobindin		Calcd.	Found
NB1	$C_{874}H_{1365}N_{231}O_{260}S_2$	19332.76	19333.99
NB2	$C_{877}H_{1371}N_{231}O_{260}S_2$	19374.84	19375.94
NB3	$C_{877}H_{1371}N_{231}O_{260}S_2$	19374.84	19375.87
NB4	$C_{880}H_{1377}N_{231}O_{260}S_2$	19416.92	19415.29
NB5	$C_{882}H_{1378}N_{232}O_{260}S_2$	19455.95	19454.12
NB6	$C_{885}H_{1376}N_{232}O_{260}S_2$	19489.97	19490.19
NB7	$C_{885}H_{1376}N_{232}O_{260}S_2$	19489.97	19488.20
NB8	$C_{885}H_{1375}N_{231}O_{260}S_2$	19474.95	19474.97
NB9	$C_{886}H_{1378}N_{232}O_{260}S_2$	19504.00	19504.53
NB10	$C_{885}H_{1376}N_{232}O_{260}S_2$	19489.97	19491.25

Table 3-3. Statistics of X-ray crystallographic data and structure refinement.

Data collection	NB4	NB5	NB6	NB9	NB10	NB4-**Rh**
X-ray source	MicroMax-007HF	SPring-8 BL44XU	SPring-8 BL44XU	SPring-8 BL44XU	SPring-8 BL44XU	MicroMax-007HF
Detector	R-AXIS VII	Rayonix MX300HE	Rayonix MX300HE	Rayonix MX300HE	Rayonix MX300HE	R-AXIS VII
Wavelength (Å)	1.54178	0.90000	0.90000	0.90000	0.90000	1.54178
Resolution (Å)	50 – 2.20	50 – 1.10	50 – 1.70	50 – 2.20	50 – 1.10	50 – 2.00
(outer shell)	(2.28 – 2.20)	(1.14 – 1.10)	(1.76 – 1.70)	(2.28 – 2.20)	(1.14 – 1.10)	(2.07 – 2.00)
Space group	$P4_1$	$P2_12_12$	$C2$	$C2$	$P2_12_12$	$P4_1$
Unit cell parameters (Å, deg.)	$a = b = 67.80, c = 130.19$	$a = 59.85, b = 79.42, c = 36.33$	$a = 88.56, b = 72.54, c = 59.80, \beta = 111.63$	$a = 88.60, b = 73.27, c = 59.52, \beta = 111.75$	$a = 59.94, b = 79.41, c = 36.48$	$a = b = 67.89, c = 129.90$
No. of total reflections	183,768	522,074	139,540	55,269	607,803	191,403
No. of unique	29,400	70,416	37,730	17,383	70,604	38,003
Completeness (%)	98.3 (97.2)	98.9 (98.8)	97.3 (94.5)	95.1 (90.3)	98.9 (97.7)	95.9 (93.0)
R_{sym} [a, b]	8.2 (34.4)	3.4 (29.3)	3.2 (29.6)	5.0 (29.4)	4.2 (33.9)	9.1 (35.7)
$I/\sigma(I)$	14.9 (3.3)	56.3 (4.7)	40.4 (3.1)	23.0 (2.8)	54.7 (3.8)	11.1 (3.0)
Refinement						
Resolution (Å)	20 – 2.20	40 – 1.10	40 – 1.70	40 – 2.20	40 – 1.10	20 – 2.00
No. of reflections	27,781	66,607	35,779	16,290	67,012	35,981
R_{cryst} / R_{free} (%)	19.4 / 24.8	14.5 / 16.6	17.8 / 21.6	20.6 / 27.1	15.8 / 18.8	23.9 / 29.5
Mean B-factor (Å^2)	34.2	19.4	26.4	36.1	23.4	35.2
No. of non-H atoms	2,570	1,471	2,613	2,506	1,477	2,619
Rmsd from native nitrobindin(2A13)	0.47	0.16	0.23	0.25	0.19	0.49
Bond lengths (Å) / angles (deg.)	0.029 / 2.674	0.025 / 2.250	0.020 / 2.154	0.016 / 1.961	0.023 / 2.194	0.009 / 4.241

[a] Numbers in parentheses are for the highest-resolution shell.

[b] $R_{sym} = \Sigma_{hkl}\Sigma_i |I_i(hkl) - <I(hkl)>| / \Sigma_{hkl}\Sigma_i I_i(hkl)$ where $<I(hkl)>$ is the average intensity of the i observations. $R = \Sigma_{hkl}|F_{obs}(hkl) - F_{calc}(hkl)| / \Sigma_{hkl}F_{obs}(hkl)$, where F_{obs} and F_{calc} are observed and calculated structure factors, respectively. R_{free} was calculated with 5% of the reflections

Table 3-4. MALDI-TOF MS results and Rh content of the rhodium complex-linked NB variants.

Biocatalysts		Calcd.	Found	Rh content[a]
NB1-**Rh**	$C_{893}H_{1387}N_{232}O_{262}S_2Rh$	19732.05	19731.24	84
NB2-**Rh**	$C_{896}H_{1393}N_{232}O_{262}S_2Rh$	19774.13	19773.89	70
NB3-**Rh**	$C_{896}H_{1393}N_{232}O_{262}S_2Rh$	19774.13	19774.10	81
NB4-**Rh**	$C_{899}H_{1399}N_{232}O_{262}S_2Rh$	19816.21	19814.52	90
NB5-**Rh**	$C_{901}H_{1400}N_{233}O_{262}S_2Rh$	19855.24	19854.62	97
NB6-**Rh**	$C_{904}H_{1398}N_{233}O_{262}S_2Rh$	19889.26	19889.56	56
NB7-**Rh**	$C_{904}H_{1398}N_{233}O_{262}S_2Rh$	19889.26	19888.29	52
NB8-**Rh**	$C_{904}H_{1397}N_{232}O_{262}S_2Rh$	19874.24	19874.45	60
NB9-**Rh**	$C_{905}H_{1400}N_{233}O_{262}S_2Rh$	19903.29	19902.29	63
NB10-**Rh**	$C_{904}H_{1398}N_{233}O_{262}S_2Rh$	19889.26	19889.98	36

[a] The concentration of Rh atom in protein matrixes was determined by ICP-OES MS and Bradford assay.

Table 3-5. A series of reengineered NB variants with the β-barrel cavity volumes.

Entry	Variants[a]	Cavity volume [Å^3][b]
NB1	H76**A**/Q96C/H158**A**	1161
NB2	H76**A**/Q96C/H158**L**	1006
NB3	H76**L**/Q96C/H158**A**	1145
NB4	H76**L**/Q96C/H158**L**	855
NB5	F44**W**/H76L/Q96C/H158L	850
NB6	L75**W**/H76L/Q96C/H158L	891
NB7	H76**W**/Q96C/H158L	827
NB8	H76L/Q96C/K127**W** /H158L	889
NB9	H76L/Q96C/V128**W** /H158L	651
NB10	H76L/Q96C/L148**W** /H158L	665

[a] In the all of variants, both Met75 and Met148 of aponitrobindin are replaced with Leu residues.   The terms, M75L and M148L are omitted to clarify.   [b] Calculated by Pocket-finder.

Table 3-6. The yield of the polyphenylacetylene.

Hybrid biocatalysts	yield / µg[a]
Mb(A125C)-**Rh**	104
NB(Q96C)-**Rh**	2.6
NB1-**Rh**	12
NB2-**Rh**	13
NB3-**Rh**	11
NB4-**Rh**	6.5
NB5-**Rh**	10
NB6-**Rh**	20
NB7-**Rh**	15
NB8-**Rh**	25
NB9-**Rh**	6.7
NB10-**Rh**	18

[a] The polymerization of phenylacetylene was performed in the presence of the hybrid biocatalyst (10 µM) in a buffer (10 mM Tris-HCl, pH 8.0) under emulsion conditions for 12 h at 25 $^{\circ}$C. The yield was determined by ^{1}H NMR.
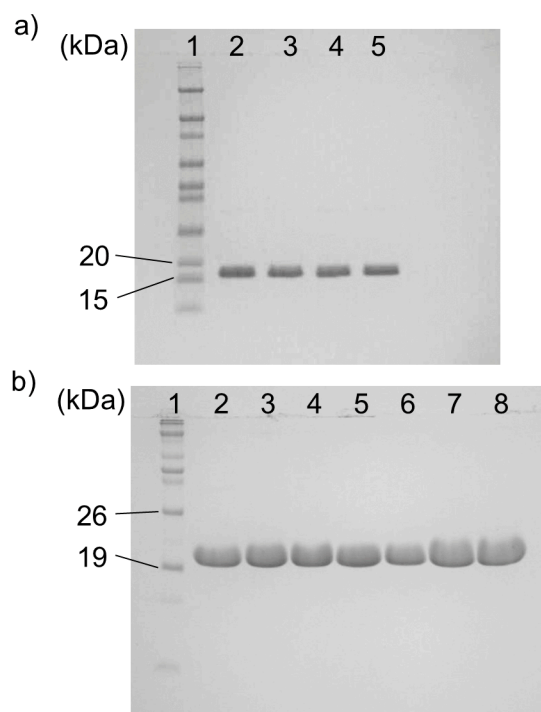
Figure 3-6. SDS-PAGE analysis of NB variants. (a) Line 1: Novex$^{®}$ sharp protein standard, Line 2: NB1, Line 3: NB2, Line 4: NB3, Line 5: NB4. (b) Line 1: BenchMark^{TM} pre-stained protein ladder, Line 2: NB5, Line 3: NB6, Line 4: NB7, Line 5: NB8, Line 6: NB9, Line 7: NB10, Line 8: NB4.
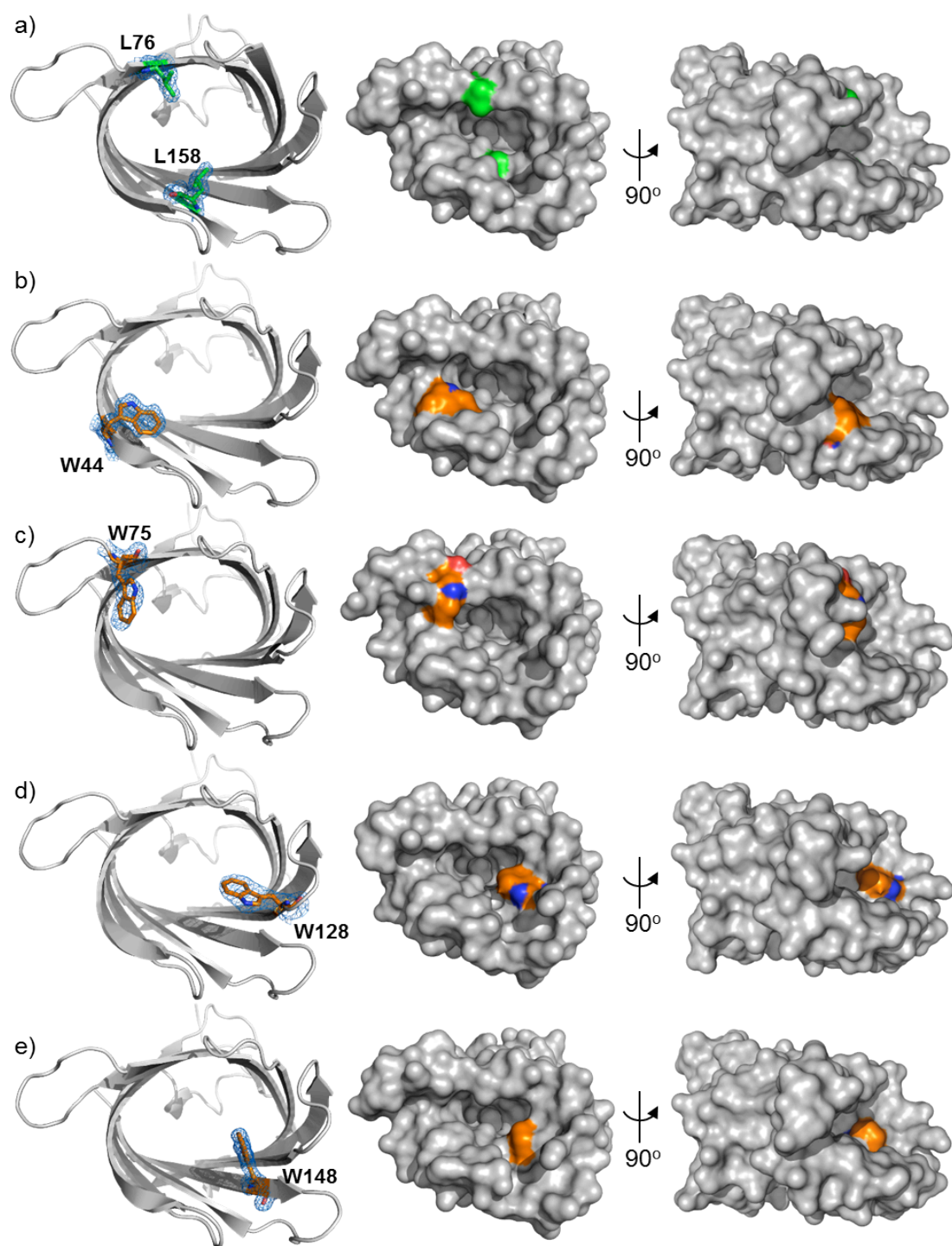
Figure 3-7. Crystal structures of (a) NB4, (b) NB5, (c) NB6, (d) NB9, and (e) NB10. Leu and Trp residues are colored in green and orange, respectively. The β-barrel structure of the variants are superimposable with that of native NB (PDB: 2A13) with a RMSD value of less than 1.0 Å.
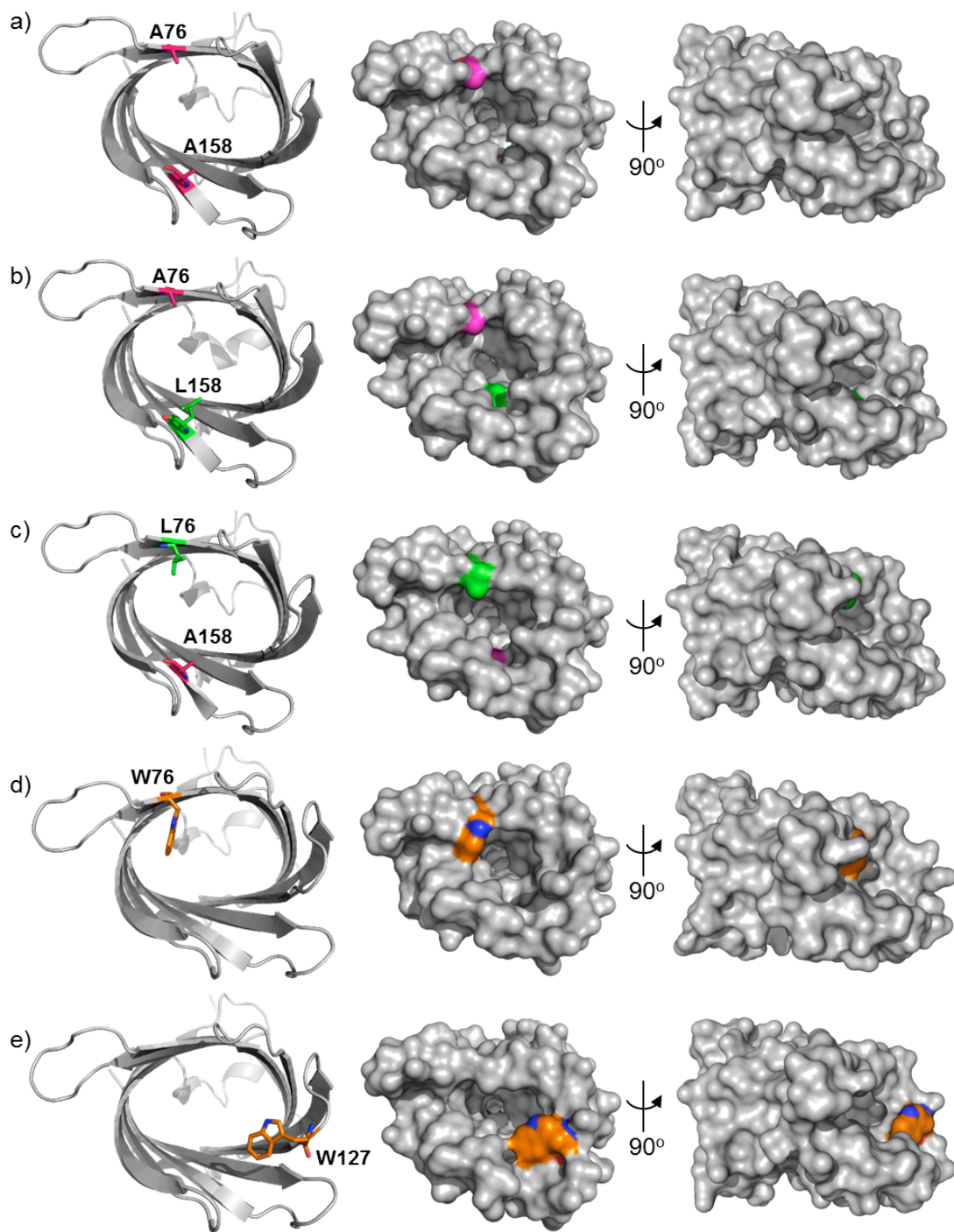
Figure 3-8. Calculated structures of (a) NB1, (b) NB2, (c) NB3, (d) NB7, and (e) NB8. Ala, Leu, and Trp residues are colored in pink, green, and orange, respectively.
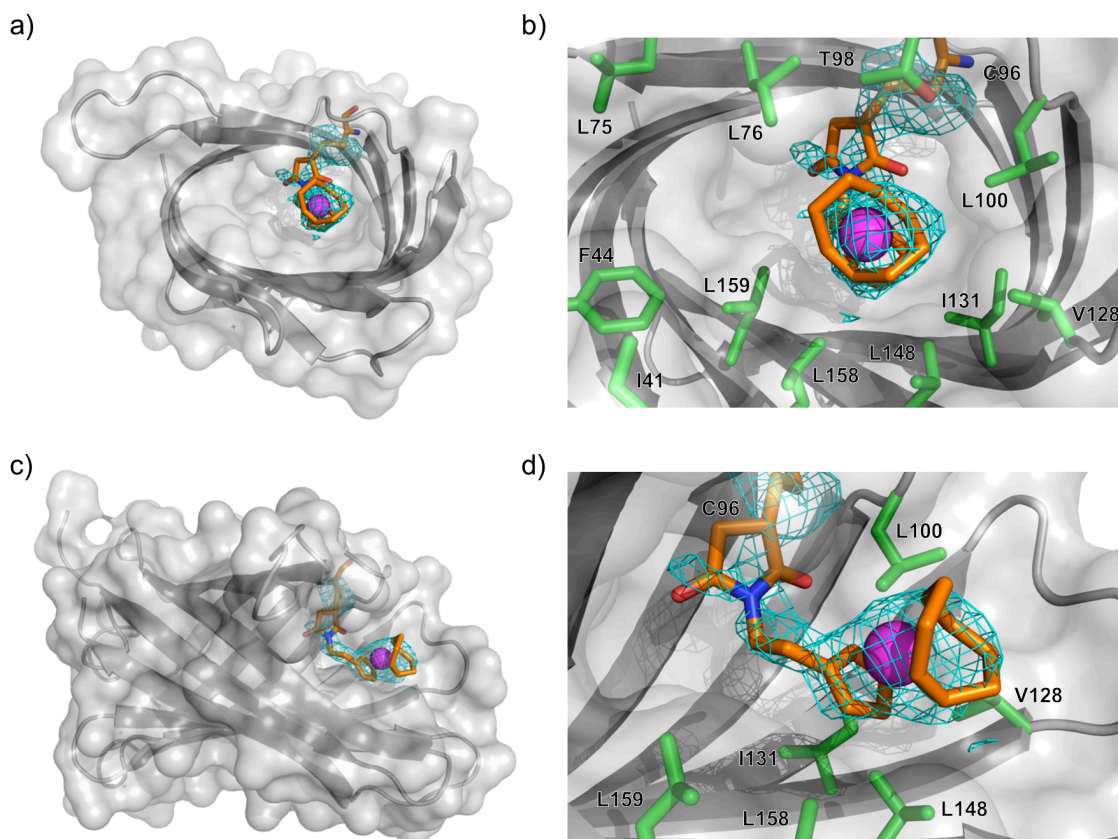
Figure 3-9. Crystal structure of NB4-**Rh**. (a) Front view, (b) enlarged front view around the rhodium moiety, (c) side view, and (d) enlarged side view around the rhodium moiety. The F_o–F_c omit map (light blue) is contoured at 3 σ, covering the rhodium complex and Cys96. (Rhodium in purple, carbon in orange, nitrogen in blue, oxygen in red, and the neighboring hydrophobic residues in green.)
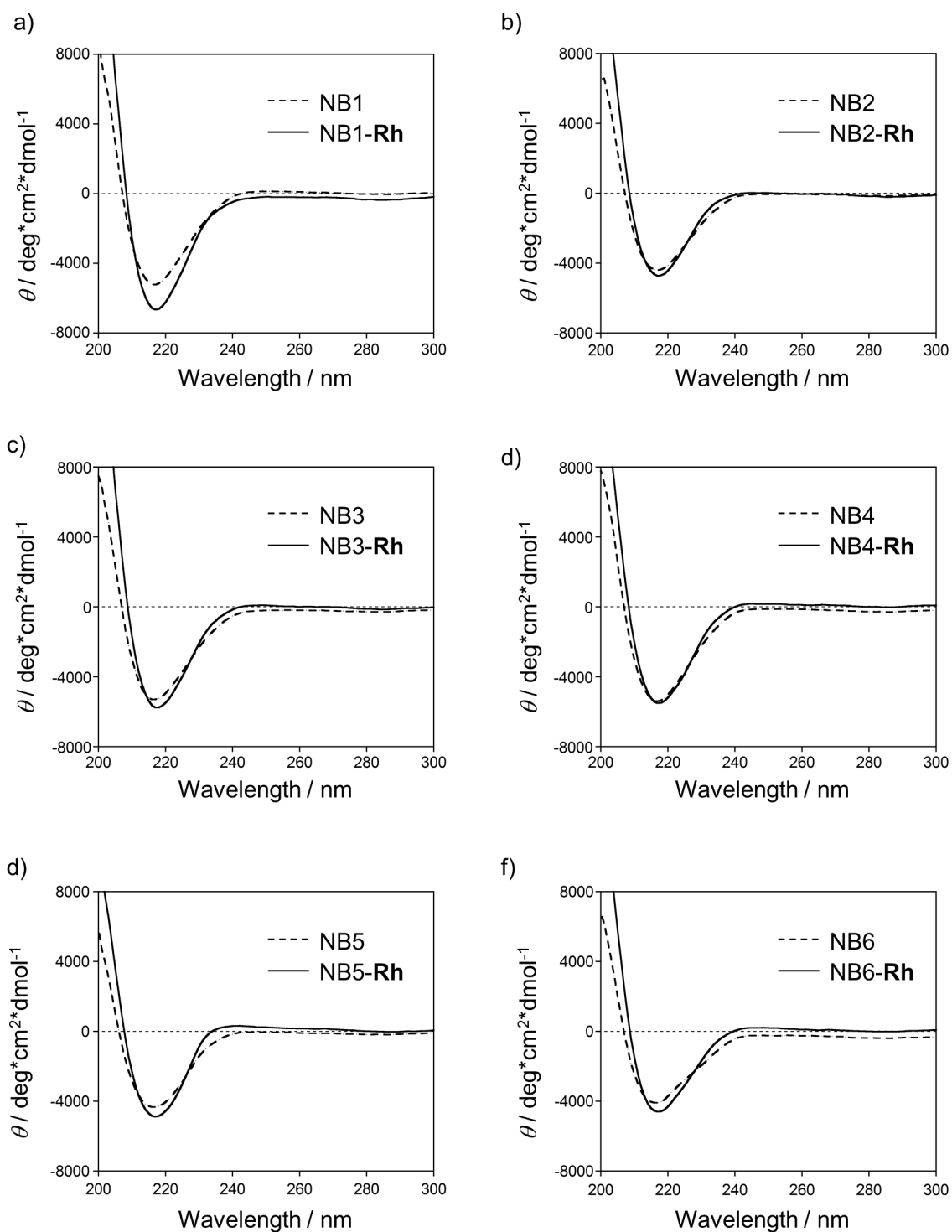
Figure 3-10. CD spectra of the rhodium complex-linked (in solid line) and apo (in dashed line) forms of (a) NB1, (b) NB2, (c) NB3, (d) NB4, (e) NB5, and (f) NB6.
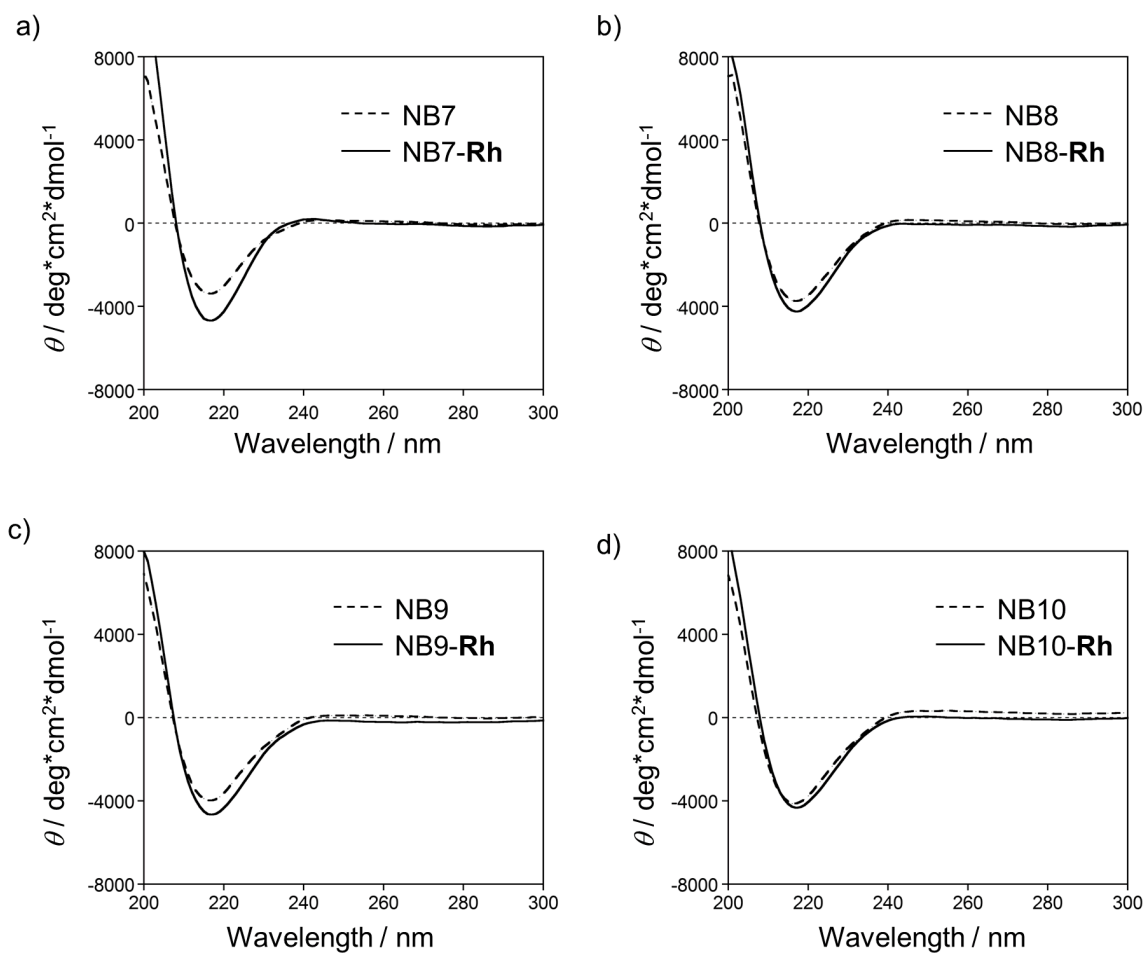
Figure 3-11. CD spectra of the rhodium complex-linked (in solid line) and apo (in dashed line) forms of (a) NB7, (b) NB8, (c) NB9, and (d) NB10.
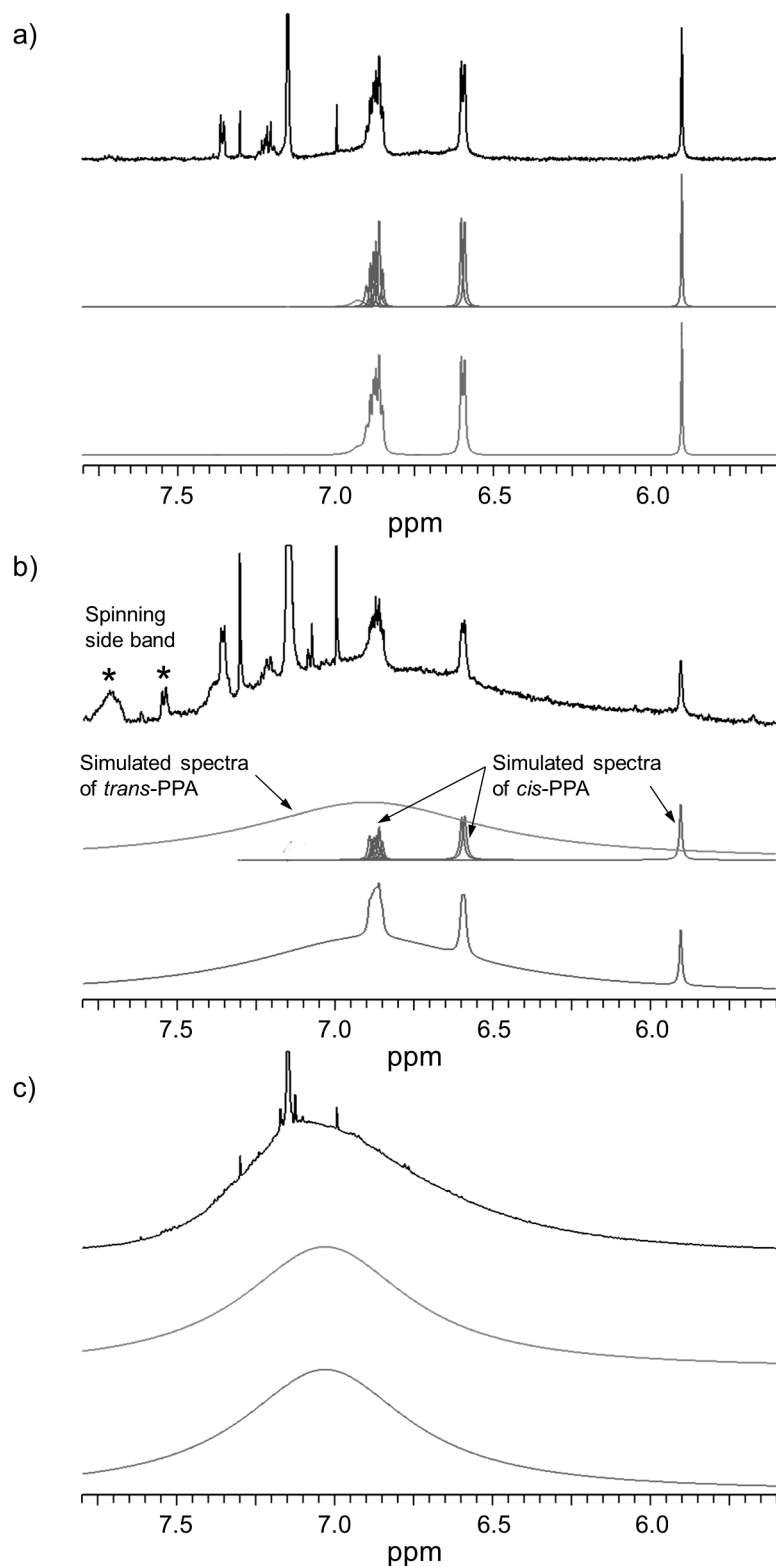
Figure 3-12. Determination of stereostructure of PPAs in CDCl₃ by ¹H NMR (600 MHz). The spectra were recorded by a high-resolution magic angle spinning (HR-MAS) method using a nano probe (spinning speed is around 2,000 Hz). The spinning side band is from the residual solvent and water. (a) PPA prepared by Mb(A125C)-**Rh**, (b) PPA prepared by NB4-**Rh**, and (c) *trans*-PPA prepared by WCl₆ catalyst. In each spectrum, the observed spectra (black and top), simulated spectra of *cis* (blue and middle) and *trans* (red and middle), and the sum of the simulated spectra (purple and bottom).
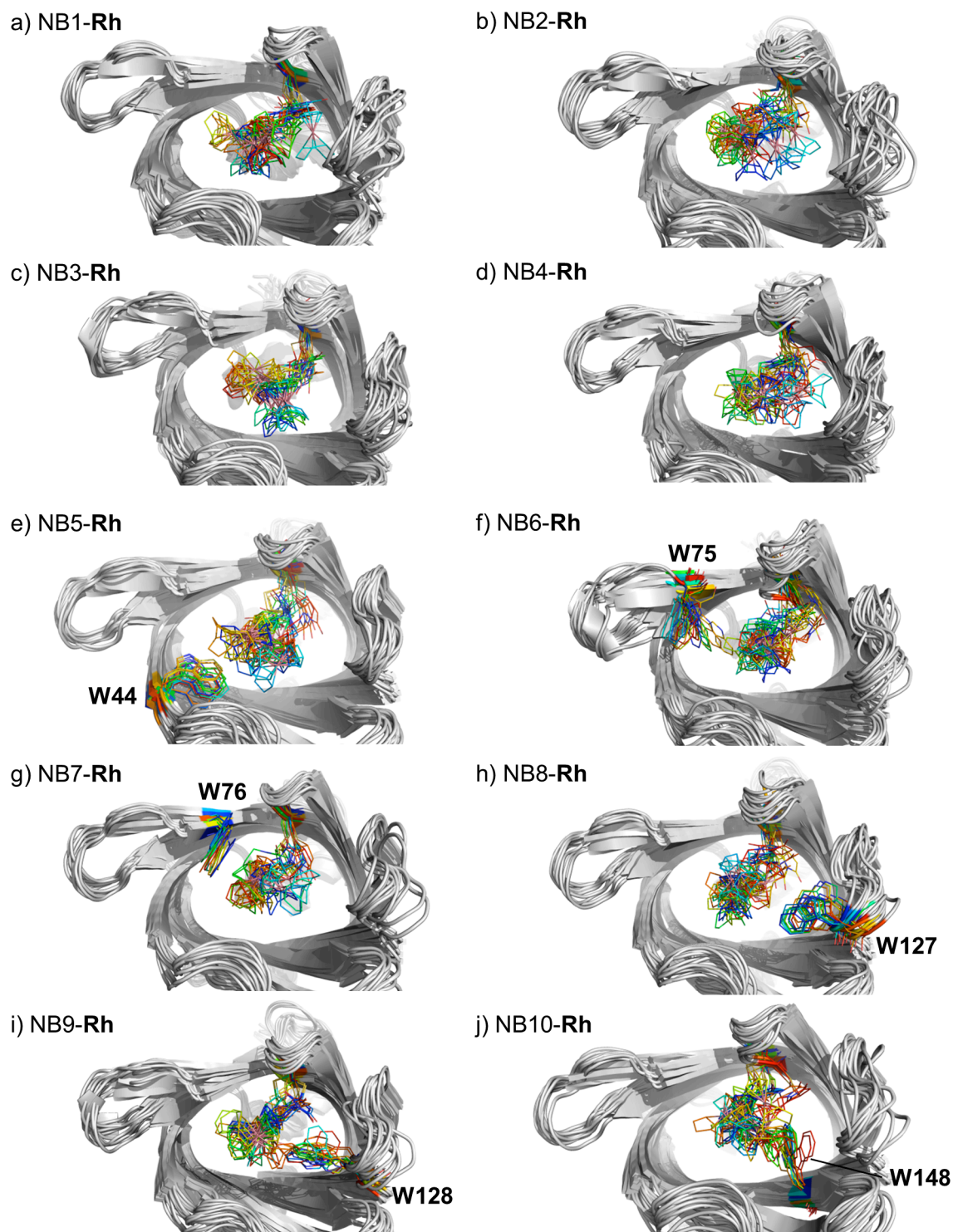
Figure 3-13. Superimposed sixteen calculated structures of (a) NB1-**Rh**, (b) NB2-**Rh**, (c) NB3-**Rh**, (d) NB4-**Rh**, (e) NB5-**Rh**, (f) NB6-**Rh**, (g) NB7-**Rh**, (h) NB8-**Rh**, (i) NB9-**Rh**, and (j) NB10-**Rh**. Selected sixteen snapshot structures were minimized after MD calculation. The rhodium moieties and Trp residues in NB5-**Rh**, NB6-**Rh**, NB7-**Rh**, NB8-**Rh**, NB9-**Rh**, and NB10-**Rh** are colored in rainbow colors.
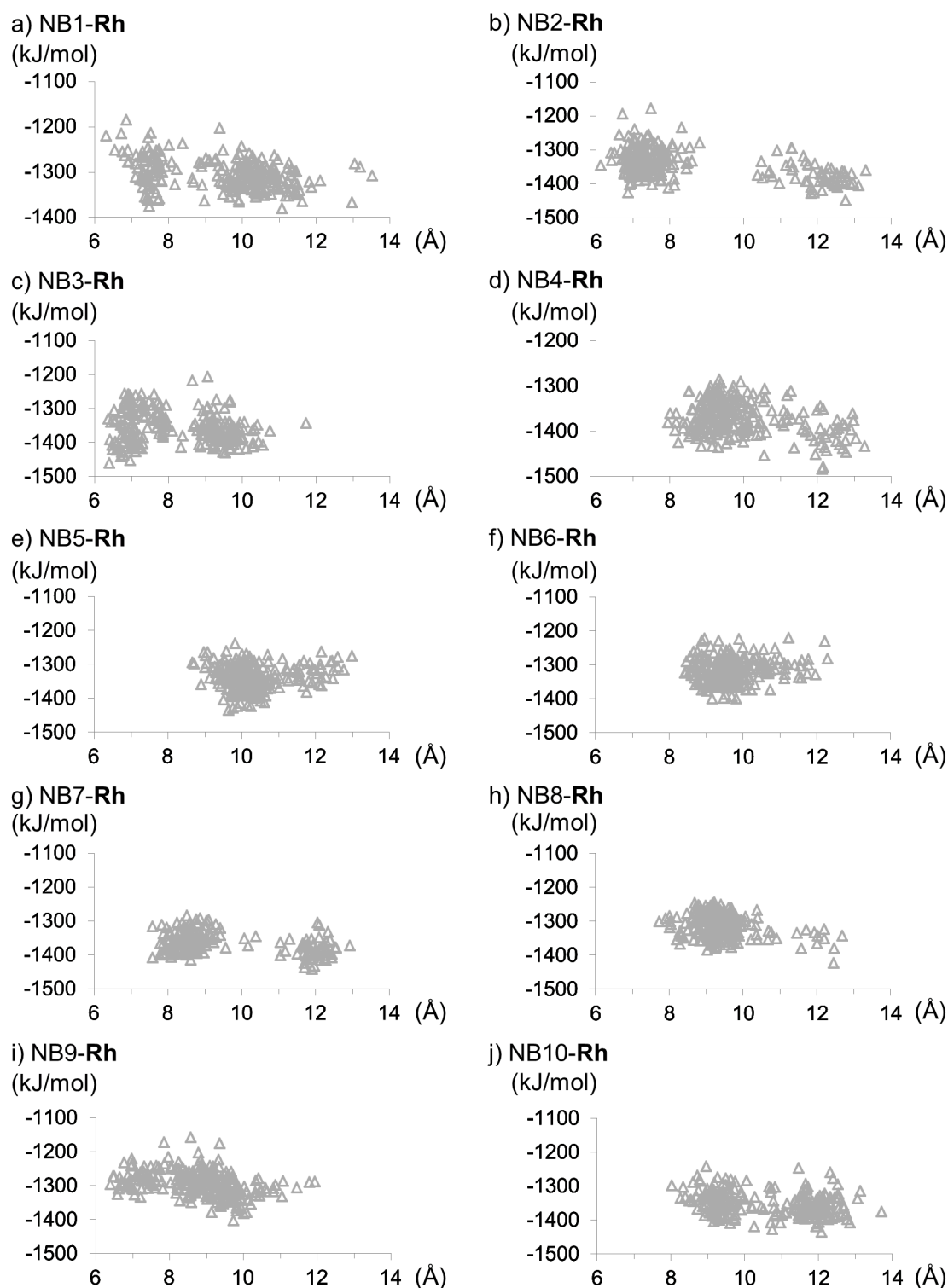
Figure 3-14. The total energy of the rhodium complex and the surrounding fourteen amino acid residues (position 41, 44, 46, 75, 76, 96, 98, 100, 127, 128, 148, 150, 158, and 159) are plotted against the distance between the rhodium ion and Cα of Leu75. Total 240 minimized structures after MD calculation in (a) NB1-**Rh**, (b) NB2-**Rh**, (c) NB3-**Rh** (d) NB4-**Rh**, (e) NB5-**Rh**, (f) NB6-**Rh**, (g) NB7-**Rh**, (h) NB8-**Rh** (i) NB9-**Rh**, and (j) NB10-**Rh** are plotted as a green triangles. The plots show the spatial distribution of the rhodium moiety within the cavity.
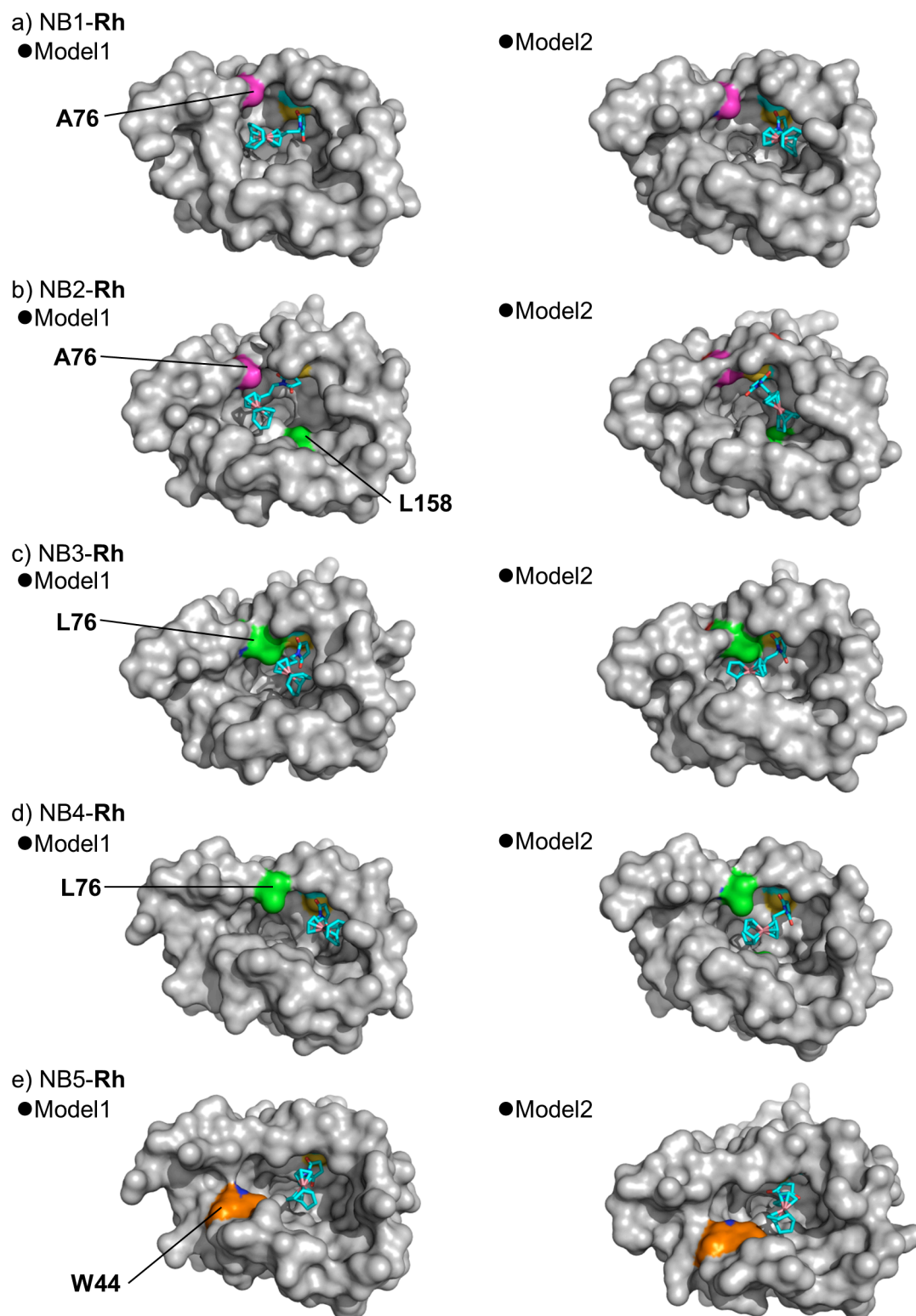
Figure 3-15. Favorable conformations of the rhodium moiety in (a) NB1-**Rh**, (b) NB2-**Rh**, (c) NB3-**Rh**, (d) NB4-**Rh**, and (e) NB5-**Rh**. Ala, Leu, Trp, and the rhodium complex are colored in pink, green, orange, and light blue, respectively.
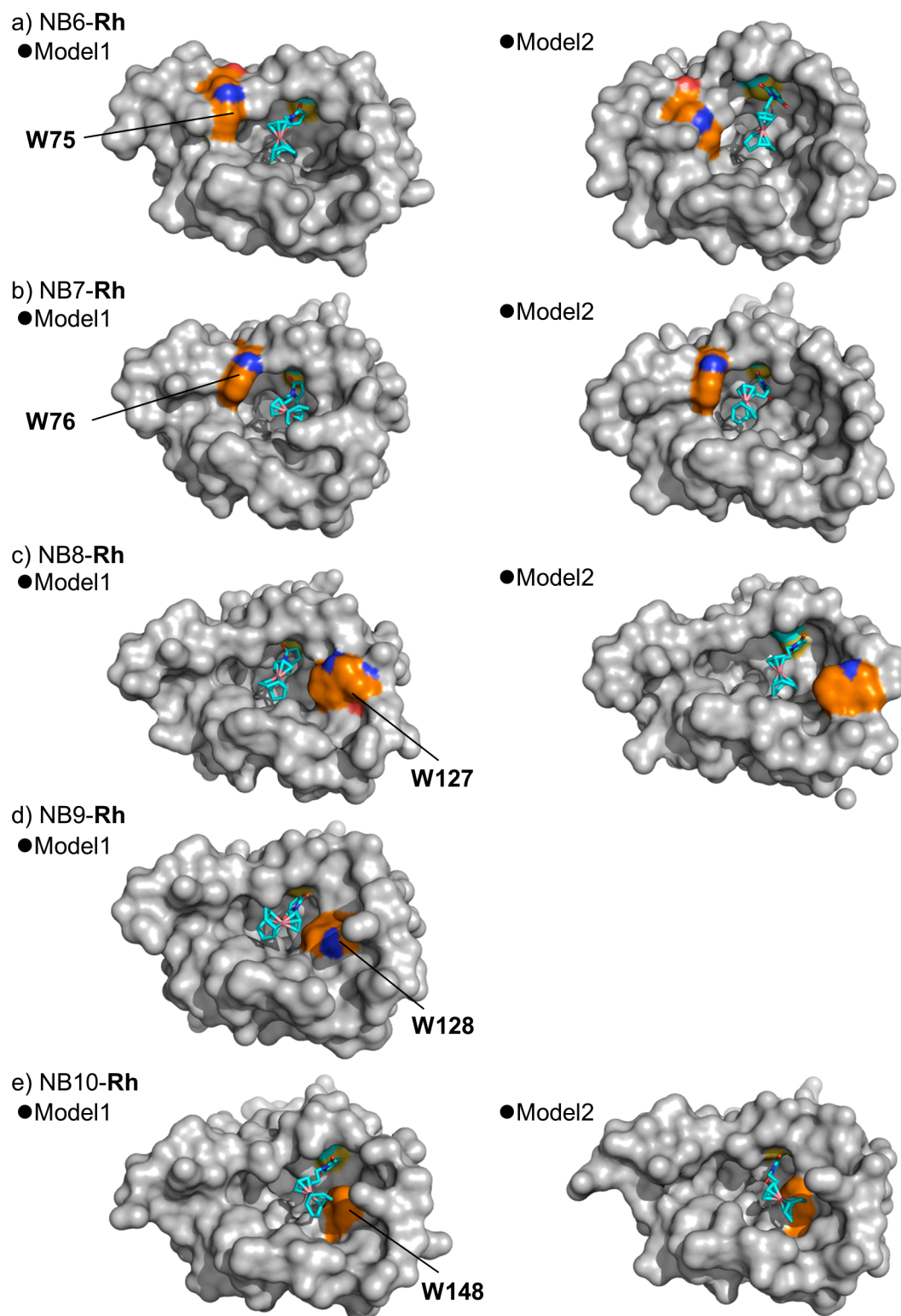
Figure 3-16. Favorable conformations of the rhodium moiety in (a) NB6-**Rh**, (b) NB7-**Rh**, (c) NB8-**Rh** (d) NB9-**Rh**, and (e) NB10-**Rh**.   The Ala, Leu, Trp residues and the rhodium complex are colored in pink, green, orange, and light blue, respectively.

References and Notes

[1] a) Y. Lu, N. Yeung, N. Sieracki, N. M. Marshall, *Nature* **2009**, *460*, 855–862; b) M. T. Reetz, M. Rentzsch, A. Pletsch, M. Maywald, P. Maiwald, J. J.-P. Peyralans, A. Maichele, Y. Fu, N. Jiao, F. Hollmann, R. Mondière, A. Taglieber, *Tetrahedron* **2007**, *63*, 6404–6414; c) T. Heinisch, T. R. Ward, *Curr. Opin. Chem. Biol.* **2010**, *14*, 184–199; d) T. R. Ward, *Acc. Chem. Res.* **2011**, *44*, 47–57; e) P. J. Deuss, R. den Heeten, W. Laan, P. C. J. Kamer, *Chem. Eur. J.* **2011**, *17*, 4680–4698; f) T. Ueno, H. Tabe, Y. Tanaka, *Chem. Asian. J.* **2013**, *8*, 1646–1660; g) T. Hayashi, Y. Hisaeda, *Acc. Chem. Res.* **2002**, *35*, 35–43; h) *Bio-inspired Catalysts (Ed.: T. R. Ward)*, Springer, Berlin, Heidelberg, **2009**.

[2] a) M. Ohashi, T. Koshiyama, T. Ueno, M. Yanase, H. Fujii, Y. Watanabe, *Angew. Chem. Int. Ed.* **2003**, *42*, 1005–1008; b) A. Mahammed, Z. Gross, *J. Am. Chem. Soc.* **2005**, *127*, 2883–2887; c) Q. Jing, K. Okrasa, R. J. Kazlauskas, *Chem. Eur. J.* **2009**, *15*, 1370–1376; d) Y. Sano, A. Onoda, T. Hayashi, *Chem. Commun.* **2011**, *47*, 8229–8231; e) T. Matsuo, A. Hayashi, M. Abe, T. Matsuda, Y. Hisaeda, T. Hayashi, *J. Am. Chem. Soc.* **2009**, *131*, 15124–15125; f) T. Matsuo, K. Fukumoto, T. Watanabe, T. Hayashi, *Chem. Asian. J.* **2011**, *6*, 2491–2499; g) F. W. Monnard, E. S. Nogueira, T. Heinisch, T. Schirmer, T. R. Ward, *Chem. Sci.* **2013**, *4*, 3269–3274; h) J. Podtetenieff, A. Taglieber, E. Bill, E. J. Reijerse, M. T. Reetz, *Angew. Chem. Int. Ed.* **2010**, *49*, 5151–5155; i) Z. T. Ball, *Acc. Chem. Res.* **2013**, *46*, 560–570.

[3] a) M. E. Wilson, G. M. Whitesides, *J. Am. Chem. Soc.* **1978**, *100*, 306–307; b) J. Collot, J. Gradinaru, N. Humbert, M. Skander, A. Zocchi, T. R. Ward, *J. Am. Chem. Soc.* **2003**, *125*, 9030–9031; c) H. Yamaguchi, T. Hirano, H. Kiminami, D. Taura, A. Harada, *Org. Biomol. Chem.* **2006**, *4*, 3571–3573; d) M. T. Reetz, J. J.-P. Peyralans, A. Maichele, Y. Fu, M. Maywald, *Chem. Commun.* **2006**, 4318–4320.

[4] a) H. L. Levine, E. T. Kaiser, *J. Am. Chem. Soc.* **1978**, *100*, 7670–7677; b) Z.-P. Wu, D. Hilvert, *J. Am. Chem. Soc.* **1989**, *111*, 4513–4514; c) D. Qi, C.-M. Tann, D. Haring, M. D. Distefano, *Chem. Rev.* **2001**, *101*, 3081–3111; d) M. T. Reetz, M. Rentzsch, A. Pletsch, M. Maywald, *Chimia* **2002**, *56*, 721–723; e) J. R. Carey, S. K. Ma, T. D. Pfister, D. K. Garner, H. K. Kim, J. A. Abramite, Z. Wang, Z. Guo, Y. Lu, *J. Am. Chem. Soc.* **2004**, *126*, 10812–10813; f) T. Matsuo, C. Imai, T. Yoshida, T. Saito, T. Hayashi, S. Hirota, *Chem. Commun.* **2012**, *48*, 1662–1664; g) P. Haquette, B. Talbi, L. Barilleau, N. Madern, C. Fosse, M. Salmain, *Org. Biomol. Chem.* **2011**, *9*, 5720–5727; h) F. Philippart, M. Arlt, S. Gotzen, S.-J. Tenne, M. Bocola, H.-H. Chen, L. Zhu, U. Schwaneberg, J. Okuda, *Chem. Eur. J.* **2013**, 13865–13871; i) J. Bos, A. García-Herraiz, G. Roelfes, *Chem. Sci.* **2013**, *4*, 3578–3582.

[5] J. M. Zimbron, T. Heinisch, M. Schmid, D. Hamels, E. S. Nogueira, T. Schirmer, T. R. Ward, *J. Am. Chem. Soc.* **2013**, *135*, 5384–5388.

[6] a) M. T. Reetz, N. Jiao, *Angew. Chem. Int. Ed.* **2006**, *45*, 2416–2419; b) J. Bos, F. Fusetti, A. J. M. Driessen, G. Roelfes, *Angew. Chem. Int. Ed.* **2012**, *51*, 7472–7475.

[7] a) T. Ueno, T. Koshiyama, M. Ohashi, K. Kondo, M. Kono, A. Suzuki, T. Yamane, Y. Watanabe, *J. Am. Chem. Soc.* **2005**, *127*, 6556–6562; b) A. Pordea, M. Creus, J. Panek, C. Duboc, D. Mathis, M. Novic, T. R. Ward, *J. Am. Chem. Soc.* **2008**, *130*, 8085–8088.

[8] T. K. Hyster, L. Knörr, T. R. Ward, T. Rovis, *Science* **2012**, *338*, 500–503.

[9] M. Creus, T. R. Ward, *Org. Biomol. Chem.* **2007**, *5*, 1835–1844.

[10] a) A. J. Heeger, *Angew. Chem. Int. Ed.* **2001**, *40*, 2591–2611; b) A. G. MacDiarmid, *Angew. Chem. Int. Ed.* **2001**, *40*, 2581–2590; c) H. Shirakawa, *Angew. Chem. Int. Ed.* **2001**, *40*, 2574–2580; d) J. Liu, J. W. Y. Lam, B. Z. Tang, *Chem. Rev.* **2009**, *109*, 5799–5867.

[11] a) Z. Ke, S. Abe, T. Ueno, K. Morokuma, *J. Am. Chem. Soc.* **2011**, *133*, 7926–7941; b) B. Z. Tang, W. H. Poon, S. M. Leung, W. H. Leung, H. Peng, *Macromolecules* **1997**, *30*, 2209–2212; c) T. Ikariya, Y. Kishimoto, P. Eckerle, T. Miyatake, M. Kainosho, A. Ono, R. Noyori, *J. Am. Chem. Soc.* **1999**, *121*, 12035–12044.

[12] a) S. Abe, K. Hirata, T. Ueno, K. Morino, N. Shimizu, M. Yamamoto, M. Takata, E. Yashima, Y. Watanabe, *J. Am. Chem. Soc.* **2009**, *131*, 6958–6960; b) Z. Ke, S. Abe, T. Ueno, K. Morokuma, *J. Am. Chem. Soc.* **2012**, *134*, 15418–15429.

[13] C. M. Bianchetti, G. C. Blouin, E. Bitto, J. S. Olson, G. N. Phillips, Jr., *Proteins* **2010**, *78*, 917–931.

[14] A. Onoda, K. Fukumoto, M. Arlt, M. Bocola, U. Schwaneberg, T. Hayashi, *Chem. Commun.* **2012**, *48*, 9756–9758.

[15] The aponitrobindin variant, M75L/Q96C/M145L, a prototype protein of the present work is abbreviated as NB(Q196C).

[16] J. V. Durme, J. Delgado, F. Stricher, L. Serrano, J. Schymkowitz, F. Rousseau, *Bioinformatics* **2011**, *27*, 1711–1712.

[17] a) D. G. Levitt, L. J. Banaszak, *J. Mol. Graphics* **1992**, *10*, 229–234; b) M. Hendlich, F. Rippmann, G. Barnickel, *J. Mol. Graphics Mod.* **1997**, *15*, 359–363; c) A. T. R. Laurie, R. M. Jackson, *Bioinformatics* **2005**, *21*, 1908–1916.

[18] The anchoring of the rhodium complex within the NB variants from NB1 to NB5 proceeded smoothly with good conversion, while the anchoring reactions of the NB variants from NB6 to NB10, which contain the bulky Trp residue were found to be slower and produced a lower yield of the rhodium complex (approximately 60%).

[19] The F_o–F_c omit map also confirms the covalent linkage between the Cys96 residue and the maleimide group of the rhodium complex.

[20] E. Krieger, T. Darden, S. Nabuurs, A. Finkelstein, G. Vriend, *Proteins: Struct. Funct. Bioinf.* **2004**, *57*, 678-683.

[21] Z. Otwinowski, W. Minor, *Method Enzymol* **1997**, *276*, 307-326.

[22] M. D. Winn, C. C. Ballard, K. D. Cowtan, E. J. Dodson, P. Emsley, P. R. Evans, R. M. Keegan, E. B. Krissinel, A. G. W. Leslie, A. McCoy, S. J. McNicholas, G. N. Murshudov, N. S. Pannu, E. A. Potterton, H. R. Powell, R. J. Read, A. Vagin, K. S. Wilson, *Acta Crystallogr. D* **2011**, *67*, 235-242.

[23] A. J. Mccoy, R. W. Grosse-Kunstleve, P. D. Adams, M. D. Winn, L. C. Storoni, R. J. Read, *J. Appl. Crystallogr.* **2007**, *40*, 658-674.

[24] P. Emsley, K. Cowtan, *Acta Crystallogr. D* **2004**, *60*, 2126-2132.

[25] G. N. Murshudov, P. Skubak, A. A. Lebedev, N. S. Pannu, R. A. Steiner, R. A. Nicholls, M. D. Winn, F. Long, A. A. Vagin, *Acta Crystallogr. D* **2011**, *67*, 355-367.

[26] Y. Duan, C. Wu, S. Chowdhury, M. C. Lee, G. Xiong, W. Zhang, R. Yang, P. Cieplak, R. Luo, T. Lee, J. Caldwell, J. Wang, P. Kollman, *J. Comput. Chem.* **2003**, *24*, 1999-2012.

[27] J. Wang, R. M. Wolf, J. W. Caldwell, P. A. Kollman, D. A. Case, *J. Comput. Chem.* **2004**, *25*, 1157-1174.

[28] A. Jakalian, D. B. Jack, C. I. Bayly, *J. Comput. Chem.* **2002**, *23*, 1623-1641.

Conclusion

The goal of this research is to create an artificial biocatalyst with high activity and selectivity by placing a synthetic metal complex within a genetically designed protein cavity. To achieve the high activity and selectivity, the author focused on both the chemical optimization of the ligand of the metal complex and the genetic optimization of the protein cavity with the guidance of computational chemistry.

In the chapter 1, the author precisely reengineered the artificial heme cofactor by the introduction of a large substrate-binding domain at one of the propionate side chains to enhance the affinity of the substrate and reactivity of the active spices "Compound I". The H64D myoglobin mutant with the reengineered artificial heme dramatically improved the peroxidase activity of myoglobin. The catalytic activity of the newly engineered myoglobin mutant was as same level as that of horseradish peroxidase, a naturally occurring peroxidase, and the engineered myoglobin exhibited the highest reactivity among any of the artificial myoglobins ever reported. The optical measurements showed that the high catalytic activity stemmed from the protein engineering *with* improved substrate access and *without* loss of the reactivities in the chemical process.

In the chapter 2, the author covalently conjugated to create rhodium complex-linked nitrobindin Q96C mutant as an artificial biocatalyst. The biocatalyst promoted phenylacetylene polymerization with approximately 50% *trans* content, although the free rhodium complex yielded only *cis*-polyphenylacetylene. The result indicates that the nitrobindin cavity could have an effect to the selectivity in phenylacetylene polymerization.

In the chapter 3, the author demonstrated the reengineering of the cavity of rhodium complex-linked nitrobindin by computationally guided site-directed mutagenesis. One of the reengineered artificial biocatalysts shows significantly-increased *trans*-stereoselectivity in phenylacetylene polymerization up to 80% *trans* content. Furthermore, the structural information of the best artificial biocatalyst was obtained by X-ray crystal structure analysis and molecular modeling. The crystal and modeled structures supported the fact that the stereoselectivity was enhanced by effective control of monomer access to the rhodium complex within the limited space of the β-barrel scaffold.

In conclusion, the artificial biocatalysts with high activity and/or selectivity are found to be prepared by the fine-tuning of the protein cavity and the ligand of the metal complex. Additionally, the both factors are important to improve the activity and selectivity, because there is the synergetic relation between the metal complex and the protein. The author is convinced that this work provides the clues for construction of an artificial biocatalyst with high active and selective catalysis. Furthermore, the author believes that the theoretical reengineering of the artificial biocatalyst will promise for the development of a homogenous catalyst with new chemical reactivity and selectivity.

List of Publications for This Thesis

1. Precise Design of Artificial Hemes for Enhancing Peroxidase Activity of Myoglobin: Myoglobin Mutant H64D Reconstituted with a "Single-winged Heme" is Equivalent to Native Horseradish Peroxidase in Oxidation Activity
   Takashi Matsuo, <u>Kazuki Fukumoto</u>, Takuro Watanabe, Takashi Hayashi
   Chem. Asian J., **2011**, *6*, 2491 – 2499.

2. A Rhodium Complex-linked β-barrel Protein as a Hybrid Biocatalyst for Phenylacetylene Polymerization
   Akira Onoda, <u>Kazuki Fukumoto</u>, Marcus Arlt, Marco Bocola, Ulrich Schwaneberg, Takashi Hayashi
   Chem. Commun., **2012**, *48*, 9756 – 9758.

3. A Rhodium Complex-linked Hybrid Biocatalyst: Stereo-controlled Phenylacetylene Polymerization within an Engineered Protein Cavity
   <u>Kazuki Fukumoto</u>, Akira Onoda, Eiichi Mizohata, Marco Bocola, Tsuyoshi Inoue, Ulrich Schwaneberg, and Takashi Hayashi
   ChemCatChem, in press.

Acknowledgments

<div align="right">

Kazuki Fukumoto

January 2014

</div>